Modelling Radon and Thoron Exhalation and Measurement of Total Natural Radiation Exposure in Mrima Hill, Kenya

Margaret Wairimu Chege (M.Sc.)

Reg. No. I84/15115/08

Thesis submitted in fulfillment of the requirement for the award of the degree of Doctor of Philosophy in Physics in the School of Pure and Applied Science of Kenyatta University

October 2014

DECLARATION

This thesis is my original work and has not been presented for a degree in any other university.

Margaret Wairimu Chege Signature……..
Department of Physics
Kenyatta University Date…….
P. O. Box43844
Nairobi,

We confirm that the work reported in this thesis was carried out by the candidate under our supervision:

Dr. N.O. Hashim Signature……
Physics Department
Kenyatta University Date…….
P.O. Box 43844
Nairobi

Dr. A. S. Merenga Signature……..
Physics Department
Kenyatta University Date……..
P.O. Box 43844
Nairobi

Dr. J. Tschiersch Signature……..
Helmholtz Zentrum München
Institute of Radiation Protection Date……..
Ingolstädter Landstraße 1
85764 Neuherberg
Germany

DEDICATION

This thesis is dedicated to fellow workmates also pursuing their doctoral studies:

"The dark of the night always give way to the light of the day"

ACKNOWLEDGEMENT

I wish to sincerely express my gratitude to my thesis supervisors, Dr. N. O. Hashim, Dr. A. S. Merenga and Dr. J. Tschiersch for their guidance throughout the course of my research. I am grateful to Dr. J. Tschiersch and the management of the Helmholtz Zentrum München – German Research Center for Environmental Health, Institute of Radiation Protection, Germany, for donating the thoron/radon measuring devices, facilitating the analysis of some of the samples and sponsoring my stay as a guest scientist at the institute and as a student at WE-Heraeus Physics Summer School that was held in Bad Honnef, Germany, from 11 - 23 August 2013. I wish to sincerely thank the organizers of the summer school especially Prof. Werner Ruehm for giving me the chance to attend the school and the opportunity to share research ideas with peers as well as experts in the field of radiation protection and measurements.

I am grateful to Dr. O. Meisenberg of the Institute of Radiation Protection, Germany, for his assistance in the sample analysis, and for the many fruitful discussions regarding indoor radioactivity particularly that due to thoron in traditional earthen buildings located in both Kenya and in Germany. I am grateful to the members of the Working Group Experimental Radioecology at the Institute of Radiation Protection in Germany for their welcome and hospitality during my stay there as a guest scientist.

Many thanks to the office of the Dean, School of Pure and Applied Sciences at Pwani University in Kilifi, Kenya for allowing the use of their facilities for water analysis, and to the Laboratory Technicians Ms. Esther Mwegu and Mr. David Samoei for their assistance in the laboratory. I am grateful to the Director's Office, Institute of Nuclear

Science and Technology, University of Nairobi, Kenya for allowing the use of their facilities for radioactivity measurements of crop and water samples. Much thanks to Mr. S. Bartilol for his assistance in the laboratory.

I am especially grateful to my fieldwork team: Mr. Charles Waigi and Mr. Saidi Kulewa of Kenyatta University, Mombasa Campus; Mr. Saidi Kibugu, a student of Environmental Studies at Kenyatta University, Mombasa Campus and a native resident of Kwale County which was the focus of this study; and to our driver, Ms. Irene Muthoni. Special thanks to the villagers of Mrima hill and Kanana for welcoming us to their homes, for their openness regarding their cultural believes and way of life, and for their assistance in collection of samples used in this study.

I am grateful to the National Council for Science and Technology (NCST), Kenya, for the financial support towards my PhD research.

Many thanks to my students at Kenyatta University, Mombasa Campus for their cooperation in the course of my PhD work.

Last but not least, I greatly appreciate the moral support from my parents and siblings, and my nephews Ricky and Ian.

TABLE OF CONTENTS

DECLARATION ii

DEDICATION iii

ACKNOWLEDGEMENT iv

TABLE OF CONTENTS vi

LIST OF TABLES x

LIST OF FIGURES xii

LIST OF PLATES xv

ABBREVIATIONS AND ACCRONYMS xvi

ABSTRACT xvii

CHAPTER 1: INTRODUCTION 1

1.1 Background 1

1.2 Background radiation 2

1.3 Heavy metals 6

1.4 Description of the study area 7

1.5 Statement of the research problem 11

1.6 Objectives 12

1.7 Rationale 12

CHAPTER 2: LITERATURE REVIEW 13

2.1 Radiation exposure 13

2.2.1 Stochastic effects 14

2.2.2 Non-stochastic effects 16

2.3 Heavy metal exposure 17

2.4 Radionuclides and heavy metals in the ecosystem.....19

2.4.1 Radioactivity in soil.....19

2.4.2 Radionuclides and other heavy metals in groundwater.....21

2.4.3 Radioactivity in crops.....23

2.3.4 Radioactivity in indoor air.....24

CHAPTER 3: THEORETICAL CONSIDERATIONS.....28

3.1 Natural radioactivity.....28

3.1.1 Origin of radioactivity.....28

3.1.2 Activity of radionuclides.....28

3.1.3 Decay series.....31

3.1.4 Radioactive equilibrium.....35

3.1.4.1 Transient equilibrium.....35

3.1.4.2 Secular equilibrium.....36

3.2 Heavy metals.....38

3.3 Identification and quantification of elements.....38

3.3.1 Alpha detectors.....38

3.3.1.1 Solid State Nuclear Track Detection (SSNTD).....38

3.3.1.2 RAD7 alpha detector.....39

3.3.2 Gamma ray detectors.....40

3.3.3 Atomic absorption spectrophotometer (AAS).....43

3.4 Modelling radon/thoron generation, exhalation and accumulation.....45

3.4.1 Thoron generation within the interstitial space of building materials.....45

3.4.2 Transport and exhalation.....48

3.4.3 Accumulation 54

CHAPTER 4: MATERIALS AND METHODS 57

4.1 Geology of the sampling region 57

4.2 Radon and thoron concentration measurements 59

4.2.1 Sampling and sample preparation 59

4.2.2 Analysis 61

4.3 Radon and thoron exhalation measurements 62

4.3.1 Sampling and sample preparation 62

4.3.2 Analysis 63

4.4 Spectral analysis of building materials, soil, crops and water samples 65

4.4.1 Sampling and sample preparation 65

4.4.2 Analysis 67

4.5 Physico-chemical analysis of water samples 68

4.5.1 Sampling and sample preparation 68

4.5.2 Analysis 69

CHAPTER 5: RESULTS AND DISCUSSION 70

5.1 Radon and thoron concentration 70

5.1.1 Internal exposure due to inhalation of indoor air 72

5.2 Radon and thoron exhalation rate 74

5.3 Specific concentrations of ^{226}Ra, ^{232}Th and ^{40}K 79

5.3.1 Building materials 79

5.3.2 Soil 81

5.3.2.1 External exposure due to soil/building materials 83

5.3.3 Groundwater 84

5.3.3.1 Internal exposure due to groundwater consumption 86

5.3.4 Cassava crop 87

5.3.4.1 Internal exposure due to cassava crop consumption 90

5.4 Physical-chemical properties of groundwater samples 90

5.5 Exposure associated with radioactivity in building materials, indoor air, crops and well water in the sampling region 94

CHAPTER 6: CONLUSION AND RECOMMENDATION 96

6.1 Conclusion 96

6.2 Recommendations 98

REFERENCES 100

APPENDICES 118

Appendix 1: ^{238}U decay chain 118

Appendix 2: Thoron decay chain 119

Appendix 3: Wall sample being collected from a typical mud wall of a hut in the Mrima hill region 120

Appendix 4: Picture of Mrima hill 121

Appendix 5: A local woman assisting in sample collection from an open well in Mrima hill region 122

Appendix 6: Calibration curves for heavy metal analysis 123

Appendix 7: Research papers and presentations 124

LIST OF TABLES

Table 1.1 World average annual radiation exposure to ionising radiation…….4

Table 2.1 Summary series of radon, thoron and actinon……..……21

Table 5.1 Summary statistics of radon and thoron concentration in the sampling regions……..70

Table 5.2 Summary statistics of radon and thoron exhalation rates from building materials……..….76

Table 5.3 Typical radon emanation coefficients for different soil types……77

Table 5.4 Summary statistics of specific concentration of ^{226}Ra, ^{232}Th and ^{40}K in building material samples……80

Table 5.5 Summary statistics of specific concentration of ^{226}Ra, ^{232}Th and ^{40}K in soil samples……..……82

Table 5.6 Summary statistics of specific concentration of ^{226}Ra, ^{232}Th and ^{40}K in groundwater samples……...…….……85

Table 5.7 Summary statistics of specific concentration of ^{226}Ra, ^{232}Th and ^{40}K in cassava tuber and leaf samples……..…….…..…88

Table 5.8 Mean values of pH, electrical conductivity and heavy metal concentration in groundwater samples…….....92

Table 5.9 Summary of annual effective dose rates due to the various factors in the sampling region……..……94

LIST OF FIGURES

Figure 2.1 Radon decay chain showing the short-lived decay products……....14

Figure 2.2 Thoron decay chain showing the short-lived decay products…….....14

Figure 3.1 Variation of activity with time for radionuclides with different decay constants…….……..15

Figure 3.2 Variation of number of atoms with time when T1<T2……34

Figure 3.3 Variation of number of atoms with time when T1>T2…….…..….34

Figure 3.4 Secular equilibrium between long-lived parent and short-lived daughter nuclide……..…….37

Figure 3.5 A reverse biased Ge semiconductor crystal……..……..37

Figure 3.6 Nebulization and atomization process……...…..…..44

Figure 3.7 Illustration of possible behavior of a thoron atom after generation in the grain of a solid particle……...…46

Figure 3.8 Possible path through a porous medium that an emanated thoron atom may follow towards the surface ……..…….…..…...…49

Figure 3.9 A schematic of a building material sample with the thickness measured from the center outwards……..……52

Figure 4.1 Map of the sampling regions indicating the sampling points…….58

Figure 4.2 Schematic of the experimental arrangement used for exhalation measurements……..…..64

Figure 4.3 Schematic of sample counting geometry for radioactivity analysis of samples…….……....67

Figure 5.1 Variation of thoron concentration with radon concentration in dwellings…….…….……71

Figure 5.2 Growth curves of radon and thoron from building material samples from Mrima hill……..……..74

Figure 5.3 Growth curves of radon and thoron from building material samples from Kanana…….….……..75

Figure 5.4 Radon and thoron exhalation rates from building material samples…….…….…..…76

Figure 5.5 A graph of measured and modelled thoron exhalation rate from building material samples…….…..……78

Figure 5.6 Distribution of specific concentration of ^{226}Ra, ^{232}Th and ^{40}K in building material samples……79

Figure 5.7 Radon and thoron exhalation rates against mother radionuclide concentration……....81

Figure 5.8 Specific concentrations of ^{226}Ra and ^{232}Th in building material samples…….……82

Figure 5.9 Distribution of Ra, Th and K in cassava tubers and leaves in Mrima hill…….88

Figure 5.10 Percentage of water samples enriched by selected heavy metals….....93

Figure 5.11 Percentage of contribution of exposure pathways to the total annual effective dose…….…...……95

LIST OF PLATES

Plate 1.1 One of the sampled shallow well in the Mrima hill region……9

Plate 1.2 A group of women and children drawing water from a closed well in the sampling region……..…..9

Plate 1.3 Dwellings in a village on the slopes of Mrima hill which were used in the current research…….…….10

Plate 3.1 Alpha track damages in CR-39 made visible by etching…….…39

Plate 4.1 Twin canisters fitted with CR-39 used in this study for discriminative measurement of radon and thoron……..……..59

Plate 4.2 Twin canisters deployed in a dwelling in Mrima hill…….……..61

Plate 4.3 A pre-treated building material sample used for exhalation measurement……63

ABBREVIATIONS AND ACCRONYMS

AAS	Atomic Absorption Spectrophotometer
DNA	Deoxyribonucleic Acid
EU	European Union
HBRA	High Background Radiation Areas
HPGe	High Purity Germanium
IAEA	International Atomic Energy Agency
ICRP	International Commission on Radiological Protection
KCPE	Kenya Certificate of Secondary Education
LET	Linear Energy Transfer
MCL	Maximum Contamination Level
SSND	Solid State Nuclear Tract Detectors
UNSCEAR	United Nations Scientific Committee on Effects of Atomic Radiation
USEPA	United States Environmental Protection Agency
WHO	World Health Organization

ABSTRACT

Mrima hill in Kwale County is one of the regions in Kenya with the highest levels of background radiation. Rich deposits of mineral ores such as niobium and manganese are also known to exist. Small-scale farming is the mainstay of the economy with cassava as the main cash as well as food crop; raw soil constitutes the primary building material while hand-dug wells serve as the source of water for the residents. The main objective of this research was to determine the exposure associated with radioactivity in indoor air, crops and well water in the region. This involved the determination of ^{222}Rn and ^{220}Rn concentration in dwellings and measurement of ^{226}Ra, ^{232}Th, and ^{40}K concentrations in building materials, soil, cassava and well water. A model on radon and thoron exhalation rates was developed and validated through exhalation measurements. In addition, physico-chemical parameters of water that included heavy metals, pH and conductivity were investigated. CR-39 SSNTD were used for simultaneous measurements of ^{222}Rn and ^{220}Rn; accumulation chamber coupled with RAD7 monitor for exhalation measurements; HPGe detectors for radioactivity measurements in crops and water samples; and the AAS for heavy metal determination in water samples. Conductivity and pH were measured on site using standard digital meters. A total annual effective dose of 24.1 mSv/y was obtained with indoor air, crops and water, and building materials contributing 56 %, 36 % and 8 % of the dose respectively. All radon concentration values were below 200 Bq m^{-3} while 65 % of thoron measurements were above 300 Bq m^{-3}. A mean thoron concentration of 652.8±397.0 Bq m^{-3} was obtained against that of radon of 35.2±13.9 Bq m^{-3}. Building materials registered average radon and thoron exhalation rates of 0.0043 Bq m^{-2} s^{-1} and 19.6 Bq m^{-2} s^{-1} respectively and average concentrations of ^{226}Ra and ^{232}Th of 134 Bq kg^{-1} and 431 Bq kg^{-1} respectively. Modelled and measured isotopes exhalation values showed good agreement which meant that exhalation rate was dependent on the content of mother radionuclide in the building material. A correlation coefficient of near unity was observed between ^{226}Ra and ^{232}Th content in building materials and in soil. Over 70 % of cassava tubers and leaves had detectable amounts ^{226}Ra with average concentrations of 60±5 Bq kg^{-1} and 141±11 Bq kg^{-1} respectively. ^{232}Th, with an average concentration of 35.3±61.5 Bq kg^{-1} was detected in 28 % of the tubers; it was not detected in the leaves. 37 % and 7 % of water samples detected for ^{226}Ra and ^{232}Th with average concentrations of 4.3±0.3 Bq kg^{-1} and 2.0±0.1 Bq kg^{-1} respectively. ^{40}K was present in all samples in averages of 842±539 Bq kg^{-1}, 1708±552 Bq kg^{-1} and 91.4 Bq kg^{-1} in cassava tubers, leaves and water respectively. In terms of heavy metals, over 90% of the water samples were enriched with at least one metal with Mn and Cd as the main contaminants. The average electrical conductivity was 862±949 µSv/cm; 17 % of the samples had pH values lower than 6.5. From the results obtained, the main source of exposure in Mrima hill region is indoor air with thoron as the main source of the radiation dose. Exposure through ingestion is mainly due to ^{226}Ra and ^{40}K. Groundwater in the region is generally of poor quality mainly due to heavy metal enrichment.

CHAPTER 1: INTRODUCTION

1.1 Background

The health and well being of the human race is to a certain extent determined by the environment. What we expose our bodies to whether externally or internally can make us either productive enough to reach our optimum potential, impact negatively on our intellect and behavior, or even make us fall sick and probably die. The World Health Organization estimates that as much as 24% of global disease can be linked directly to environmental factors (WHO, 2006). Some of the consequences of exposure are however not easy to detect as they manifest later in adulthood, or their origins are not well understood. Consequently, they are often blamed on other factors. As an example, among the Kikuyu community in Kenya, ringworm of the skin is in some cases misconstrued to be as a result of *githemengu* (evil eye) while in reality it is caused by a fungus and may spread through interaction with infected items: sharing of items is a common practice among rural communities in the country.

The recent past has seen a steady rise in global awareness over environmental pollution particularly with regard to contaminants such as radionuclides and heavy metals. This is as a result of the increasing evidence being advanced on their effects on the health and well being of the human race (Briggs, 2003; WHO, 2007). While some radionuclides and heavy metals have many positive applications especially in the industrial, medical and energy sectors, they can become potentially dangerous if the exposure is not well controlled or in some cases the concentration exceeds certain threshold values.

1.2 Background radiation

Radionuclides have been in existence since the beginning of time. They are present in the air we breathe, the water we drink and the food we eat. They are in the soil in which we grow our crops, in the building materials we use to construct our houses, in our hospitals and in our industries. These radionuclides give rise to a cloud of background radiation that eternally engulfs us, never to escape from.

Sources of radionuclides and subsequently background radiation can be categorized as either artificial/anthropogenic or natural. Anthropogenic radiation results from some form of human activity such as the use of nuclear medicine, nuclear power generation, military operation, agricultural, mining and industrial activities as well as use of consumer products such as smoke detectors. Radiation from these sources is generally small as its function is regulated. Its application is restricted in such a way that a balance is struck between the benefits it offers and the risks it imposes on people and the environment. Nonetheless, uncontrolled exposure can occur for example in the event of nuclear accidents as happened following the Chernobyl nuclear disaster of 1986 in the former USSR and the 2011 Fukushima disaster in Japan.

Natural sources of radiation consist primarily of cosmic rays and terrestrial radiation. Cosmic rays are a type of radiation that comes from outer space consisting primarily of charged particles (85 % protons, 12 % alpha particles and 3 % heavier nuclei). The earth's atmosphere absorbs some of this radiation and in the process produces secondary radiation of reduced intensity consisting of subatomic particles such as muons and electrons. At higher altitudes where the air is thinner, less cosmic radiation

is absorbed compared to lower altitudes where the air is thicker. For this reason, people who live on higher elevations or fly on commercial airplanes are exposed to cosmic radiation of higher intensity than those who, for instance, live at sea level. Air is thickest at sea level and here cosmic radiation consists mainly of muon at 68 %. Electrons make up 30 % while protons are reduced to less than 1 %.

Terrestrial radiation on the other hand comes from radionuclides that occur naturally in rock and soil. ^{238}U, ^{232}Th, their decay products and the singly occurring ^{40}K contribute the greatest fraction of this radiation (UNSCEAR, 2000). Terrestrial radionuclides are of particular concern with respect to radiation protection due to their ability to migrate to other compartments of the ecosystem such as indoor air, groundwater and crops, and eventually to the human body thus adding to the total radiation dose. Data on this aspect of radiation exposure is limited in Kenya, relative to that on exposure due to radionuclide concentration in soil.

Table 1.1 shows the contribution of different sources of radiation to the total global annual radiation dose (UNSCEAR, 2008). From the UNSCEAR data, natural sources are responsible for over 80 % of the radiation dose contributing an average annual exposure of 2.4 mSv/y. The largest proportion of this exposure (about 42 %) comes from inhalation of indoor air (UNSCEAR, 2008). In most parts of the world, rock and soil serve as the main building materials and as they naturally contain trace amounts of ^{238}U and ^{232}Th, they can be important sources radioisotopes ^{222}Rn (radon) and ^{220}Rn (thoron) in their respective decay chains (Appendix 1 and 2 respectively), which are considered responsible for the inhaled dose. Being gases, the isotopes can escape from the building material where they are formed and into indoor air. Their movement and

exhalation from the building materials, and eventual build-up in indoor air is dependent on the nature of the building material and the level of ventilation of the building (Al-Sharif, 2001; El-Taher *et al*., 2013).

Table 1.1: World average annual radiation exposure to ionising radiation (UNSCEAR, 2008)

Radiation source	**Exposure (mSv/y)**
Inhalation of air	1.26
Ingestion of food & water	0.29
Terrestrial radiation from ground	0.48
Cosmic radiation from space	0.39
Subtotal (natural)	**2.4**
Medical	0.6
Consumer items	-
Atmospheric nuclear testing	0.005
Occupational exposure	0.005
Chernobyl accident	0.002
Nuclear fuel cycle	0.0002
Other	-
Subtotal (artificial)	**0.61**
Total	**3.01**

In some developed countries, radiation exposure from artificial sources is as high as that from natural sources. In the US for instance, almost half the annual dose comes

from artificial sources with diagnostic medical procedures accounting for 48 % of the dose (NCRP, 2009).

Radiation exposure from natural sources typically ranges from 1.5 mSv/y to 3.5 mSv/y. In parts of the world referred to as high background radiation areas (HBRA), the exposure can be as high as 50 mSv/y or even more. The highest exposure ever recorded is 260 mSv/y in the HBRA of Ramsar city in Northern Iran (Ghiasi-nejad *et al.*, 2002). Other well known HBRA include Yangjiang region in China, Guarapari in Brazil and Kerala in India. In Kenya, Mrima hill in the south coast of the port city of Mombasa is one of the regions in the country with the highest level of background radiation, with documented outdoor gamma exposure of up to 106mSv/y (Patel, 1991) and absorbed dose rates of between 253 and 733 nGy/h (Kebwaro *et al.,* 2011). The lower absorbed dose rate is over 4 times higher than the global average of 60 nGy/h (UNSCEAR, 2000). It is worth noting that the reported exposure and dose rates in the region do not take into account the contributions of radon and thoron in indoor air and radionuclides ingested through food and water. The radiation exposure and consequently the effective dose are therefore likely to be much higher than has been previously reported.

Because it is impossible to completely do away with radiation exposure, it is recommended that the exposure be maintained 'As Low As Reasonably Achievable' (ALARA principle). The ALARA philosophy is based on the hypothetical 'Linear No-Threshold' (LNT) assumption that the risk from radiation exposure is directly proportional to the dose. The risk of low radiation doses is based on extrapolation from the risk assessed at high doses (ICRP, 2006). There exists opponents of the LNT

model who argue that living organisms have the ability to build defenses against toxic agents at low concentrations and that the defenses are overwhelmed only at high doses (Tubiana *et al.*, 2009). In contrast, proponents of the model such as UNSCEAR regard complex DNA damage as difficult to repair correctly and that even at low radiation doses, there is a non-zero chance of production of mutant DNA that increase the risk of cancer developing (UNSCEAR, 2010). The committee on Biological Effects of Ionizing Radiation (BEIR) on the other hand considers the model to offer reasonable description of the relation between low-dose exposure to ionizing radiation and the incidence of radiation-induced solid cancers and consequently find it a computationally convenient starting point with respect to radiation protection (BEIR VII, 2006).

In support of the LNT model, the ICRP came up with recommendations and guidelines aimed at preventing acute radiation exposure and limiting chronic exposure to what may be considered an acceptable level. In its publication 60 report (1991), the ICRP recommended an exposure level for radiation workers of not more than 20 mSv/y averaged over five years with the maximum dose in any one year not exceeding 50 mSv. For the general public, the report recommended a maximum dose of 1 mSv/y averaged over five years.

1.3 Heavy metals

Apart from being radioactive, ^{226}Ra and ^{232}Th are heavy metals. A heavy metal is a metallic chemical element that has a relatively high density, is toxic or poisonous at relatively low concentrations and cannot be degraded or destroyed (Duruibe *et al.*,

2007). Radionuclides usually co-exist with other types of non-radiative elements. This is evident in Mrima hill where in addition to the high background radiation, the region is documented as having rich deposits of rare earth elements such as manganese, lead, iron, zircon, phosphate, gypsum, niobium, titanium, molybdenum, monazite, nepheline and gorceite (Kwale District Environmental Assessment Report, 1985; Gaciri, 1991; Kariuki, 2002). Copper and zinc ores are also known to exist, according to the Government of Kenya State of the Coast report (2008).

At trace level, some metals such as copper, manganese and zinc are needed for metabolic and chemical processes essential for proper functioning of the human body. All metals radioactive or otherwise are however toxic at high concentrations (Salem *et al.*, 2000). Thus, to get a fuller picture of the state of the environment vis-à-vis public health in a given region, it is important to incorporate the study of some common heavy metals in the environment alongside that of radioactivity.

Groundwater which serves as the main source of drinking water for many people particularly in Africa is an important source of heavy metals. Heavy metals principally arise from the dissolution of naturally occurring minerals in rock and soil the water comes into contact with, or those dislodged by rainfall while penetrating down. In regions with a rich background of mineral resources such as Mrima hill, notable enrichment of groundwater may therefore be experienced.

1.4 Description of the study area

The present study is mainly centered on a rural village nestled on the lower slopes and the foot of Mrima hill. The region is inhabited by the indigenous Digo sub-tribe of

the Mijikenda community, interspersed by the Kamba and the Kisii communities. The residents of Mrima hill are typical rural dwellers whose livelihood depends on the environment. They mainly practice small-scale farming for subsistence, and as the region is drought prone, cassava is largely grown as both a cash and food crop given its ability to withstand dry conditions. Both the tubers and the leaves are consumed, with the tubers being eaten mainly as snacks while the leaves are used as vegetables (Karuri *et al.,* 2001).

The water table in the region is relatively high. Intriguing though is the fact that the villagers do not use groundwater to carry out irrigation as would be normally expected. But then again living organisms to some extent are guided by intuition and will often instinctively react to situations in such ways so as to evade impending danger. Nonetheless, for lack of an alternative source of water, the villagers use the groundwater abstracted from indiscriminately hand-dug wells for drinking and other domestic purposes, water that they use without any form of prior treatment. The wells are generally shallow with depth ranging from less than a meter to approximately 50 m. Most of the wells are open (Plate 1.1) while a few are closed and fitted with a hand pump (Plate 1.2).

Plate 1.3 is a picture of dwellings typically found in the Mrima hill region. The dwellings are constructed primarily using soil which is dug near the site of construction. To form the wall, lumps of wet mud are fixed in a shell formed by joining together pieces of thin wooden poles (Appendix 3).

Plate 1.1: One of sampled shallow wells in the Mrima hill region

Plate 1.2: A group of women and children drawing water from a closed well in the sampling region

Plate 1.3: Dwellings in a village on the slopes of Mrima hill which were used in the current research

The dwellings are thatched using *makuti* (dry coconut leaves) and usually have no ceiling; the floor is left as bare earth. The walls are normally not smoothened after construction and therefore the mud lumps fall off with time and have to be replaced with fresh ones. The dwellings are small in size but due to the hot climatic condition that characterizes the coastal region, they are not as airtight as dwellings in parts of the world where heat needs to be conserved.

In most African traditional cultures, *uchawi* (witchcraft) which is considered to be vile and *uganga* (traditional healing) which is considered to be good exist side by side. Among the Mijikenda community for instance *mganga* (traditional healer) promotes his cures publicly and is usually a respected member of the community; *mchawi* (witchdoctor) on the other hand casts his spells in secret and is feared and

avoided if known or suspected (Sperling, 1988). To some Mijikenda, diseases and other ailments are believed to be the result of *uchawi* and as a result villagers often seek help from *waganga* instead of trained health professionals (Tinga, 1998). Consequently, data on prevalent diseases and their probable causes in the community is limited. Generally, the education standards are relatively low in the region, with the literacy level in the larger Kwale County being placed at 62.8% in 2000, the lowest in the country at the time (UNESCO, 2005). In the 2013 national KCPE examination, the county was ranked 41 out of the 47 counties in the country.

1.5 Statement of the research problem

The geological setting coupled with the close interaction the villagers of Mrima hill maintain with the environment predisposes them not only to the external exposure resulting from the presence of elevated concentration of radionuclides in soil documented by various researchers, but also to internal exposure through pathways such as food and water given the ability of radionuclides to migrate to other compartments of the ecosystem. Moreover, the external exposure is not limited to outdoor settings only; the risk exists indoors as well given the type of building materials used in the region and the fact that people generally spend most of their time indoors. Despite the apparent risk, no data exists on internal exposure or external exposure inside local dwellings with regard to Mrima hill. This research seeks to fill this knowledge gap.

1.6 Objectives

The main objective of this research was to determine the exposure associated with radioactivity in building materials, indoor air, crops and well water (groundwater) in Mrima hill region.

The specific objectives were:

i. Determination of radon and thoron concentration inside mud dwellings in the sampling region.
ii. Measurement of radon and thoron exhalation rates from the building materials.
iii. Measurement of terrestrial radionuclides in crops, well water and soil samples.
iv. Modelling radon and thoron exhalation rate from the building materials.
v. Analysis of non-radioactive physico-chemical parameters in the well water samples

1.7 Rationale

The data obtained in this research can be used in various ways such as:

i. Formulation of policies regarding public health and the environment.
ii. Creating public awareness on the possible consequences of radiation exposure and metal toxicity.
iii. Model results can be used as cost-effective test bench for improved designs of thoron (and radon) mitigation and preventive measures.
iv. Baseline data for future reference.

CHAPTER 2: LITERATURE REVIEW

2.1 Radiation exposure

Exposure occurs when human beings are subjected, internally or externally, to ionising radiation. External exposure is mainly attributed to irradiation by gamma rays emitted by radionuclides located outside the body. Gamma rays being the most penetrating of the ionising radiation can easily pass through the human skin and into the underlying soft tissue. However, their linear energy transfer (LET) is low which to a certain extent reduces the risk of radiation-inflicted tissue damage.

Internal exposure occurs when radionuclides emit ionising radiation while inside the human body. Radiation of most concern is alpha radiation (helium nuclei). Helium particles are relatively massive and barely penetrate more than a fraction of a millimeter in the tissue. The resulting highly localized LET makes alpha radiation the most damaging to human cells than any other form of radiation. The energy deposited by a single alpha particle is sufficient to damage intracellular DNA and trigger cancerous growth of cells, even allowing for substantial repair (Krewski *et al*., 1999).

The kind of health effects ionising radiation causes depends on the amount of radiation received as well as the duration of exposure. On this basis, radiation exposure effects are grouped into two categories; (1) stochastic effects and (2) non-stochastic effects. Stochastic effects are mainly associated with chronic exposure to low level background radiation while non-stochastic effects are associated with exposure to high levels of radiation over a short period of time (acute exposure).

2.2.1 Stochastic effects

Lung cancer is one of the well known possible effects of chronic exposure to radon and in some circumstances thoron. According to WHO report of 2009, radon is responsible for the largest proportion of lung cancer cases among non-smokers and the second leading cause of lung cancer after cigarette smoking. While radon has been considered responsible for nearly the whole radiation dose attributable to inhalation of air, more recent studies have shown that thoron can significantly add to the inhaled dose particularly in regions where the main building material is soil (Tschiersch *et al*., 2007; Meisenberg and Tschiersch, 2011).

Radon and thoron contribute to the radiation dose through their respective short-lived daughters shown in Figures 2.1 and 2.2.

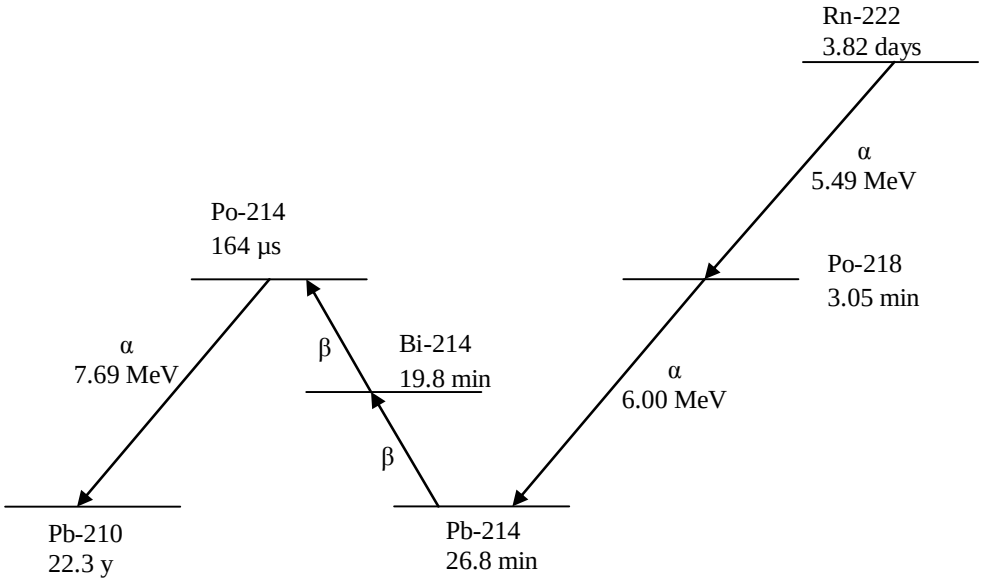

Figure 2.1: Radon decay chain showing the short-lived decay products

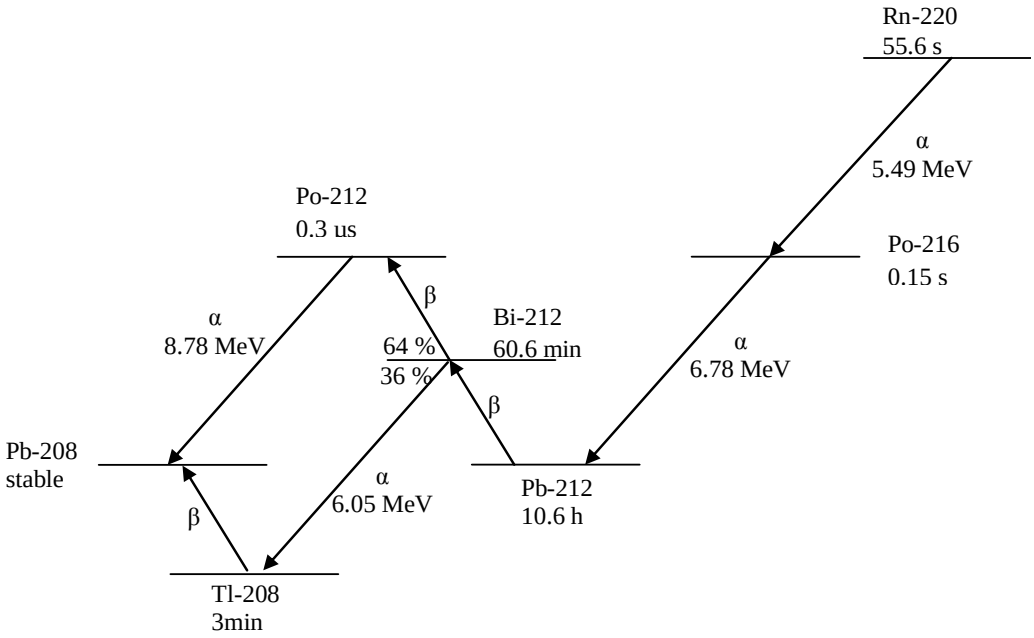

Figure 2.2: Thoron decay chain showing the short-lived decay products

The radon and thoron daughters are charged particles and upon formation agglomerate into small molecular clusters or attach to aerosols in indoor air; only a small fraction of the progeny remain free, and this depends on the concentration and size of the aerosols together with the ventilation level of the dwelling under consideration (Bochicchio *et al*., 1995; Vaupoti and Kobal, 2007). Upon inhalation, the particles have the potential to lodge in various parts of the lungs depending on their state (free or attached) and gradually build-up with time with every breath taken.

In the radon decay chain, ^{218}Po and ^{214}Po are the most significant in relation to inhaled dose since their subsequent decays are accompanied by the release of alpha energies of 6 MeV and 7.69 MeV respectively. In the case of thoron, ^{212}Pb is considered of most concern despite being a beta emitter. ^{212}Pb has a relatively long half-life of 10.6

hours and therefore has ample time to accumulate to significant levels in breathable air. It subsequently decays to ^{212}Bi, another relatively long lived progeny with a half-life of 60.6 minutes. ^{212}Bi undergoes a double split with 36 % decaying by emitting alpha particles of energy 6.05 MeV while the remaining fraction (64 %) decay by beta emission to ^{212}Po which almost instantly undergoes alpha decay whereby 8.78 MeV of energy is released. Thus, it is not the radon isotopes *per se* that deliver the critical dose of radioactivity said to cause lung cancer but rather the short-lived progeny (Bailey, 1994; European Commission, 1998).

In some households in Mrima hill, children especially sleep on mats laid out on the floor. This puts them in very close proximity to the thoron exhaling surface thereby increasing their chances of inhaling the thoron progeny, including the relatively short-lived ^{216}Po. ^{216}Po decays by emitting alpha radiation of energy 5.49 MeV.

Radionuclides can be inadvertently ingested with food and water. Some radionuclides are heavy metals and constant ingestion can result in their accumulation in different organs of the body. ^{226}Ra in the decay chain of ^{238}U for instance is deposited in the bone tissue as it is chemically similar to calcium. As its level builds up, the increased radiation from its subsequent alpha decays increases the risk of certain types of cancer such as bone and sinus cancer (Kurttio *et al*., 2005).

2.2.2 Non-stochastic effects

Non-stochastic effects are mainly associated with artificial sources such as medical procedures, nuclear accidents, criminal activities or acts of war. During radiotherapy for instance where patients are subjected to high burst of ionising radiation, side

effects such as radiation burns, vomiting, weakness and hair loss often occur. Moreover, radiotherapy can induce thyroid abnormalities (Jereczek-Fossa *et al.,* 2004) and ototoxicity (Bhandare *et al.,* 2007) in patients receiving radiation treatment of head and neck cancer.

Ionising radiation can effect changes in DNA blueprints such that damaged cells fail to reconstitute fully thus leading to the creation of mutant cells (Han and Yu, 2010). Such mutant genes when formed in foetus or growing children can result in developmental abnormalities such as mental retardation (Strom, 2003). If the mutations involve the genetic code, the defects can be passed on to future generations, even years after the initial exposure.

2.3 Heavy metal exposure

Majority of people particularly in rural Kenya do not have access to clean piped water and normally use alternative sources such as groundwater abstracted through hand-dug wells or boreholes. The sinking of the wells in most cases is unregulated and no prior assessment is carried out to determine the suitability of the water for human use.

The quality of groundwater evolves with time as a consequence of human activity or due to natural settings. Compounds resulting from anthropogenic sources such as chemicals and fertilizers, landfills and pit latrines can find their way into the groundwater leading to its degradation. Even in the absence of the human influence, groundwater is never in a pure state as it will always contain elements picked from the geological material it comes into contact with, or those added by the recharge water

while penetrating down. Depending on their type and concentration, the elements can be toxic and therefore harmful to human beings.

The elements in groundwater may be organic or chemical in nature. Most concern is centered on organic pollution particularly that arising from human activity while chemical compounds such as heavy metals arising from natural sources are relegated to the background. This is despite the fact that all heavy metals irrespective of their origin are chemical toxins at high concentrations and when ingested can adversely affect the health and general well being of humans.

The first target organ of metal toxicity is the kidney due to its ability to reabsorb and accumulate divalent metals. The extent of damage inflicted depends on the type of metal involved and the dose received. Cd, Pb and radioactive heavy metals such as ^{226}Ra have been associated with renal damage at relatively low concentrations while Mn and Cu are associated with renal damage at higher concentrations (Zamora *et al*., 1998; Kurttio *et al*., 2002; Barbier *et al*., 2005; Sabath and Robles, 2012). Besides, Cd is carcinogenic and can lead to cancer; it can also cause osteoporosis and hearing impairment (Nawrot *et al*., 2006; Prasher, 2009; WHO, 2011). Pb exposure can result in delays in physical and mental development in newborns and growing children, irreversible damage of the nervous and reproductive systems, high blood pressure and chronic anemia (Smith *et al*., 1989).

Chronic exposure to high doses of Mn can lead to intellectual impairment in school going children leading to reduced IQ scores (Momodu *et al*., 2009). It is a neurotoxicant and has been linked to conditions such as loss of libido and in some

cases impotence, and to manganism which is a Parkinson-like condition characterized by muscle stiffness, weakness and tremors (USEPA, 2004). High intakes of Cu can cause gastro-intestinal distress and liver damage (USEPA, 2003); Zn toxicity can result in stomach cramps, skin irritations, vomiting, nausea and anemia (WHO, 2003) and intake of very high levels of Mg (50mg/l) may result in undesired laxative effects (WHO, 2011).

Chronic exposure to most heavy metals leads to neurological damage and neurobehavioral disorders that may be similar to the effects experienced by narcotic addicts (USEPA, 2004; Pabello and Bolivar, 2005; Patrick, 2006). Drugs temporarily restore neurotransmitter functions that are abnormal, and therefore in some cases, substance abuse is often used as a crude self-medication in response to the effects of metal toxicity (Masters, 1999).

2.4 Radionuclides and heavy metals in the ecosystem

The environment contains an abundance of radionuclides and heavy metals, and their accumulation and subsequent health effects are a matter of serious concern globally. It is in cognizance with this that researchers the world over have embarked on intensive research aimed at establishing the concentration of radionuclides and heavy metals in different compartments of the ecosystem.

2.4.1 Radioactivity in soil

All soils naturally contain trace amounts of radionuclides and therefore their presence is not necessarily indicative of contamination. In the absence of human influence,

their concentration in soil depends on the geology of the parent material from which they were formed and since geological formations differ spatially, it is not unusual for different areas in the world to report different concentrations of given radionuclides.

The presence of particular geological formations augments the occurrence of certain radionuclides. Radionuclides in the decay chain of ^{238}U for instance are mainly associated with igneous rock formations and phosphates ores. In the HBRA of Ramsar, Iran, where extremely high concentration of ^{226}Ra (in ^{238}U decay chain) in soil samples with a mean of up to 59,100 Bq kg^{-1} has been reported, the local geology is characterized by igneous rock formation (Ghiassi-nejad *et al*., 2001; Saghirzadeh *et al*., 2008). In Sudan on the other hand, ^{238}U concentration up to 3960 Bq/kg has been measured in Uro phosphates ores of Eastern Nuba Mountains of the country (Adam and Eltayeb, 2009).

Presence of ^{232}Th is mainly associated with carbonatite rock formations and monazite deposits. In India, elevated concentration of ^{232}Th was observed in regions characterized with monazite deposits. Such regions were Kollam region of Kerala, where ^{232}Th concentration as high as 1342 Bq kg^{-1} was measured in soil (D'Cunha and Narayan, 2012) and Erasama Beach where mean concentration of ^{232}Th of 2828 Bq kg^{-1} was obtained in the beach sand (Mohanty *et al.*, 2004). The HBRA of Kenya such as Mrima hill, Lambwe East on the western shores of Lake Victoria and Mt. Homa on the eastern shores of the same lake are mainly by characterized by carbonatite formations. Soil samples collected from villages around Mrima hill reported ^{232}Th concentrations with a mean of 500 Bq kg^{-1} and a high of 869 Bq kg^{-1} (Kebwaro *et al.*, 2011). Similar samples from Lambwe East were found to contain

^{232}Th concentration with a mean of 1215 Bq kg^{-1} (Mustapha *et al*., 2012) while those from Mt. Homa reported ^{232}Th concentration with a mean of 409.5 Bq kg^{-1} (Otwoma *et al*., 2012). The migratory effect of the radionuclides to other compartments of the ecosystem such as indoor air, crops and groundwater is not documented in the fore mentioned research on HBRA in Kenya.

2.4.2 Radionuclides and other heavy metals in groundwater

Radionuclides and nonradioactive heavy metals in groundwater are mainly mobilized from soil and rock, their concentration to a large extent reflecting their presence and abundance in these materials. The elemental concentration is also dependent to some extent on the geochemical characteristics of water such as the pH, oxidation reduction potential and presence of complexing ions as well as attenuation processes such as adsorption of the metals on soil particles and organic matter.

In Egypt, groundwater abstracted through wells was analysed for ^{226}Ra and ^{232}Th and the results compared with that of tap water. Although the content of the radionuclides was found to be within the acceptable limits, higher values were reported in groundwater than in tap water (Ahmed, 2004). In Tanke-Ilorin, Nigeria, the effective dose resulting from radionuclides in groundwater was found to be much higher at 1.30 mSv/y than the WHO recommended level of 0.1 mSv/y (Nwankwo, 2013). According to the research, the high radiation dose was due to the radium isotopes ^{226}Ra and ^{228}Ra whose concentrations in groundwater ranged from 0.81 to 7.4 Bq l^{-1} and 1.8 to 5.6 Bq l^{-1} respectively.

Babu *et al*. (2008) reported ^{238}U concentration of up to 1.44 Bq l^{-1} in groundwater from Kolar Distric in India, with 21 % of groundwater sampled exceeding WHO prescribed limits. A study carried out on the Disi acquifer in Southern region of Jordan said to be the future source of water for the local residents reported extremely high concentrations of radium isotopes that exceeded the recommended level in drinking water by about 2000 % (Vengosh *et al*., 2009).

Further afield in Northwestern Connecticut, USA, elevated total uranium concentration with a high of 7.780 Bq l^{-1} and an average of 0.620 Bq l^{-1} was observed in some domestic wells (Orloff *et al*., 2004). According to the study, nearly 80 % of the wells had uranium content beyond the USEPA recommended limit of 0.02 Bq l^{-1}.

In Kenya, data on radioactive heavy metals in groundwater is scarce although concentration of radon (^{222}Rn) is documented. A screening survey by Mustapha *et al*., (2002) on radon concentration in drinking water obtained from different parts of the country reported a mean concentration of 100 Bq l^{-1} and maximum 1160 Bq l^{-1}. The highest radon concentration according to the study was in water samples obtained from groundwater sources and in the basements of buildings. Some of the samples had radon concentration that exceeded the internationally recommended reference levels.

Non-radioactive heavy metal contamination of groundwater is generally viewed as an anthropogenic problem and as a result, most researchers tend to focus more on metal concentration in groundwater in industrial settings, dumpsites, urban centers and agricultural zones where fertilizers and pesticides are extensively used (Shakeri *et. al*.,

2009; Oyeku and Fludoyn, 2010; Mandour *et al*., 2011); naturally, elevated levels of heavy metals were observed in these studies. Nonetheless, enrichment of groundwater can occur due to natural sources particularly in regions with a rich background of minerals in the geology. In some parts of rural Nigeria for instance, elevated levels of Fe, Mn and Pb was observed in groundwater and attributed to dissolution of the elements in the natural ecosystem (Ocheri and Ogwuche, 2012). Mrima hill is documented as being rich in mineral resources and it will be interesting to see the effect if any this has on the groundwater quality.

2.4.3 Radioactivity in crops

Radionuclides such as ^{137}Cs released following nuclear disasters and those occurring naturally in groundwater and soil can be taken up by food crops thereby adding their quota of radiation dose when ingested. Radionuclides released during nuclear fallout affect crops and vegetation located far and wide from the initial fallout zone as was witnessed in mushrooms following the Fukushima Daiichi accident (Yamada, 2013). On the other hand, transfer of naturally occurring radionuclides to crops and vegetation is localized and affects mainly a small radius around the zone of origin. In Tanzania for instance, wild and edible leaf vegetation in areas around Minjingu phosphate mine reported high concentrations of ^{226}Ra with average activities of 650 Bq kg^{-1} and 393 Bq kg^{-1} respectively relative to selected control sites (Banzi *et al*., 2000).

Farm inputs such as fertilizer while increasing the crop yield can also enhance the radioactivity level in the same crop. In Tanzania, maize and rice crops analysed for

^{238}U content registered concentration levels of 13.23 Bq kg^{-1} and 5.02 Bq kg^{-1} respectively (Mlwilo *et al*., 2007). Although the calculated dose resulting from consumption of the crops was lower than the guideline values, the study attributed the higher concentration of ^{238}U in maize to the use of phosphate fertilizer.

2.3.4 Radioactivity in indoor air

Radioactivity in indoor air is mainly attributed to radon isotopes. Radon occurs as three different isotopes namely radon, thoron and actinon (^{219}Rn), one from each of the three natural radioactive decay series of ^{238}U, ^{232}Th and ^{235}U (Table 2.1). The radon isotopes are gases unlike their predecessors and once they are formed, and subject to the nature of the building material, they can diffuse out of the solid matrix and into indoor air. Actinon however is not considered much of a risk due to its scarcity as well as its relatively short half-life of 4 s. Radon on the other hand is almost always present in air while thoron is encountered in some instances.

Table 2.1: Summary series of radon, thoron and actinon

Radon isotope	Half-life	Mother Nucleus	Half-life	Stable Final nuclide
^{220}Rn	55.6 s	^{232}Th	1.4×10^{10} y	^{208}Pb
^{222}Rn	3.82 d	^{238}U	4.5×10^{9} y	^{206}Pb
^{219}Rn	4 s	^{235}U	7.1×10^{8} y	^{207}Pb

For more compact building materials such as those used in most western countries, the likelihood of any thoron generated decaying before being exhaled is higher given its short half-life. It is probably for this reason that thoron was not viewed as a significant contributor to indoor radioactivity and consequently the radiation dose. In most parts of rural Africa and Asia on the other hand, raw soil constitutes the main component of building materials. As it is highly porous, thoron atoms have substantial ease of movement and therefore increased probability of being exhaled before decaying. Once in the air, decay of the thoron atoms no longer acts as a sink but rather as an important source of inhalation dose through the daughters formed.

Numerous studies on radon and more recently thoron have been carried out the world over. In Kenya and prior to the current work, indoor radioactivity measurements did not discriminate between radon and thoron concentrations and therefore the measurements taken were reported as belonging to radon. Radon concentration in the country was found to vary widely between locations. Chege *et al*. (2009) found notable radon concentration of up to 315 Bq m^{-3} in some otherwise well ventilated model traditional mud huts that were situated in Kenyatta University, Nairobi, while Maina *et al*. (2004) obtained indoor radon concentration in the coastal region of up to 704 Bq m^{-3}. Mustapha *et al.* (1999) reported indoor radon concentration for different parts of the country of up 200 Bq m^{-3}.

Further afield in Europe, indoor radon concentration with an average of less 25 Bq m^{-3} was observed in the Netherlands, the UK and Cyprus and over 100 Bq m^{-3} in Estonia, Finland, Sweden, Luxembourg, the Czech Republic, Hungary and Albania (UNSCEAR, 2000). Some dwellings in Finland, Norway, Sweden, Belgium,

Germany, Switzerland, the UK, the Czech Republic and Spain were reported to have extremely high indoor radon concentration of over 10 000 Bq m^{-3}. The variation in radon concentration was attributed to differences in geology and climate, in building materials and construction techniques, and in the domestic customs of the inhabitants.

Some materials naturally contain high concentrations of radium and thorium. Examples of such materials include fly ash bricks, gypsum, alum shale, volcanic tuffs and pozzolana, some of which may contain radium and thorium content of several hundred Bq kg^{-1} (UNSCEAR, 1982; Battaglia *et al*., 1990; European commission, 2000). Such materials when used for construction can therefore enhance indoor radon concentration, as is the case for phosphogypsum which essentially is waste gypsum from fertilizer production (Maged and Ashraf, 2005).

The development of measuring devices capable of discriminating between thoron and radon has made it possible to simultaneously measure radon and thoron in dwellings. In Ireland, such measurements resulted in indoor radon concentration with a mean of 75 Bq m^{-3} against that of thoron of 22 Bq m^{-3} (McLaughlin *et al*., 2011). Similar measurements were carried out in Winnipeg City in Canada, one of the cities previously reported to have dwellings with elevated levels of radon (Chen *et al*., 2009). In this study, thoron was detected in about half the homes sampled and ranged from 5 to 297 Bq m^{-3}. Radon however was still the major source of exposure with concentration ranging from 20 to 483 Bq m^{-3}.

Buildings constructed using raw soil often exhibit high concentration of thoron. In Hyderabad city, India, where dwellings of different construction types were sampled

for thoron, dwellings with mud flooring registered the highest thoron concentration with a maximum of 330 Bq m^{-3} (Sreenath *et al*., 2004). In a study by Shang *et al*. (2005) in China, residential dwellings constructed using loam bricks or soil wall were found to contain significantly higher thoron levels as compared to radon. The average thoron concentration was 318 Bq m^{-3} while that of radon was 72.4 Bq m^{-3}. Some dwellings had thoron concentration as high as 1860 Bq m^{-3}. In the same country, cave dwellings of the Chinese Loess Plateau were found with thoron and radon concentrations of up to 865 Bq m^{-3} and 195 Bq m^{-3} respectively (Tokonami *et al*., 2004). Dwellings constructed using soil dominate in Mrima hill and rural Kenya in general and therefore for such reason as mitigation purposes, there is need to establish the concentration of both radon and thoron in the dwellings.

CHAPTER 3: THEORETICAL CONSIDERATIONS

3.1 Natural radioactivity

3.1.1 Origin of radioactivity

Radioactive decay or radioactivity is the disintegration of unstable nuclei (radionuclides) with the release of ionising radiation. Nuclear instability occurs when the forces within the nucleus can no longer hold it together. This causes the radionuclide to break down and in so doing releases nuclear energy in form of (or combination of) alpha (α), beta (β) and gamma (γ) radiation.

Alpha radiation is equivalent to a helium nucleus while beta particles are electrons or positrons. A nucleus is theoretically unstable with respect to alpha and beta decay if its atomic mass is greater than the sum of the masses of its nucleons. Gamma radiation is a form of electromagnet radiation similar to but more energetic by several orders of magnitude than atomic radiation. Following alpha or beta decays, a nucleus may be left in one of the excited states. The nucleus de-excites by releasing nuclear energy in the form of gamma radiation.

3.1.2 Activity of radionuclides

The activity (A) of a radionuclide is the measure of the intensity of radiation emitted during radioactive decay. The intensity of radiation depends on the number of radionuclides present and as this number reduces with time, so does the activity. If N be the number of atoms of a radionuclide, say, X present at some time t, then,

$$\frac{dN}{dt} = -\lambda N \qquad (1)$$

λ is the constant of proportionality referred to as the decay constant and is usually characteristic of the radionuclide involved. The negative sign signifies the diminution of the number of radionuclides with time.

Equation (1) represents what is termed as the decay law and its solution gives the number of radioactive atoms present at any time t. For the boundary conditions $N = N_0$ at $t = 0$, equation (1) solves to

$$N = N_0 e^{-\lambda t} \qquad (2)$$

The activity A of a radionuclide is defined as the absolute change in the number of nuclides with time, i.e. $A = \left|\frac{dN}{dt}\right| = \lambda N$. Thus if A_0 be the activity at time $t = 0$, equation (2) becomes

$$A = A_0 e^{-\lambda t} \qquad (3)$$

The half-life $T_{1/2}$ of a radionuclide is the time taken for the activity of the radionuclide to reduce to half its original value i.e. at $t = T_{1/2}$, $A = \frac{A_0}{2}$. Substituting these in equation (3) gives the half-life of a radionuclide as

$$T_{1/2} = \frac{0.693}{\lambda} \qquad (4)$$

A simulation of equation (3) for three radionuclides with different half-lives (hence decay constants) but the same initial activity is shown in Figure 3.1. Clearly, the activity of the longer-lived nuclides reduces with time more slowly than that of the shorter-lived ones.

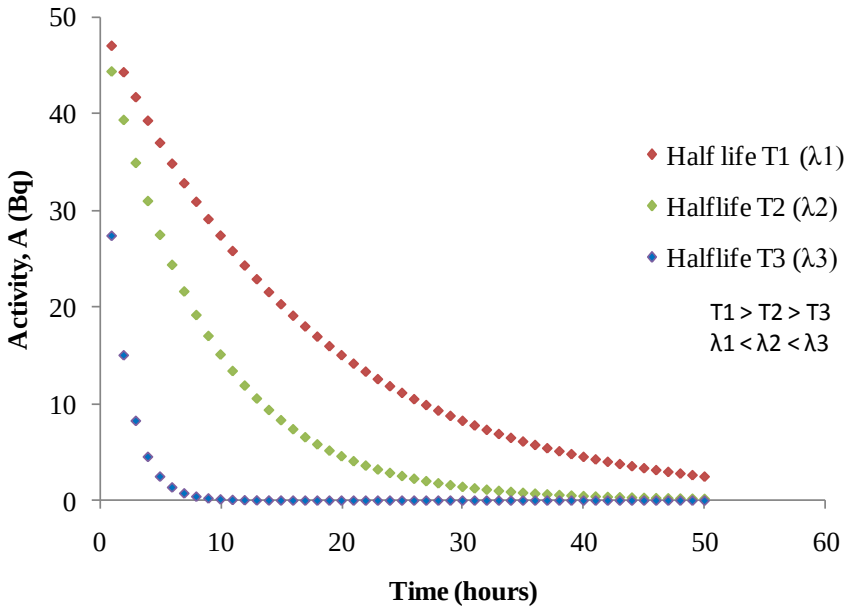

Figure 3.1: Variation of activity with time for radionuclides with different decay constants

The activity of a radionuclide falls by a factor of $1/2^n$ after n half-lives and reduces to practically zero after about 10 half-lives. A long-lived radionuclide such as ^{232}Th would therefore require over 140 billion years for its activity to become negligible. Assuming that ^{232}Th atoms came into existence at the time the earth came into being and bearing in mind that the earth is approximately 4.5 billion years old, then time has barely dented the activity of ^{232}Th atoms. The activity of isolated ^{220}Rn atoms on the other hand will be practically gone in less than 10 minutes.

3.1.3 Decay series

Most radioactive decays do not occur in isolation but rather are a part of a series decay chain) whereby the existence of one radionuclide is dependent on the existence of another. ^{220}Rn for instance cannot cease to exist unless ^{232}Th becomes extinct first. Radionuclide at the top of a decay chain is referred to as the parent while its decay products are called progeny or daughter radionuclides.

We consider a parent radionuclide, say X, with decay constant λ_1. If N_1 be the number of X atoms at some time t, then by decay law,

$$\frac{dN_1}{dt} = -\lambda_1 N_1 \qquad (5)$$

The solution of equation (5) given the boundary condition $N_1 = N_{10}$ at $t = 0$ becomes,

$$N_1 = N_{10} e^{-\lambda_1 t} \qquad (6)$$

Suppose X decays and transmutes to another radionuclide, Y. It follows that the rate of production of Y must be equal to the rate of decay of X ($= \lambda_1 N_1$). Y also decays with time at the rate of $\lambda_2 N_2$ where λ_2 is its decay constant and N_2 the number of atoms at some time t. The rate of change of Y atoms with time therefore is the difference between the production rate and the decay rate, i.e.

$$\frac{dN_2}{dt} = \lambda_1 N_1 - \lambda_2 N_2 \qquad (7)$$

Equation (7) is solved by first assuming its solution to be

$$N_2 = f(t)e^{-\lambda_2 t} \tag{8}$$

where $f(t)$ is the number of Y atoms that were present at time $t = 0$. The differential form of equation (8) with respect to time gives the rate of change of Y atoms with time, i.e.

$$\frac{dN_2}{dt} = \left(\frac{df}{dt} - f\lambda_2\right)e^{-\lambda_2 t} \tag{9}$$

A comparison of equations (7) and (9) indicates that the LHS of the equations are equal which means that the RHS of the equations must also be equal. Therefore

$$\left(\frac{df}{dt} - f\lambda_2\right)e^{-\lambda_2 t} = \lambda_1 N_1 - \lambda_2 N_2 \tag{10}$$

Using the values of N_1 and N_2 given in equations (6) and (8) respectively in equation (10) results in the expression

$$\left(\frac{df}{dt} - f(t)\lambda_2\right)e^{-\lambda_2 t} = \lambda_1 N_{10} e^{-\lambda_1 t} - \lambda_2 f(t)e^{-\lambda_2 t}$$

which simplifies to

$$\frac{df}{dt} = \lambda_1 N_{10} e^{-(\lambda_1 - \lambda_2)t} \tag{11}$$

On integration, equation (11) becomes

$$f(t) = -\frac{\lambda_1 N_{10}}{\lambda_1 - \lambda_2} e^{-(\lambda_1 - \lambda_2)t} + C \qquad (12)$$

where C is the integrating constant.

The constant C is obtained by applying boundary conditions. If $f(t) = 0$ at $t = 0$, then $C = \frac{\lambda_1 N_{10}}{\lambda_1 - \lambda_2}$. Substituting this in Equation (12) yields

$$f(t) = \frac{\lambda_1 N_{10}}{\lambda_1 - \lambda_2}\left(1 - e^{(-\lambda_1 - \lambda_2)t}\right) \qquad (13)$$

Using equation (13) in equation (8) gives the number of Y atoms present at some time t as

$$N_2 = \left[\frac{\lambda_1 N_{10}}{\lambda_1 - \lambda_2}\left(1 - e^{-(\lambda_1 - \lambda_2)t}\right)\right] e^{-\lambda_2 t}$$

which simplifies to

$$N_2 = \frac{\lambda_1 N_{10}}{\lambda_1 - \lambda_2}\left(e^{-\lambda_2 t} - e^{-\lambda_1 t}\right) \qquad (14)$$

Figure 3.2 shows a simulation of equations (6) and (14) when the parent X is short-lived (half-life T1) and daughter Y (half-life T2) is long-lived (T1 < T2). Figure 3.3 is a simulation of equations (6) and (14) for a longer-lived parent X and shorter-lived daughter Y (T1>T2).

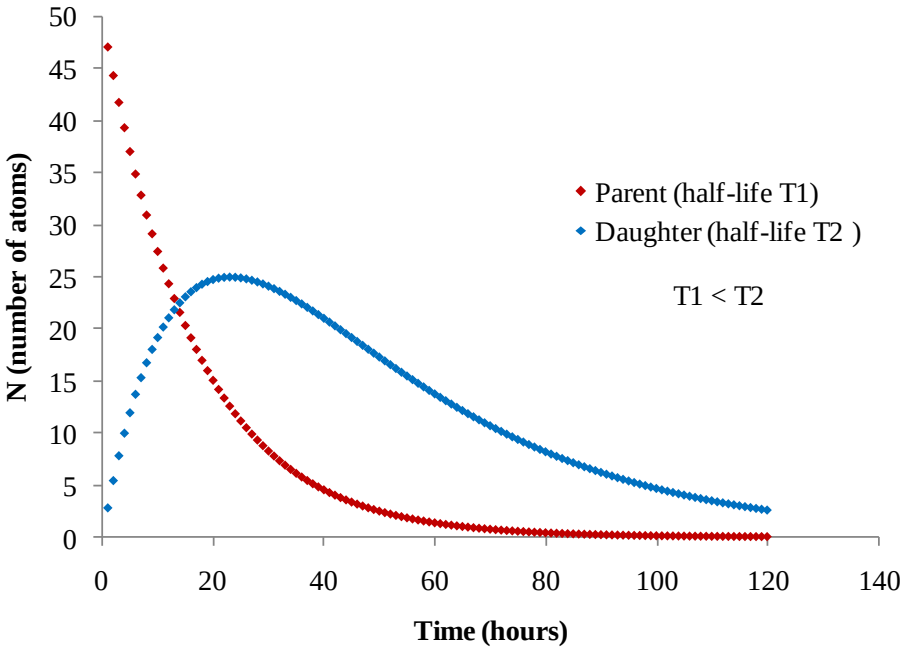

Figure 3.2: Variation of number of atoms with time when $T1 < T2$

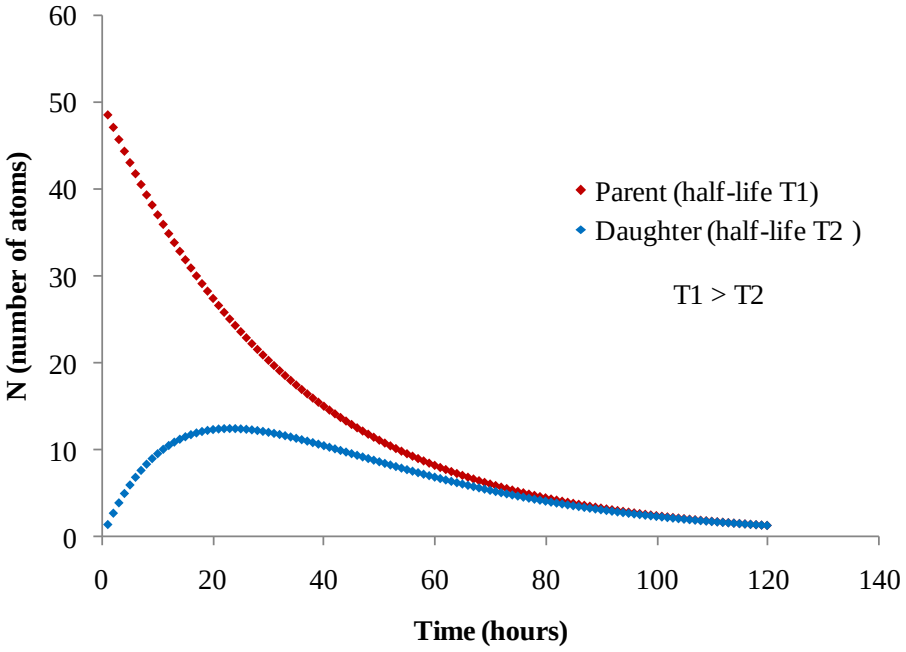

Figure 3.3: Variation of number of atoms with time when $T1 > T2$

In both cases, the atoms of the daughter nuclide increases with time up to a maximum value before starting to decrease. After a long time, the number of atoms of daughter nuclide decreases exponentially with its own half-life in the first case, while in the second case, the daughter atoms decreases exponentially with the half-life of the parent.

3.1.4 Radioactive equilibrium

When the parent is more long-lived than the daughter as illustrated in Figure 3.3, two types of equilibrium can occur: transient equilibrium or secular equilibrium.

3.1.4.1 Transient equilibrium

This is established between the numbers of the parent and the daughter atoms after a long time compared to the half-life of the daughter. In this case, and with reference to equation (14), $\lambda_2 t >> 1$ hence $e^{-\lambda_2 t}$ becomes negligibly small compared to $e^{\lambda_1 t}$ such that it can be assumed to be zero. Equation (14) therefore reduces to

$$N_2 = \frac{\lambda_1}{\lambda_2 - \lambda_1} N_{10} e^{-\lambda_1 t} \qquad (15)$$

But $N_{10} e^{\lambda_1 t} = N_1$ (equation (6)). Using this in equation (15) results in

$$\frac{N_2}{N_1} = \frac{\lambda_1}{\lambda_2 - \lambda_1} = \text{constant} \qquad (16)$$

Equation (16) shows that after a long time, the ratio of the number of daughter atoms to that of the parent atoms remains constant. When this happens, the two nuclides are said to be in transient equilibrium.

3.1.4.2 Secular equilibrium

This is obtained when the half-life of the parent is very long compared to that of the daughter such that $\lambda_1 << \lambda_2$ and therefore $\lambda_2 - \lambda_1 \approx \lambda_2$. In addition, for observation time that is much less than the half-life of the parent, $\lambda_1 t << 1$ such that $e^{-\lambda_1 t} \approx 1$. Taking these into consideration, equation (14) takes the form

$$N_2 = \frac{\lambda_1 N_{10}}{\lambda_2}\left(1 - e^{-\lambda_2 t}\right)$$

$$N_2\lambda_2 = \lambda_1 N_{10}(1 - e^{-\lambda_2 t}) \qquad (17)$$

By definition, $N_2\lambda_2$ represents the activity of the daughter (A_2) and $\lambda_1 N_{10}$ that of the parent (A_{10}). Thus,

$$A_2 = A_{10}(1 - e^{-\lambda_2 t}) \qquad (18)$$

If the observation time is much longer than the half-life of the daughter, then $e^{-\lambda_2 t} \approx 0$ and equation (18) reduces to;

$$A_2 = A_{10} \qquad (19)$$

Equation (19) indicates that the rate of production of daughter atoms equals the rate of decay of parent atoms. When this happens, the parent and the daughter are said to be

in secular equilibrium. It is this property that is employed in the evaluation of activity concentration of long-lived radionuclides. Simulation of secular equilibrium (equations (18) and (19)) is shown in Figure 3.4

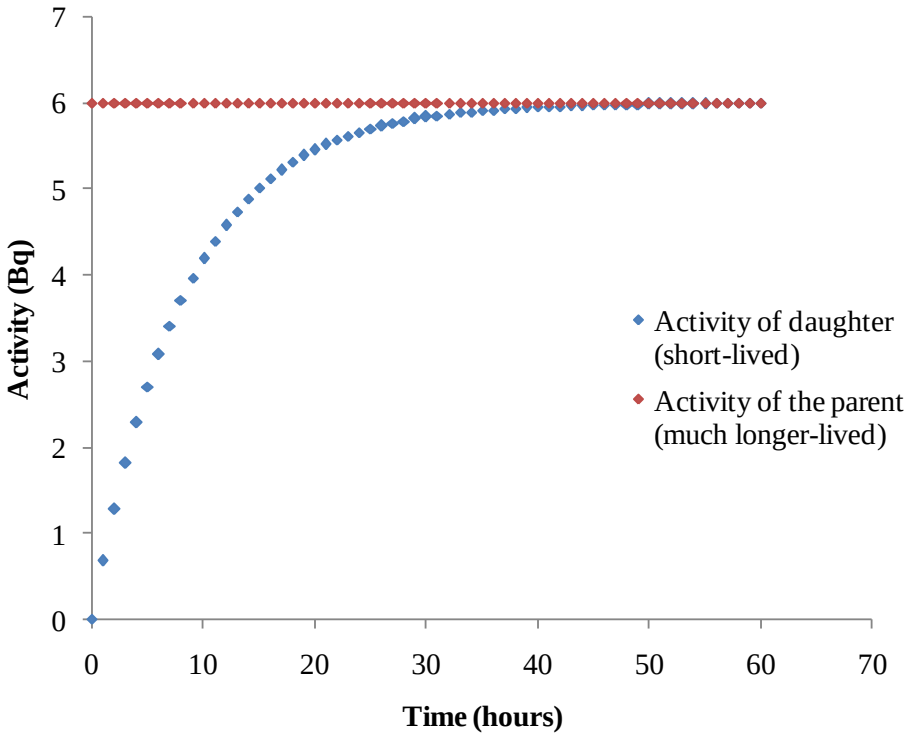

Figure 3.4: Secular equilibrium between long-lived parent and short-lived daughter nuclide

Secular equilibrium is maintained as long as the parent element and the daughter product remain together. If separation occurs, then the equilibrium is disturbed. Nonetheless, the number of daughter atoms starts to grow again and with time, secular equilibrium is re-established.

3.2 Heavy metals

Many different definitions of the term heavy metal have been proposed; some based on density, others on atomic weight, and yet others on the chemical properties or toxicity. In this thesis, a heavy metal will be considered to be a metallic element which is toxic at relatively low concentration.

3.3 Identification and quantification of elements

3.3.1 Alpha detectors

By virtual of the fact that radon and thoron are gases, their measurements are usually carried out *in situ*. For this reason, most measuring devices are alpha-detection based since it is possible to design alpha detectors which are easy to transport to sampling sites and at the same time of high sensitivity. Radiation detection and quantification mechanism of these detectors employ the ability of alpha radiation to form damage tracks on some types of materials on interaction. Some alpha-based detectors use alpha energy spetra emitted by the radon isotopes and their progeny for identification and the ionising power of the alpha particles for quantification of the isotope of interest.

3.3.1.1 Solid State Nuclear Track Detection (SSNTD)

When alpha particles interact with some solids such as the poly allyl diglycol carbonate used as the CR-39 alpha detector, they leave behind damage tracks at the point of impact. If such a detector is exposed to air containing radon and thoron, the alpha particles emitted by the isotopes when they decay leave damage tracks on the

detector examples of which are shown in Plate 3.1. The detector however cannot discriminate between tracks from radon and those from thoron. Since thoron has a relatively short half-life and diffusion length through solids much less than that of radon, discrimination is achieved by enclosing the alpha detector inside a container that retards the entry of air to an extent that thoron atoms decay before gaining access in to the container. Any resulting damage tracks on the detector will consequently be as a result of alpha particles emanating from the decay of radon and progeny.

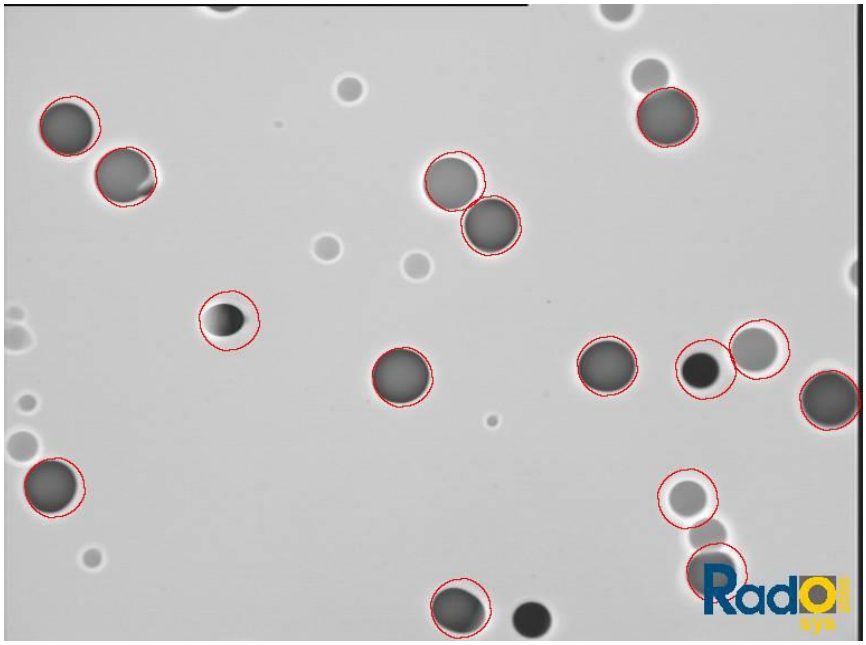

Plate 3.1: Alpha track damages in CR-39 made visible by etching

3.3.1.2 RAD7 alpha detector

The Rad7 comprises of a hemisphere chamber coated on the inside with a conducting material with silicon alpha detector implanted at the centre. A high voltage in the range of 2000-2500 V is applied to the conductor relative to the detector hence

creating an electric field throughout the volume of the cell. The cell is equipped with a built-in pump with adjustable flow rate which draws in sample air through a hose. The hose is fitted with a filter which allows the gas to pass through while blocking the entry of the particulate progeny.

When the isotopes decay within the cell, the transformed nuclei are accelerated by the electric field towards the detector where they stick on the detector surface. Subsequent decays of the progeny lead to the emission of characteristic alpha radiation directly into the silicon detector. Alpha particles are highly ionising and interaction of the radiation with the silicon chip leads to the production of an electric current characteristic of the alpha radiation. This is then used to identify and quantify the isotope. The charged particles tend to accumulate on the detector surface with time and the detector must be purged every few hours by flushing dry isotope-free air.

3.3.2 Gamma ray detectors

The gamma-ray energies emitted by various radionuclides are unique for each species and can therefore be used to generate information about the emitting radionuclide. Gamma rays interact with matter through three processes namely photoelectric effect, Compton scattering and pair production in which they transfer all or part of their energy to an electron. When an electron absorbs an entire gamma photon, it is emitted from the atom leaving behind a vacancy (hole) which behaves like a positive charge. It is the electron-hole pairs created that provide information regarding the incident gamma ray and the emitting radionuclide.

The Photoelectric effect is significant for detection of low gamma energies of up to 150 keV while Compton scattering dominates at photon energies between 150 keV and 8.5 MeV. In Compton scattering however, the entire gamma photon is not absorbed and therefore the last interaction must be a photoelectric one for electron-hole pairs to be generated. If this does not happen, or if multiple Compton interactions occur outside the detector volume, the pulse generated forms part of the Compton continuum. Pair-production can lead to the total absorption of the incident gamma photon as long as the gamma photon has energy of at least 1.02 MeV.

Solids usually have sufficient density to absorb gamma photon in their entirety and are used in the construction of gamma detectors. As radionuclides usually emit a cascade of gamma rays of different energies, a good gamma detector must come equipped with a high energy resolution capability. This is achieved by using semiconductor materials such as germanium (Ge) which have a narrow band gap between the valence and the conduction band. However, the narrow band gap means that such a detector cannot be operated at room temperature as this would result in the production of large quantities of leakage current. The detector must therefore be cooled when in use, done using liquid nitrogen. In addition, the detector must be placed in a vacuum tight cryostat to inhibit thermal conductivity between the crystal and the surrounding air.

Semiconductors generally contain inherent impurities which may lower the energy required to create an electron-hole pair thus creating too much noise. This is corrected by using a reverse biased p-n junction diode (Figure 3.5).

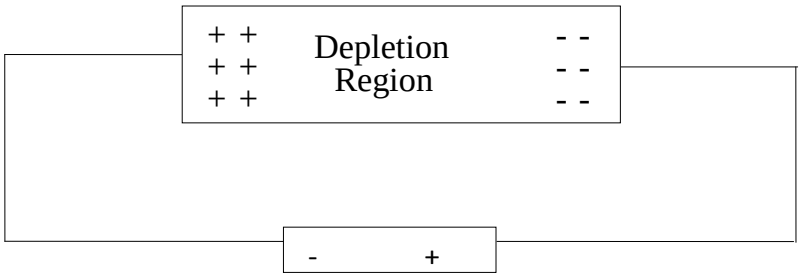

Figure 3.5: A reverse biased Ge semiconductor crystal

The resulting depletion region created allows almost nil current to flow in the absence of gamma radiation, thus improving on the noise properties of the detector and consequently its performance.

The performance of the detector increases with the depletion depth. The depth of the depletion region, d is related to the applied voltage and the impurities in the semiconductor material according to the expression;

$$d = \left(\frac{2\beta V_{bias}}{eN_{imp}} \right)^{1/2} \qquad (20)$$

where β is the dielectric constant of the medium, V_{bias} is the reverse bias voltage and N_{imp} is the net impurity concentration in semiconductor material. Impurities reduce the depletion depth and therefore the Ge crystal must be processed further to improve the efficiency of the detector. This is achieved through a process referred to as zone refining which involves locally heating the crystal and slowly passing a melted Ge zone over it. Impurities are preferentially transferred to the molten Ge leading to the creation of a high purity germanium (HPGe) detector.

HPGe detector uses coaxial geometry in which the outer surface serves as one electrode and a central conducting cylindrical core as the other electrode. A high voltage is applied across the electrodes. When gamma rays from a sample interact with the Ge crystal, electron-hole pairs created are collected at the electrodes under the influence of the electric field. The electric pulse generated is related to the gamma ray that caused it based on calibration data and subsequently the source radionuclide. The identification and quantification of long-lived radionuclides are based on the establishment of secular equilibrium between the parents and their short-lived daughter products.

3.3.3 Atomic absorption spectrophotometer (AAS)

Atomic absorption spectrophotometry (AAS) is an analytical technique that employs the absorption of light by free atoms to determine the elemental concentration of heavy metals contained in a liquid sample. A free atom is most stable when in ground state. However adding thermal energy may cause the atom to be excited to a higher energy state. When this takes place in the presence of light, some of the light is absorbed with elements absorbing characteristic wavelengths. The reduction in the intensity of light is used to quantify the element of interest.

The main components of the AAS include a nebulizer/burner, a hollow cathode lamp, monochromator and photomultiplier detector. The working of the nebulizer/burner is illustrated in Figure 3.6. The liquid sample is sucked into the nebulizer and released as a fine spray. This is mixed with acetylene and air and flamed at a temperature of 2100-2400 ^{o}C. After the disolvation, the dry sample is broken down into neutral

atoms though a process called volatilization. These neutral atoms are ionized and thus become excitable and capable of absorbing light. The cathode lamp provides the source of light and is usually made from the element of interest. As such, each element is analysed using a specific cathode lamp as a source of light. Light from the cathode lamp, after passing through the sample, is received by the monochromator which isolates the photon energy of interest. The photon falls on the photomultiplier detector and through photoelectric effect, an electric signal is generated. The strength of the electrical signal is then related to the concentration of the element of interest via calibration curves.

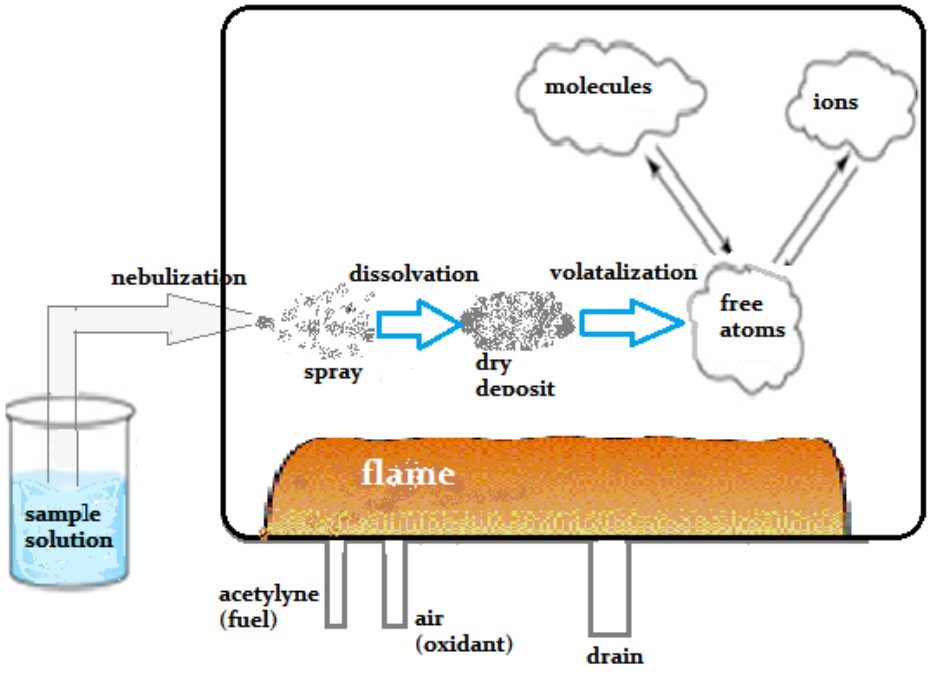

Figure 3.6: Nebulization and atomization process

3.4 Modelling radon/thoron generation, exhalation and accumulation

The processes involved in thoron generation, transport and exhalation and eventual build-up in confined space is similar to that of radon. While the model discussed in this thesis is in reference to thoron, it can be equally applied to radon with minimal adjustments.

The build-up of thoron concentration due to a sample inside a sealed chamber is best understood by studying three interdependent processes

i. Thoron generation within the interstitial space (pores) of the sample
ii. Transport and exhalation
iii. Accumulation in the chamber

The various assumptions employed in the model development are mentioned in the body of the discussion.

3.4.1 Thoron generation within the interstitial space of building materials

We consider a piece of building material of volume dV (m^3) and bulk density ρ (kg m^{-3}). We assume that at the start of observation $(t = 0)$ the piece of building material contains N_{R0} atoms of ^{224}Ra, assumed to be in secular equilibrium with the primordial nuclide ^{232}Th. If N_R be the number of ^{224}Ra atoms at a later time t, then by decay law $N_R = N_{R0}e^{-\lambda_R t}$ where λ_R is the decay constant of ^{224}Ra.

^{224}Ra decays directly to thoron and therefore the number of thoron atoms created in time t (N_{TC}) equals the number of ^{224}Ra atoms that have decayed in that time, i.e.

$$N_{TC} = N_{R0}(1-e^{-\lambda_R t}) \quad (21)$$

When ^{224}Ra decays, part of the disintegration energy serves as recoil energy for the generated thoron atoms and is sufficient to move it some distance from the point of generation. Depending on the nature of the building material and the initial position of the parent nuclide, the generated thoron atom ends up in one of the scenarios listed below and depicted in Figure 3.7.

A. The thoron atom is displaced but remains embedded within the grain

B. The atom travels across the interstitial space between the grains and embeds in another grain

C. The atoms ends up in the interstitial space between the grains

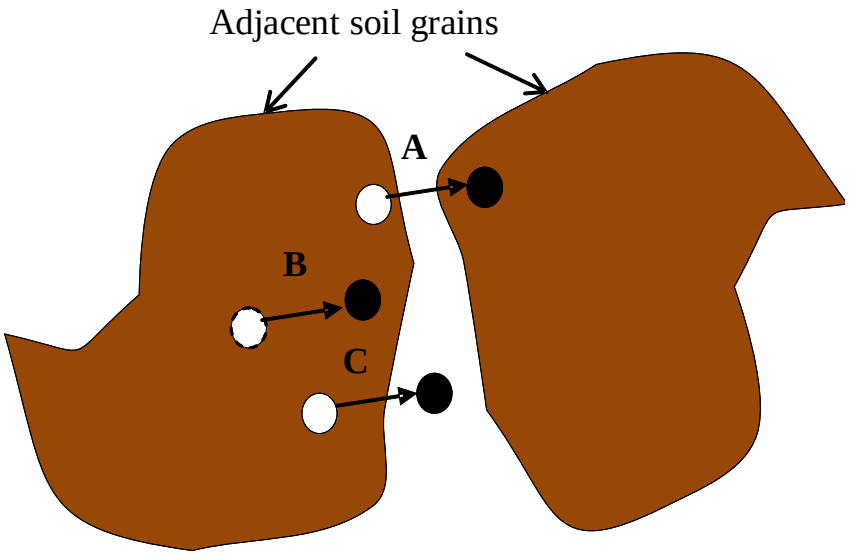

Figure 3.7: Illustration of possible behavior of a thoron atom after generation in the grain of a solid particle

Only those atoms that end up in the interstitial space are available for transport. The ratio between the number of thoron atoms available for transport (N_T) and the

number of thoron atoms created (N_{TC}) is called emanation coefficient (η) (Sakoda *et al*., 2010; Schumann, 1993). Thus $\eta = \frac{N_T}{N_{TC}} \Rightarrow N_T = \eta N_{TC}$. Using this in equation (21) gives the number of thoron atoms available for transport as

$$N_T = \eta N_{R0}(1 - e^{-\lambda_R t}) \tag{22}$$

Thoron is radioactive and its activity changes with time according to the equation

$$\frac{dT_T}{dt} = \lambda_T N_T \tag{23}$$

where λ_T is the decay constant of thoron. Using equation (22) in (23) gives

$$\frac{dN_T}{dt} = \lambda_T \eta N_{R0}(1 - e^{-\lambda_R t}) \tag{24}$$

If we consider an observation time that is much longer than the half-life of thoron, then the last term on the RHS of equation (24) reduces to zero. Hence

$$\frac{dN_T}{dt} = \lambda_T \eta N_{R0} \tag{25}$$

We consider the situation whereby the N_R atoms of ^{224}Ra are homogeneously distributed within the building material. If C_R (Bq kg^{-1}) be the concentration of ^{224}Ra, then by definition, $N_{R0} = \rho C_R dV$. Using this in equation (25) yields

$$\frac{dN_T}{dt} = \lambda_T \eta \rho C_R dV \tag{26}$$

We assume that the piece of building material has a solid volume dV_s and pore volume dV_p such that $dV_s + dV_P = dV$. If the material has uniform porosity ε, then $dV = \frac{dV_p}{\varepsilon}$, and using this in equation (26) and rearranging leads to

$$\left(\frac{dN_T}{dV_P}\right)\frac{1}{dt} = \frac{\lambda_T \eta \rho C_R}{\varepsilon} \tag{27}$$

The term on the LHS of equation (27) is the change in thoron concentration with time (Bq m^{-3} s^{-1}) and represents thoron production/input rate (S). Thus

$$S = \frac{\lambda_T \eta \rho C_R}{\varepsilon} \tag{28}$$

3.4.2 Transport and exhalation

Transport of the emanated thoron atoms through the interstitial space of building materials occurs primarily by diffusion (Csige *et al*., 2013). Figure 3.8 presents the possible path that may be followed by an emanated thoron atom. Fick's laws describe the diffusion of a substance through a homogeneous media (Zapalac, 1981). Assuming the building material sample to be homogeneous and considering that only thoron atoms moving towards the surface (taken to be the x-direction) are exhaled, then the transport equation by Fick's second law can be expressed as (Griffiths *et al*., 2010)

$$\frac{\partial C(x,t)}{\partial t} = D\frac{\partial^2 C(x,t)}{\partial x^2} - \lambda_T C(x,t) + S \tag{29}$$

where D is the effective diffusion coefficient. The term on the LHS of equation (29) represents the change in emanated thoron concentration with time, the first term on RHS the change of thoron concentration with distance, second term loss due to decay and the last term the input rate of thoron given in equation (28).

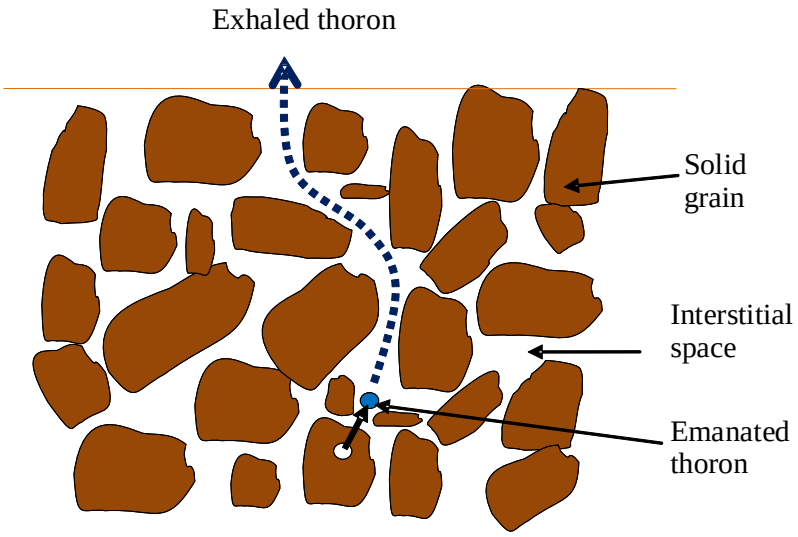

Figure 3.8: Possible path through a porous medium that an emanated thoron atom may follow towards the surface

At steady state, equation (29) reduces to a linear differential equation of the second order;

$$\frac{\partial^2 C}{\partial x^2} - \frac{\lambda_T}{D} C = -\frac{S}{D} \qquad (30)$$

Equation (30) is solved by breaking it up into two functions, complementary function (C.F.) and the particular integral (P.I.). These are solved and their solutions added up, with the resulting equation being taken as the solution of equation (30). The C.F. is obtained by equating the LHS of equation (30) to zero i.e.

$$\frac{\partial^2 C}{\partial x^2} - \frac{\lambda_T}{D} C = 0 \tag{31}$$

We let the complementary solution of equation (31) be

$$C(x) = Ae^{mx} \tag{32}$$

where A is an arbitrary constant and m the roots of the function. Differentiating equation (32) twice yields $\frac{d^2 C}{dx^2} = m^2 C$, and putting this in equation (31) leads to

$$\left(m^2 - \frac{\lambda_T}{D} \right) C = 0 \tag{33}$$

The concentration C cannot be zero, which means that the first term on the LHS of equation (33) must be zero i.e.

$$m^2 - \frac{\lambda_T}{D} = 0$$

$$\Rightarrow m = \pm \sqrt{\frac{\lambda_T}{D}} \tag{34}$$

Equation (32) expressed in terms of the roots thus becomes

$$C(x) = A_1 e^{\sqrt{\frac{\lambda_T}{D}} x} + A_2 e^{-\sqrt{\frac{\lambda_T}{D}} x} \tag{35}$$

A_1 and A_2 are arbitrary constants.

For the P.I. part, we assume the particular solution of equation (30) is a constant, say A_3, i.e. $C(x) = A_3$. Differentiating this twice gives $\frac{d^2C}{dx^2} = 0$, which on substituting in equation (30) leads to

$$A_3 = \frac{S}{\lambda_T} \tag{36}$$

The sum of equations (35) and (36) gives the complete solution of equation (30) as

$$C(x) = A_1 e^{\sqrt{\frac{\lambda_T}{D}}x} + A_2 e^{-\sqrt{\frac{\lambda_T}{D}}x} + \frac{S}{\lambda_T} \tag{37}$$

Taking $\sqrt{\frac{D}{\lambda_T}} = l_d$ where l_d is the diffusion length, equation (37) becomes

$$C(x) = A_1 e^{\frac{x}{l_d}} + A_2 e^{-\frac{x}{l_d}} + \frac{S}{\lambda_T} \tag{38}$$

To find the values of the constants A_1 and A_2, we consider a piece of building material with two surfaces (and therefore finite width). We suppose that the piece of building material has a uniform thickness $2a$ measured along the x-axis, and define a coordinate system where the origin is in the middle. This is illustrated in Figure 3.9. Assuming that $C(x = -a) = C(x = a) = C_0 = 0$, then the constants A_1 and A_2 are calculated as

$$A_1 = A_2 = -\frac{S}{\lambda_T}\left[\frac{1}{e^{\frac{a}{l_d}} + e^{-\frac{a}{l_d}}}\right] \tag{39}$$

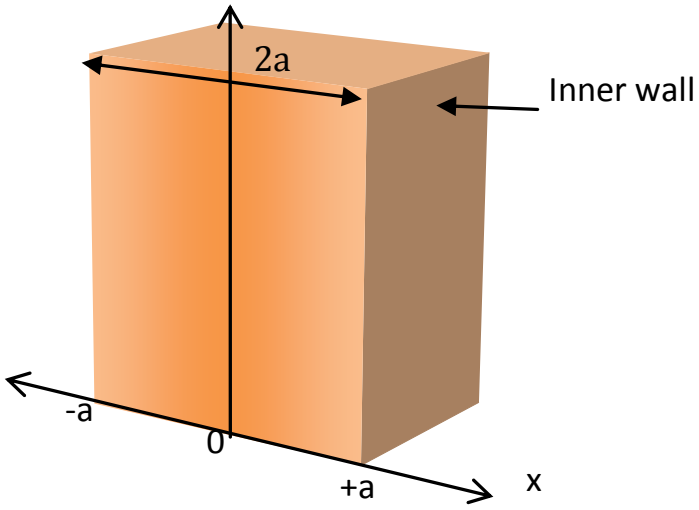

Figure 3.9: A schematic of a building material sample with the thickness measured from the center outwards

Using equation (39) in (38) lead to

$$C(x) = -\frac{S}{\lambda_T}\left(\frac{e^{\frac{x}{l_d}} + e^{-\frac{x}{l_d}}}{e^{\frac{a}{l_d}} + e^{-\frac{a}{l_d}}}\right) + \frac{S}{\lambda_T}$$

or

$$C(x) = \frac{S}{\lambda_T}\left(1 - \frac{\cosh\frac{x}{l_d}}{\cosh\frac{a}{l_d}}\right) \qquad (40)$$

Gas transport in an unsaturated solid zone occurs through molecular diffusion; this means that thoron exhalation rate E (Bq m^{-2} s^{-1}) at the air-solid boundary can be calculated from Fick's first law: $E = -D\varepsilon \frac{dC(x)}{dx}$ (Duenas *et al*., 1997). Thus

$$E = -D\varepsilon \frac{S}{\lambda_T} \frac{d}{dx} \left(1 - \frac{\cosh \frac{x}{l_d}}{\cosh \frac{a}{l_d}} \right) \tag{41}$$

Given that exhalation of thoron in to indoor air occurs from only one surface (inner surface) of the building material and is independent of the other (outer) surface, the exhalation rate is determined by solving equation (41) at $x = a$, i.e.

$$E = -D\varepsilon \frac{S}{\lambda_T} \frac{d}{dx} \left(1 - \frac{\cosh \frac{x}{l_d}}{\cosh \frac{a}{l_d}} \right)_{x=a}$$

$$E = -D\varepsilon \frac{S}{\lambda_T} \left(- \frac{\sinh \frac{x}{l_d}}{\cosh \frac{a}{l_d}} \cdot \frac{1}{l_d} \right)_{x=a} = D\varepsilon \frac{S}{\lambda_T} \frac{1}{l_d} \left(\frac{\sinh \frac{a}{l_d}}{\cosh \frac{a}{l_d}} \cdot \right) = S\varepsilon \frac{D}{\lambda_T} \frac{1}{l_d} \tanh \frac{a}{l_d}$$

With $S = \frac{\lambda_T \eta \rho C_R}{\varepsilon}$ (equation (28)) and $D = \lambda_T l_d^2$ (from definition of diffusion length), the exhalation rate becomes

$$E = l_d \lambda_T \eta \rho C_R \tanh \frac{a}{l_d} \tag{42}$$

Equation (42) shows that the thickness as well as the inherent properties of the building material such as density and the content of the parent radionuclide to a large extent affect the rate at which thoron is exhaled. Also to note is that at $a >> l_d$, the last term of equation (42) reduces to unity in which case the exhalation rate depends entirely on the intrinsic properties of the building material i.e.

$$E = l_d \lambda_T \eta \rho C_R \tag{43}$$

3.4.3 Accumulation

We consider an accumulation chamber of volume V_c. Suppose that the piece of building material sample with only one side exposed is enclosed in the chamber. Let A_s be the area of the exposed side and E thoron exhalation rate. If C_{ch} (Bq m^{-3}) be the concentration of thoron atoms released into the chamber and E (Bq m^{-2} s^{-1}) the exhalation rate, then by dimensional analysis, the build-up of concentration with time is given by

$$\frac{dC_{ch}}{dt} = \frac{EA_s}{V_c} \tag{44}$$

There are two sinks for thoron atoms released into the chamber: loss through decay and loss through ventilation, given respectively as $\frac{dC_{ch}}{dt} = -\lambda_T C_{ch}$ and $\frac{dC_{ch}}{dt} = -\lambda_v C_{ch}$

where λ_V is the leakage or the ventilation rate. Putting this into consideration, the rate of change of concentration becomes

$$\frac{dC_{ch}}{dt} = \frac{EA_s}{V_c} - (\lambda_T + \lambda_V)C_{ch} \tag{45}$$

The integral of equation (45) gives the concentration C_{ch} of thoron in the chamber at any time t. To solve for C_{ch}, equation (45) is first expressed in terms of an integrating factor and rearranged i.e.

$$e^{(\lambda_T+\lambda_v)t}\frac{dC_{ch}}{dt} + (\lambda_T + \lambda_V)C_{ch}e^{(\lambda_T+\lambda_v)t} = \frac{EA_s}{V_c}e^{(\lambda_T+\lambda_v)t}$$

$$d\left(e^{(\lambda_T+\lambda_v)t}C_{ch}\right) = \frac{EA_s}{V_c}e^{(\lambda_T+\lambda_v)t}dt \tag{46}$$

Integrating both sides of equation (46) and rearranging;

$$e^{(\lambda_T+\lambda_v)t}C_{ch} = \frac{EA_s}{V_c}\int e^{(\lambda_T+\lambda_v)t}dt$$

$$C_{ch}(t) = \frac{EA_s}{V_c}\frac{1}{\lambda_T+\lambda_v} + Be^{-(\lambda_T+\lambda_v)t} \tag{47}$$

B is an arbitrary constant.

To find the constant B, we apply boundary condition $C_{ch}(t=0) = 0$ which leads to

$B = -\frac{EA_s}{V_c(\lambda_T+\lambda_v)}$. Using this in equation (47) gives the concentration of thoron as a function of time as

$$C_{ch}(t) = \frac{EA_s}{V_c(\lambda_T + \lambda_v)}\left(1 - e^{-(\lambda_T + \lambda_v)t}\right)$$

or

$$C_{ch}(t) = \frac{EA_s}{V_c \lambda_{eff}}\left(1 - e^{-\lambda_{eff} t}\right) \tag{48}$$

where $\lambda_T + \lambda_v = \lambda_{eff}$.

Steady state is achieved after a long observation time compared to the half-life of thoron $(t \to \infty)$ whereby $e^{-\lambda_{eff} t} \approx 0$. At steady state, equation (48) consequently reduces to

$$C_{ch} = \left.\frac{EA_s}{V_c \lambda_{eff}}\right|_{t \to \infty} \Rightarrow E = \frac{C_{ch} V_c \lambda_{eff}}{A_s}$$

In general,

$$E_i = \frac{C_{ch-i} V_c \lambda_{eff}}{A_s} \tag{49}$$

where E_i is the exhalation rate of isotope i and C_{ch-i} the steady state concentration of isotope i in the accumulation chamber.

CHAPTER 4: MATERIALS AND METHODS

4.1 Geology of the sampling region

The study primarily focused on the region around Mrima hill bounded by the latitudes -4.469700 and -4.513056 and longitudes 39.237200 and 39.285833. The hill (Appendix 4) is roughly located at a latitude of -4.488301 and a longitude of 39.262512 and has an approximate circumference of 2.5 km, rising about 250 m above the sea level. For comparison purposes, Kanana Village located about 12 km from Mrima hill and bounded by the latitudes -4.523685 and -4.534882 and longitudes 39.365477 and 39.374800 was studied. Both areas are within Kwale County in the coastal region of Kenya with Mrima hill located approximately 70 km south of the Port City of Mombasa. The sampling region is shown Figure 4.1.

The study areas are within the coastal plain that is characterized by coral limestone of Pleistocene age and Magarini sands derived from the Duruma sandstone series and deposited during the tertiary ages, and the coarse-grained Taru and fine-grained Maji-ya-chumvi formations (Horkel *et. al*., 1984; Osoro *et al*., 2011). Mrima hill, which represents the carbonatite phase of the intrusive alkaline formation centered on the nearby Jombo, is intruded into the Mesozoic sandstones and is covered with igneous residue deposits except for isolated exposures (Harris, 1965).

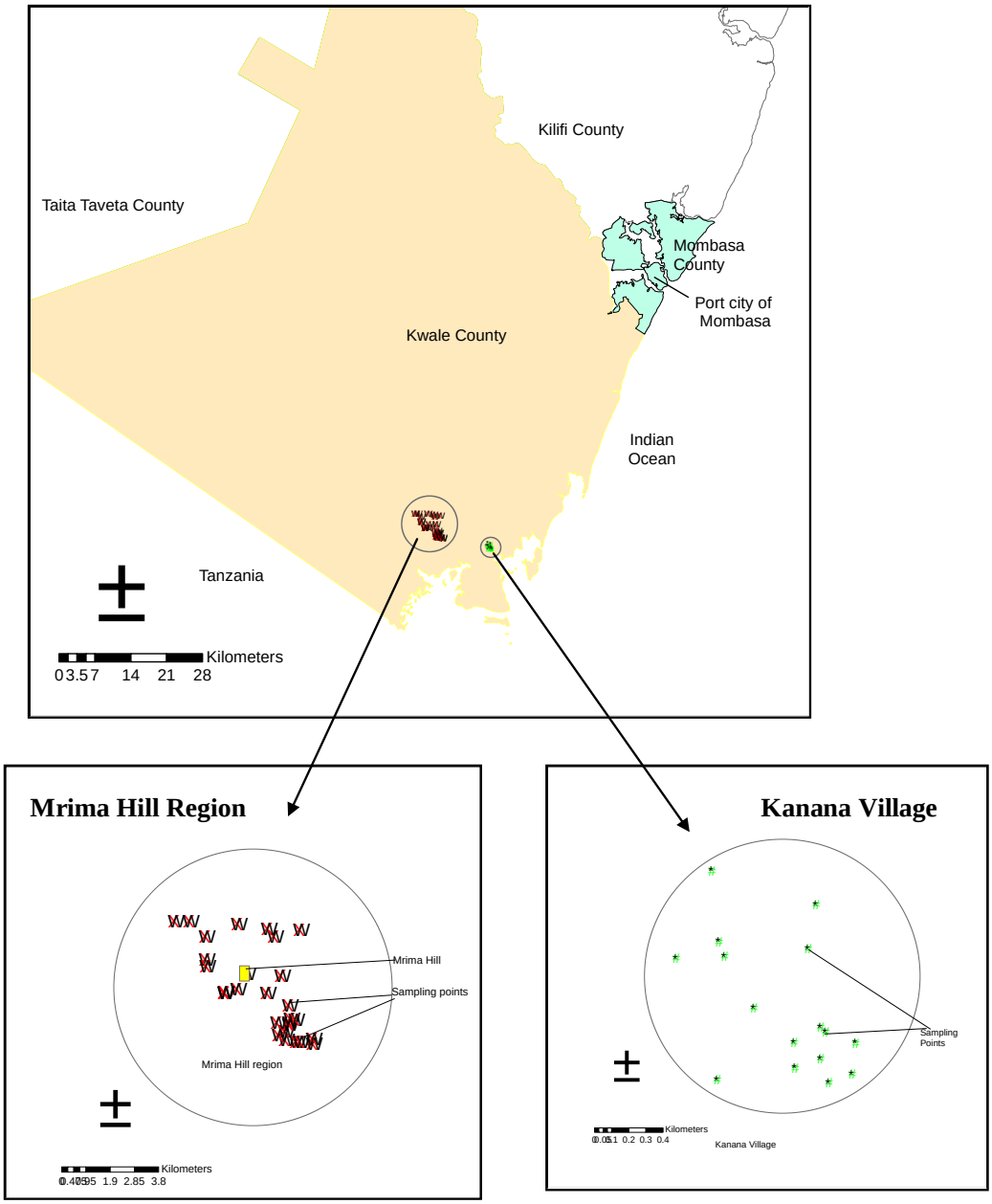

Figure 4.1: Map of the sampling regions indicating the sampling points

4.2 Radon and thoron concentration measurements

4.2.1 Sampling and sample preparation

CR-39 solid state nuclear track detectors (SSNTD) were used for simultaneous measurement of radon and thoron concentrations in air (Meisenberg *et al*., 2013). This was facilitated by placing 1 cm CR39 plastic polymer platelets at the bottom of 3.6 cm tall plastic canisters. One platelet was used in each canister. Discrimination between radon and thoron measurements was achieved using pairs of the measuring devices (Plate 4.1); one for measuring the concentration of both radon and thoron and the other radon only.

Plate 4.1: A picture of twin canisters fitted with CR-39 used for discriminative measurements of radon and thoron in this study

The canister used for measurement of both radon and thoron was fitted with a screw cap that contained several holes (B). Besides, it was covered with a membrane filter

and conductive foam through which the radon isotopes but not their progenies entered the canister. The canister used for measurement of radon only had a solid screw cap (A) with air entering the canister through the cap thread. The measurement devices were calibrated against a RAD7 active radon and thoron measurement device (Durridge Inc.) in a 1 m calibration chamber. Pairs of canisters (A and B) were packed in air-tight casings and only unpacked at the sampling site during deployment. For control purposes, two pairs of canisters were not deployed and stayed in their casings throughout the sampling period.

Dwellings were randomly selected in both Mrima hill and Kanana regions. Majority of the dwellings sampled were constructed in the Digo fashion whereby the dwelling basically comprised of two sections separated by a narrow corridor (measuring about 1.5 - 2 m in width and 3 - 4 m in length). The narrow corridor was used for indoor air sampling. Before deployment, each pair of canisters was fixed on a paper holder which was then fixed on the wall of the dwelling (Plate 4.2) at a height of at least 1.5 m from the floor. The paper holders kept the canisters at a constant distant of 10 cm from each other and their screw caps at a distance of 20 cm from the wall of the dwelling. One pair of canisters was used per dwelling. A total of 30 pairs of canisters were deployed in Mrima hill region and an equal number in Kanana village, where they were left for a period of about three months. At the end of the sampling period, the canisters were repacked in air-tight casings to avoid the possibility of contamination.

Plate 4.2: Twin canisters deployed in a dwelling in Mrima Hill

4.2.2 Analysis

Analysis of the samples was done at the Institute of Radiation Protection in Munich, Germany. The exposed and control substrates were removed from the canisters and etched in Na OH solution at 94°C for 4 h. The density of the enhanced tracks was then determined using an automated Radosys counting system. The concentrations of radon (C_R) and thoron (C_T) were calculated based on track densities, time of exposure and calibration factors using the equations

$$C_R = \frac{(N_R - N_B)CF_R}{t} \tag{50}$$

$$C_T = \frac{[(N_{RT} - N_B) \times CF_R - C_R]CF_T}{t} \tag{51}$$

Where N_R is the track density in radon substrate, N_B the track density in blank/control substrate, N_{RT} the track density in the radon and thoron substrate, CF_R (0.52 kBq m^{-3} h^{-1} per track) and CF_T (2.1 kBq m^{-3} h^{-1} per track) the calibration factors for radon and thoron respectively, and t the exposure time in hours (2280 h).

The calibration factors were obtained by exposing blank substrates to different known concentrations of radon/thoron for a given period of time and the track density obtained in each case. CF_R and CF_T were then obtained by relating the densities of the tracks to the respective isotope concentration. To ensure consistency of results, inter-comparison tests of the detectors were carried out at the National Institute of Radiological Science (NIRS) in Japan and at the Physikalisch-Technische Bundesanstalt (PTB) (German Metrology Agency) in Germany. The tests at PTB made the calibration traceable to a national standard.

4.3 Radon and thoron exhalation measurements

4.3.1 Sampling and sample preparation

10 pieces of the mud lumps were carefully pried off the walls of dwellings randomly selected from those sampled for radon and thoron concentration measurements. Each sample was wrapped tightly and firmly with rolls of water-proof polyethylene paper to keep them from breaking up and also from possible contamination. Analysis of the samples was done at the Institute of Radiation Protection in Munich, Germany.

The dimensions of the building material samples were evaluated using approximation method due to their irregular shape. To conform to the exhalation model described in Chapter 3, all but one side of the building material samples were thickly coated with

lacquer (10 layers) effectively reducing thoron and radon exhalation to nearly zero. A picture of one of the samples thus treated is shown in Plate 4.3.

Plate 4.3: A pre-treated building material sample for exhalation measurement

4.3.2 Analysis

The closed chamber (accumulation) method coupled with continuous measurement of radon and thoron concentrations were employed in the determination of the exhalation rates (Hassan *et al*., 2011). The accumulation chamber basically consisted of a 3-litre stainless steel barrel fitted with an air tight lid with inlet and outlet ports. A small fan located near the bottom of the chamber kept the air inside well mixed. The two ports on the top of the barrel connected the accumulation chamber to the RAD7 continuous detector via silicon hoses. As the RAD7 monitor is designed to measure the concentration of radon and thoron atoms in air and not that of their decay product, the hose leading to the detector was fitted with a thin filter to suppress the radon and

thoron decay products while allowing free movement of air. A saturated salt (potassium carbonate) provided a stable humidity condition of about 45 %.

The pre-treated building material sample was enclosed in the accumulation chamber and after allowing a growth time of about 24 h, the RAD7 monitor was connected to collect and analyse the gas for thoron and radon concentration. A schematic diagram of the experimental arrangement is shown in Figure 4.2. Radon was quantified based on the ^{218}Po and ^{214}Po peaks at alpha energies 6 MeV and 7.69 MeV respectively and thoron from the ^{216}Po peak at alpha energy 6.78 MeV. The concentrations measurements were regularly recorded for over a period of 300 h. Plots of the isotopes concentrations as a function of exposure time were obtained and the exhalation rates of radon and thoron calculated at steady-state concentrations using equation (49). The data fitting was done using the equation (48).

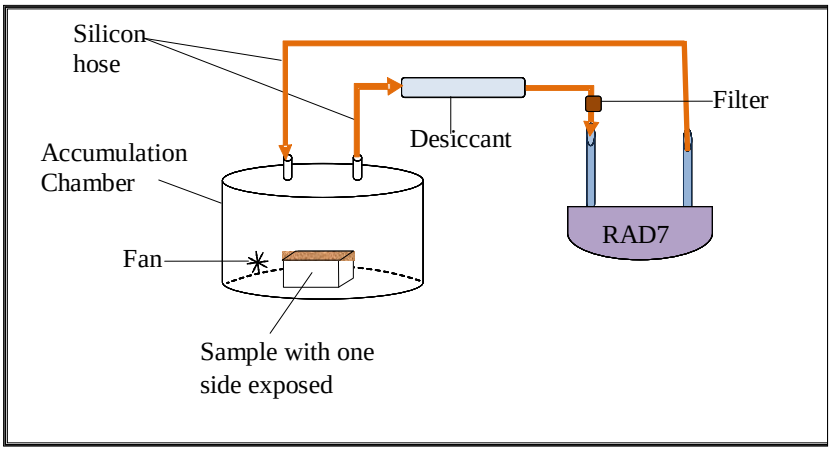

Figure 4.2: Schematic of the experimental arrangement used for exhalation measurements

4.4 Spectral analysis of building materials, soil, crops and water samples

4.4.1 Sampling and sample preparation

The earthen building material samples used for exhalation measurements were investigated for their content of ^{226}Ra and ^{232}Th as well as ^{40}K. After cutting off the resin coat, each sample was crushed so as to pass through a 2-mm mesh-sieve for homogenization and packed in a standard 250 ml air-tight polyethylene containers having the same geometry as that for the reference material (Callegari *et al.*, 2013). The containers were hermetically sealed and stored for at least 21 days to allow ^{226}Ra and ^{232}Th atoms to attain secular equilibrium with their respective short-lived progeny (Hafez *et al.*, 2005; Xhixha *et al.*, 2013; Mauring and Gäfvert, 2013).

Samples of soil were obtained from the site of randomly selected dwellings among those sampled for exhalation measurements. The soil was dug after removing the top debris much in the same way that the local residents do it. About 2 kg of soil sample was obtained per location. The samples were homogenised by crushing and sieving through 2-mm mesh-sieve. They were then dried to a constant weight in an oven at an approximate temperature of 100 ^{o}C for about 24 hours (Garzia *et al*., 2013): drying of samples enables a straightforward calculation of the specific activity of radionuclides (Benke and Kearfott, 1999). A portion of each sample was filled in standard 250 ml polyethylene containers in a manner similar to that of the building material samples. They too were stored for at least 21 days before measurements.

Cassava tubers and their leaves were randomly collected from farms in the Mrima hill region only. To form a representative, three samples were obtained from different

parts of each farm and combined together to form a single sample. The outer skin of the cassava tubers was peeled off and the tubers cut into small cubes. These together with the leaves were sun dried to a constant weight after which each sample was ground so as to pass through a 2-mm mesh-sieve. The samples were dry-weighed, sealed in 250 ml polyethylene containers and likewise allowed to sit for 21 days before analysis.

Groundwater sampling was carried out during the dry season. The samples were collected from both open and closed wells using 500 ml recycled PVC bottles. Before use, the bottles were cleaned with detergent and water, rinsed off with 10% nitric acid to remove any metals that may have adsorbed on to the bottle surfaces, then by distilled water and finally with the sample water before collection. Water samples were obtained from the open wells in a manner similar to that used by the local residents –using a tin tied to a rope as shown in Appendix 5. The samples were taken to the laboratory where they were acidified using concentrated nitric acid to a pH of less than two as a preservation measure (USEPA, 2005; Hamzah *et al.*, 2011). A portion of each sample was filled in 250 ml PVC containers and stored for at least 21 days before analysis.

Spectral analysis of the building material and soil samples was carried out at the Institute of Radiation Protection in Munich, Germany while that of cassava and groundwater samples was done at the Institute of Nuclear Science and Technology, University of Nairobi, Kenya.

4.4.2 Analysis

The spectral data acquisition and analysis for all the samples were done using high purity germanium (HPGe) detectors interfaced with multichannel analysers. The detectors were calibrated using internationally accepted standards with the same geometry as the samples. Reproducible positioning of samples was ensured with a platform that held the sample container coaxial with the detector during counting. A schematic diagram of the sample counting geometry is shown in Figure 4.3.

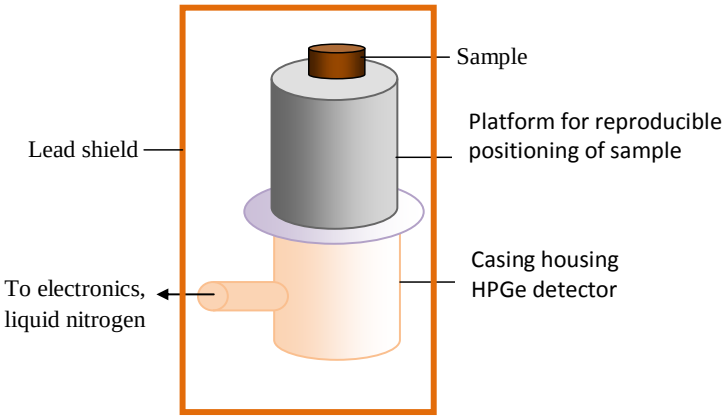

Figure 4.3: Schematic of sample counting geometry for radioactivity analysis of samples

Each sample was counted for at least 12 h with samples having very low concentration being counted for a couple of days. ^{226}Ra specific concentration was determined from gamma energies of 295.22, 351.93, 609.31 and 1764.49 keV; ^{232}Th from gamma energies 968.97, 911.2, 238.63, 727.33, 1620.5 and 583.19 keV; and ^{40}K from gamma energy 1460 keV. The specific concentration (C_s) of each nuclide was determined from the relation (Tzortzis and Haralabos, 2002).

$$C_s = \frac{N_\gamma}{b\chi mt} \quad (52)$$

where N_γ is the average net intensity of the gamma rays of interest, b the emission probability of the gamma rays of interest, χ the detection efficiency of the gamma lines of interest, m the mass of the sample in kg and t the measurement time in seconds.

4.5 Physico-chemical analysis of water samples

4.5.1 Sampling and sample preparation

Sampling of groundwater is discussed in the preceding section. Analysis of pH and electrical conductivity of the samples was done *in situ*. For heavy metal analysis, the preserved water was left to sit for at least 72 hours before analysis (Lintern *et al.*, 1984). This was to facilitate the liberation of any metals that may have adsorbed on to the sampling bottles' surfaces.

Sample preparation was carried out according to EPA method 200.2: for digestion, 2 ml concentrated nitric acid and 1 ml concentrated hydrochloric acid were added to 100 ml of each sample, and the resulting solution was heated at a solution temperature of 95 ^{0}C until the volume reduced to 20 ml. The digestion process removes organic materials that may be present in the water samples and also augments the release of metals adsorbed on particulate matter. The concentrate was allowed to cool, then topped up to 100 ml using double distilled water and filtered using 0.45µm pore size filters into 100 ml conical flasks. The procedure was repeated for all the samples. To

correct for the acids used in the digestion process, a blank was prepared in the same manner as the samples using the double distilled water.

4.5.2 Analysis

Analysis of pH and electrical conductivity was done using standard digital meters while that of heavy metals was done using GF-990 flame atomic absorption spectrophotometer (AAS) at the School of Pure and Applied Sciences, Pwani University, Kilifi, Kenya. The AAS was calibrated using standard stock solutions of known concentrations and a calibration curve obtained. Examples of calibration curves used in this study are shown in Appendix 6.

A portion of each sample and the blank were put in 15 ml vials and the vials fixed in a rack on a turn table interfaced with the AAS. With cathode lamp corresponding to the metal of interest as a source of light, the samples (and the blank) were aspirated into the acetylene – air flame of the AAS one at a time and the absorbance of light measured in each case. The concentration of the given metal was obtained in reference to the calibration curve less the concentration of the blank (if any). The procedure was repeated with cathode lamps corresponding to each metal of interest.

CHAPTER 5: RESULTS AND DISCUSSION

5.1 Radon and thoron concentration

Table 5.1 gives the summary statistics of radon and thoron concentrations in mud dwellings located in Mrima hill region and Kanana village. The dwellings studied had detectable concentrations of both radon and thoron, although the concentration of thoron was higher than that of radon. A strong positive correlation (R^2=0.814) was however observed between the two isotopes (Figure 5.1).

The main source of thoron and radon is usually the soil. In most modern houses, higher radon concentration is normally found in the basement where radon enters by diffusing through the foundation or through cracks and crevices. The presence of thoron in such a case is detected mainly near the cracks and crevices, as the solid foundation inhibits its diffusion into the dwelling. All the dwellings sampled in this study had earthen walls and floor and consequently both isotopes had nearly equal chances of being exhaled into the indoor air which explains the positive correlation between indoor radon and thoron concentration.

Table 5.1: Summary statistics of radon and thoron concentration in the sampling regions

	Concentration (Bq m^{-3})	
	Radon	**Thoron**
	Average (range)	**Average (range)**
Mrima hill	35.2 ± 13.9 (16.3 - 55.6)	652.8 ± 397.0 (132.4 - 1295.1)
Kanana	8.9 ± 2.7 (3.0 - 16.1)	34.9 ± 18.4 (10.0-70.5)

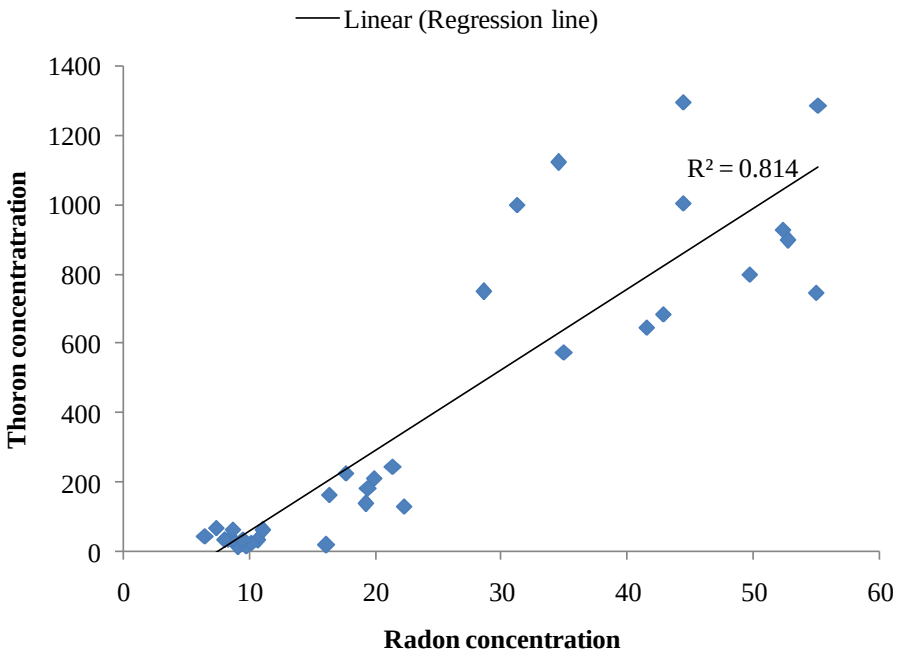

Figure 5.1: Variation of thoron concentration with radon concentration in dwellings

Higher radon and thoron concentrations were observed in dwellings located in Mrima hill as compared to Kanana. In the Mrima hill region, radon concentration varied from 16.3 - 55.6 Bq m^{-3}, with an average of 35.2 ± 13.9 Bq m^{-3} while that of thoron varied from 132 - 1295 Bq m^{-3} with an average of 652.8 ± 397.0 Bq m^{-3}. Kanana dwellings on the other hand had radon concentration of 3.0 - 16.1 Bq m^{-3} with an average of 8.9 ± 2.7 Bq m^{-3} and thoron concentration of 10.0 - 70.5 Bq m^{-3} with an average of 34.9 ± 18.4 Bq m^{-3}. The differences in radon and thoron concentration between the sampling regions can be attributed to the geology while that between radon and thoron in dwellings can be attributed to differences in concentrations of mother radionuclides in the building materials as shown in section 5.3.

Radon is a recognised carcinogen and as a result, agencies and countries the world over have come up with reference levels beyond which radon mitigation measures are recommended. Majority of these reference levels are within the range of 200-600 Bq m^{-3}. All the dwellings sampled registered radon concentration below the lower limit of 200 Bq m^{-3}. In terms of radiation protection therefore, radon does not appear to be a major source of indoor radioactivity in the sampling regions.

In cognisance of thoron as a potential source of internal exposure, the EU proposed a thoron reference level in dwellings of 300 Bq m^{-3}. All the dwellings sampled in Kanana and 35 % of those sampled in Mrima hill region had thoron concentration below the EU proposed guideline value. 40 % of the sampled dwellings in Mrima hill region had concentration levels between 300-1000 Bq m^3 while the remaining 25 % had thoron concentration of over 1000 Bq m^3. Dwellings located on the slopes of Mrima hill registered among the highest thoron concentration, which is not surprising since the hill according to literature (Patel and Mangala, 1994) is the source of the high background radiation that characterise the region. Besides, similar results have been observed in dwellings constructed mainly using soil in China (Tokonami *et al*., 2004; Tschiersch and Müsch, 2005; Shang *et. al*., 2005; Yamada *et. al*., 2006) and India (Reddy *et al*., 2008).

5.1.1 Internal exposure due to inhalation of indoor air

As discussed in chapters 1 and 2, the health risk associated with exposure to radon and thoron principally arises due to inhalation of the short-lived decay products and the consequent alpha particle irradiation of the bronchial airways. This exposure,

quantified in terms of the annual effective dose (E), depends on the progeny concentration as well as the exposure time. Where direct measurements of radon and thoron progeny are difficult, the dose may be calculated on the basis of equilibrium equivalent concentration (EEC), given by the relation $EEC = C_i F_i$ (C_i is the measured concentration of isotope i and F_i its progeny equivalent factor). The effective dose is then evaluated from the relation (UNSCEAR, 2000)

$$E_i = C_i F_i Q_i t \qquad (53)$$

where Q_i is the dose conversion factor for isotope i (9 nSv/Bq m^{-3} h for radon and 40 nSv/Bq m^{-3} h for thoron) and t the indoor occupancy (in hours) per year. Equivalent factors (F_i) of 0.4 for radon and 0.1 for thoron were adopted from Yamada *et. al*., 2006. The global average time spent indoors is 80 %. In Kenya, the average indoor occupancy time is about 60 % (Mustapha *et al*., 1999; Kinyua *et al*., 2011; Kebwaro *et al*., 2011). This occupancy period was adopted in the exposure assessment.

In the Mrima hill region, effective dose due to radon ranged from 0.32 to 1.04 mSv/y with an average of 0.67 mSv/y while that due to thoron ranged from 2.78 – 27.23 mSv/y with an average of 13.70 mSv/y, resulting in a total inhaled dose of 14.37 mSv/y. The dose in this region was of the same order of magnitude as that reported in cave dwellings of the Chinese loess plateau (12.13 mSv/y) calculated using the same UNSCEAR formula (Yamada *et. al*., 2006). Effective dose in Kanana was much lower with a total of 0.9 mSv/y. Of this, 0.17 mSv/y was attributed to radon and 0.73 mSv/y to thoron.

The ICRP recommends effective dose action levels of 3-10 mSv/y (ICRP, 1993). The effective dose rate due to radon in both sampling regions and that due to thoron in Kanana was below the ICRP lower limit of 3 mSv/y. The average dose rate in Mrima hill together with that registered in 65 % of dwellings in the region was above 10 mSv/y. Clearly, the contribution of thoron to the inhaled dose in Mrima hill is significant.

5.2 Radon and thoron exhalation rate

Figures 5.2 and 5.3 are examples of radon and thoron growth curves in the accumulation chamber.

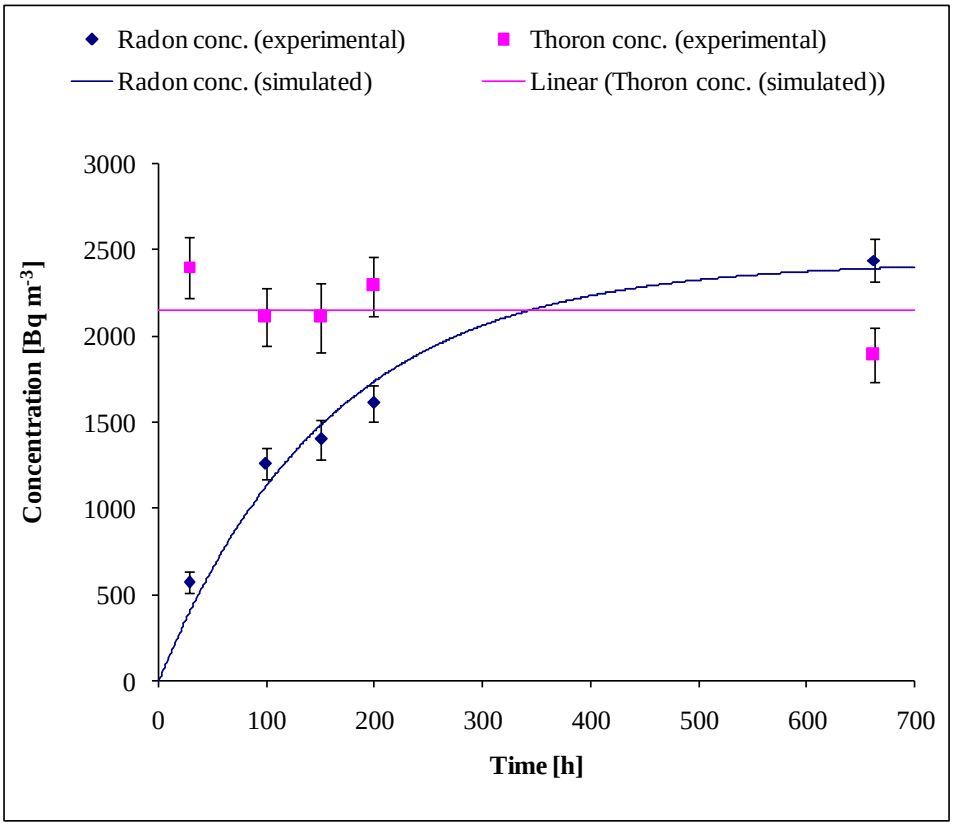

Figure 5.2: Growth curves of radon and thoron from building material sample from Mrima hill

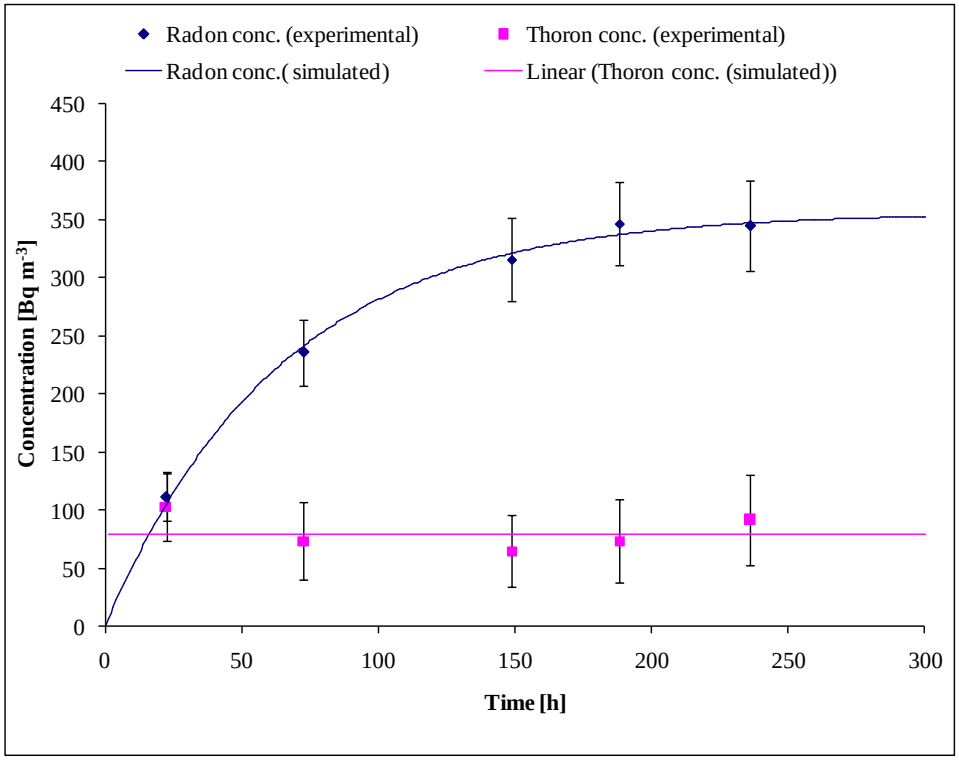

Figure 5.3: Growth curves of radon and thoron from building material sample from Kanana

Thoron activity was detected almost instantly due to its short half-life and also took a much shorter time for the atoms to reach secular equilibrium with short-lived daughters. This is in comparison with the longer-lived radon whereby it took over 300 hours for secular equilibrium between radon and its short-lived progeny to be achieved. For both isotopes though, the measured concentration values fitted well with simulated results obtained from equation (48) in which input parameters included effective decay constant of 0.00627, volume of the accumulation chamber of 3 litres and surface area of the exposed surfaces of 4 cm^2.

Figure 5.4 shows the radon and thoron exhalation rates while Table 5.2 gives the summary statistics.

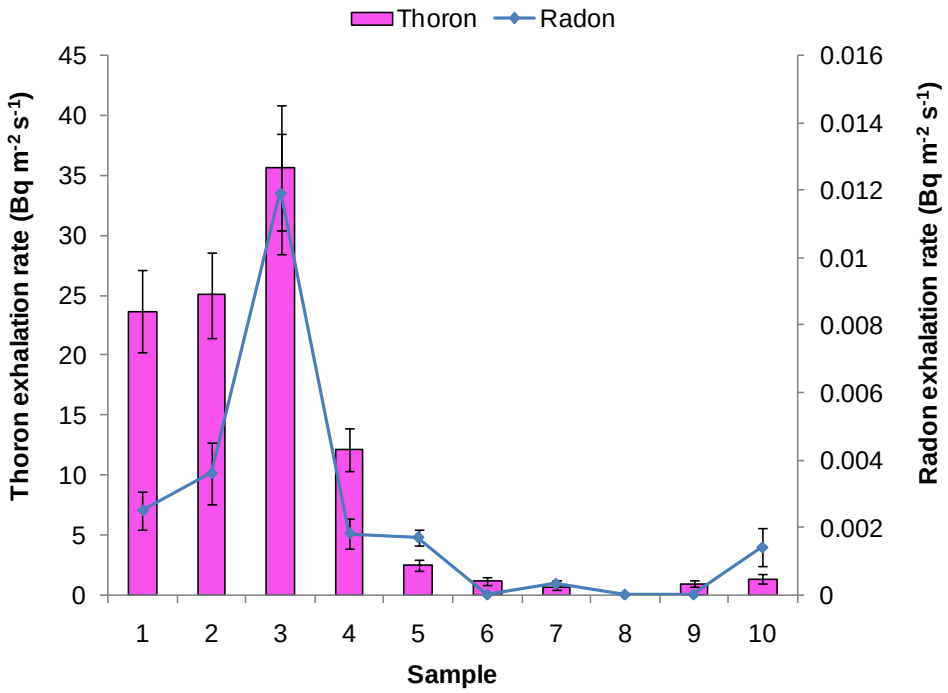

Figure 5.4: Radon and thoron exhalation rates from building material samples

Table 5.2: Radon and thoron exhalation rates from building materials

	Exhalation rate (Bq m^{-2} s^{-1})	
	Thoron	**Radon**
	Average/range	**Average (range)**
Mrima hill	19.8 ± 3.2	0.0043 ± 0.0008
	(2.5 ± 1.8 - 35.7 ± 5.2)	(0.0017 ± 0.0002 - 0.0119 ± 0.0018)
Kanana	0.8 ± 0.2	0.0003 ± 0.0001
	(BD - 1.3 ± 0.3)	(BD - 0.0014 ± 0.0006)

The exhalation rate of thoron was generally higher than that of radon by about three orders of magnitude. However, the decay rate of thoron is usually higher than that of radon by nearly the same order of magnitude thus reinforcing the earlier observation that both isotopes had nearly equal chances of being exhaled. Building materials that exhibited higher exhalation rates coincided with those from Mrima hill region, with an average of 19.8 ± 3.2 Bq m^{-2} s^{-1} and a high of 35.7±5.8 Bq m^{-2} s^{-1}. Radon exhalation rate in the region was significantly lower with an average of 0.0043 ± 0.0008 Bq m^{-2} s^{-1}. Samples from Kanana on the other hand registered radon and thoron exhalation rates with averages of 0.0003 ± 0.0001 Bq m^{-2} s^{-1} and 0.8 ± 0.2 Bq m^{-2} s^{-1} respectively. The highest thoron exhalation rate was 1.3±0.3 Bq m^{-2} s^{-1}, which is about half the lowest thoron exhalation rate in Mrima hill samples.

One of the factors affecting thoron (and radon) exhalation rate is the emanation coefficient. Table 5.3 gives the typical radon emanation coefficient for different soil types.

Table 5.3: Typical radon emanation coefficient for different soil types (Guo *et al.*, 2004)

Soil Type	Emanation coefficient
Sand	0.14
Sandy loam	0.21
Loam	0.24
Silty loam	0.25
Clay	0.28

The study area is characterized by sandy loam soil and therefore for the model given by equation (42), the emanation coefficient of 0.21 was used as one of the input parameters. Other input parameters included thoron diffusion length of 0.011 m (Meisenberg and Tschiersch, 2011), density of sandy loam of 1440 kg m^{-3}, thoron decay constant of 0.0125 and thickness of the materials of 4 cm. As shown in Figure 5.5., the measured and modelled exhalation values showed good agreement, an indication that the concentration of the mother radionuclide to a large extent was responsible for the exhalation rate of the corresponding isotope.

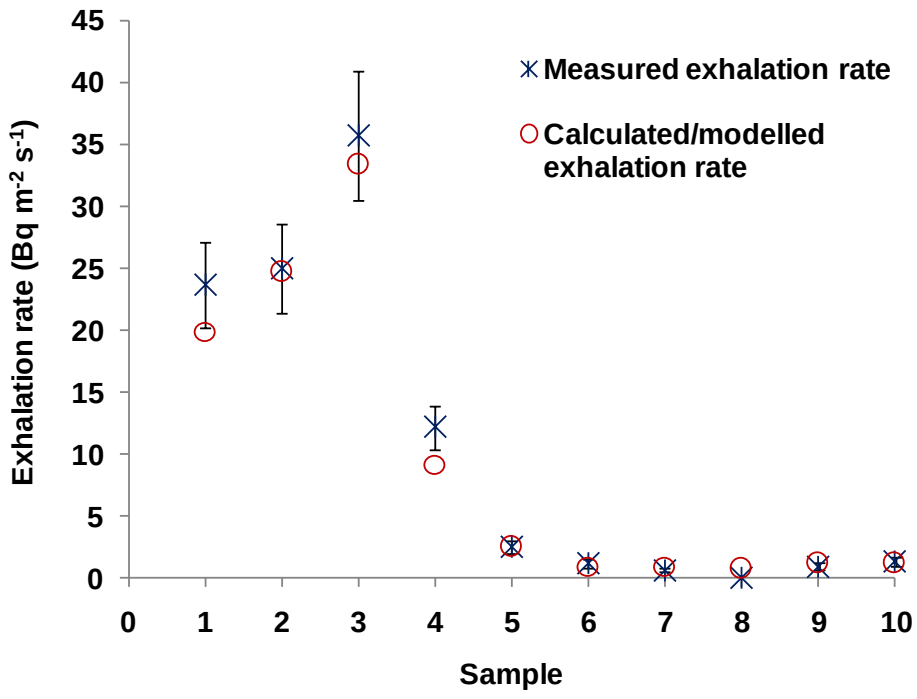

Figure 5.5: A graph of measured and modeled thoron exhalation rate in the different building material samples

5.3 Specific concentrations of ^{226}Ra, ^{232}Th and ^{40}K

5.3.1 Building materials

Figure 5.6 shows the distribution of specific concentration of ^{226}Ra, ^{232}Th and ^{40}K in samples of building materials while Table 5.4 provides the summary statistics. Conforming to the results on exhalation measurements, higher specific concentrations of ^{226}Ra, ^{232}Th and ^{40}K were observed in samples from the Mrima hill region, with average values of 134±10 Bq kg^{-1}, 431±19 Bq kg^{-1} and 249±27 Bq kg^{-1} respectively. The concentrations ranged from 61±3 - 221±10 Bq kg^{-1} for ^{226}Ra, 59±3 - 804 ±34 Bq kg^{-1} for ^{232}Th, and 98±11 - 407±46 Bq kg^{-1} for ^{40}K. Samples from Kanana on the other hand registered average concentrations of 20±1 Bq kg^{-1}, 23±1 Bq kg^{-1} and 92±11 Bq kg^{-1} with maximum values of 25±1 Bq kg^{-1}, 27±2 Bq kg^{-1} and 118±14 Bq kg^{-1} for ^{226}Ra, ^{232}Th and ^{40}K respectively.

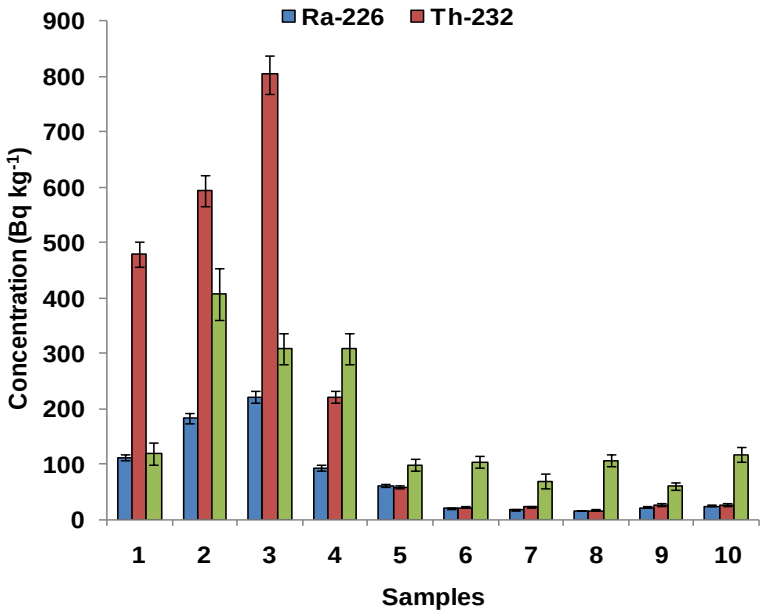

Figure 5.6: Distribution of specific concentration of ^{226}Ra, ^{232}Th and ^{40}K in building material samples

Table 5.4: Summary statistics of specific concentrations of ^{226}Ra, ^{232}Th and ^{40}K in building material samples

	Specific concentration (Bq kg^{-1})		
	^{226}Ra	^{232}Th	^{40}K
	Average (range)	Average (range)	Average (range)
Mrima hill	134±10 (61±3 - 221±10)	431±19 (59±3 - 804 ±34)	249±27 (98±11 - 407±49)
Kanana	20±1 (16±1 - 25±1)	23±1 (17±1 - 27±2)	92±11 (60±7 - 118±14)

As shown in Figure 5.7, a positive correlation was observed between radon/thoron exhalation rates and the specific concentrations of ^{226}Ra/^{232}Th. Similar dependence of exhalation rate on the concentration of mother radionuclide in soil was observed in the HBRA of Ramsar where radon exhalation rate of up 15.4 Bq m^{-2} s^{-1} was reported (Dehghani, *et. al.*, 2013). The main source of background radiation in this region is ^{226}Ra.

The stronger correlation (R^2=0.99) between thoron exhalation rate and the content of ^{232}Th in the building material was attributed to the fact that thoron is only able to escape from the first few layers of soil due to its relatively shorter diffusion length (of approximately 1.1 cm in soil) and therefore is unlikely to be affected significantly by temporal variation in meteorological parameters. Radon on the other hand has a much longer diffusion length in soil (~1 m) and therefore its exhalation rate is more likely to be affected by factors other than the content of ^{226}Ra in building materials.

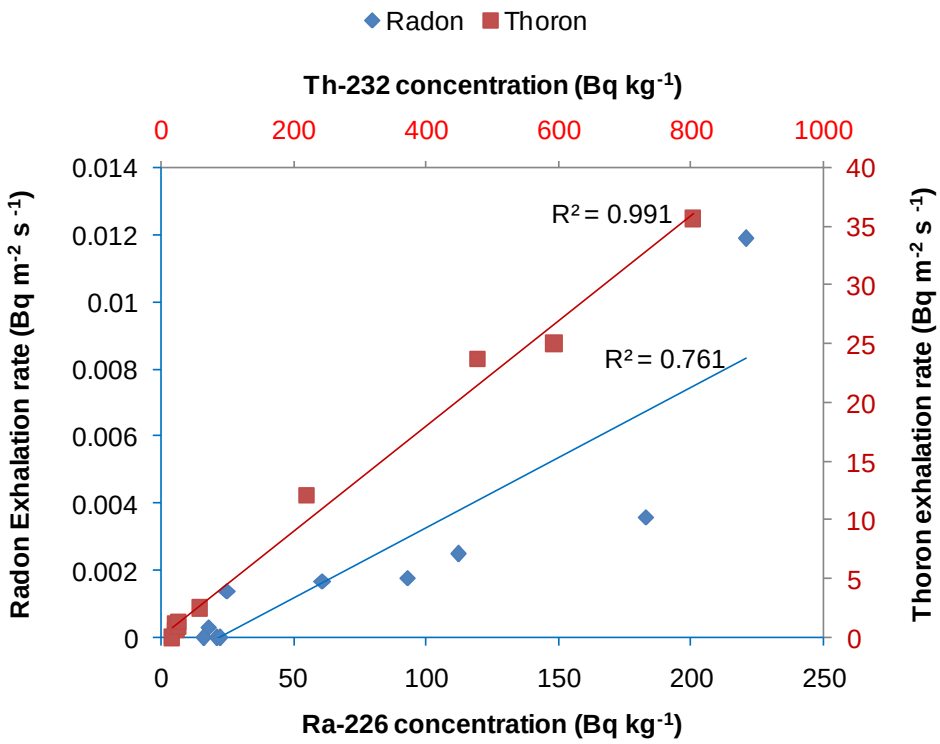

Figure 5.7: Radon/thoron exhalation rates against mother radionuclide concentration

5.3.2 Soil

A plot of specific concentrations of ^{226}Ra and ^{232}Th in soil and in building materials is shown in Figure 5.8 while Table 5.5 gives the summary statistics of ^{226}Ra, ^{232}Th and ^{40}K concentrations in soil. The concentration of ^{226}Ra and ^{232}Th in soil is comparable to that in building materials thus conforming that the building materials originated from the local soil. In addition, higher concentrations of ^{226}Ra, ^{232}Th and ^{40}K were measured in samples from Mrima hill region resulting in average concentrations of 142±9 Bq kg^{-1}, 457±27 Bq kg^{-1} and 247±17 Bq kg^{-1} and maximum concentrations of 250±23 Bq kg^{-1}, 854±72 Bq kg^{-1} and 324±28 Bq kg^{-1} respectively.

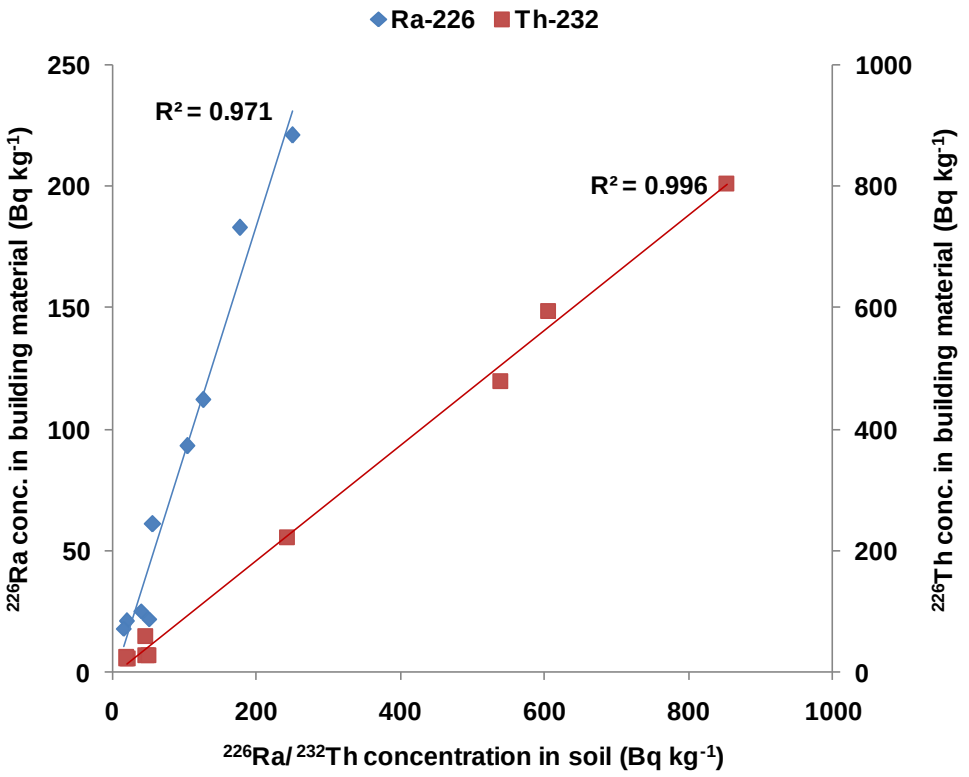

Figure 5.8: $^{226}Ra/^{232}Th$ concentration in building material samples

Table 5.5: Summary statistics of specific concentration of ^{226}Ra, ^{232}Th and ^{40}K in soil samples

	Specific concentration (Bq kg^{-1})		
	^{226}Ra	^{232}Th	^{40}K
	Average (range)	Average (range)	Average (range)
Mrima hill	142±9 (56±3 - 250±23)	457±27 (46±3 - 854 ±72)	247±17 (84±3 - 324±28)
Kanana	31±2 (15±1 - 50±2	35±3 20±2 - 50±3)	137±13 (87±12 - 167±15)

^{226}Ra and ^{232}Th concentration values in soil samples from Mrima hill were similar to those reported by Kebwaro *et al*., 2011. Although the levels of both ^{226}Ra and ^{232}Th were higher than the world average values of 33 and 45 Bq kg^{-1} respectively, ^{232}Th was still the dominant radionuclide in the region. The region appeared depleted of ^{40}K, with the maximum concentration of 324±28 Bq kg^{-1} being less that the world average (420 Bq kg^{-1}) by nearly 20 %.

Soil samples from Kanana registered low values of ^{226}Ra, ^{232}Th and ^{40}K with average specific concentrations of 31±2 Bq kg^{-1}, 35±3 Bq kg^{-1} and 137±13 Bq kg^{-1} and maximum values of 50±2 Bq kg^{-1}, 50±3 Bq kg^{-1} and 167±15 Bq kg^{-1} respectively. This is not unique to Kanana as similarly low concentration values have been reported in other parts of Kwale County. In the proposed titanium mining areas, Osoro *et al*., (2011) reported concentrations of ^{226}Ra, ^{232}Th and ^{40}K in soil samples with average values of 20.9 Bq kg^{-1}, 27.6 Bq kg^{-1} and 69.9 Bq kg^{-1} respectively. Hashim *et al*., (2004) reported average concentrations of ^{226}Ra, ^{232}Th and ^{40}K in soil from Gazi of 11.9 Bq kg^{-1}, 10.8 Bq kg^{-1} and 206 Bq kg^{-1} respectively.

5.3.2.1 External exposure due to soil/building materials

Due to the nature of building materials used in the sampling regions, there exists a risk of external gamma exposure inside dwellings. The indoor risk (E) due to gamma irradiation was thus investigated using the relation (UNSCEAR, 2000);

$$E = 1.4 F_d t \sum F_i C_i \qquad (54)$$

The term $\sum F_i C_i$ represents the absorbed gamma dose rates (n Gy h^{-1}) with F_i (taken as 462, 0.604 and 0.047 $nGyh^{-1}/Bq\ kg^{-1}$ for ^{226}Ra, ^{232}Th and ^{40}K respectively) as the absorbed dose rate conversion factor for radionuclide i and C_i the corresponding specific concentration; F_d (=0.7 $nGyh^{-1}/Svh^{-1}$) is the outdoor gamma dose conversion factor. The outdoor dose is converted to indoor dose by the factor 1.4 (UNSCEAR 1993; Colgan *et al*., 2008), given that the indoor gamma dose is about 1.4 times the outdoor gamma dose. t (h/y) is the indoor occupancy time which in Kenya is 60 %.

An effective indoor gamma dose rate of 1.8 mSv/y was observed in dwellings located in Mrima hill. This value is nearly twice the prescribed limit of 1 mSv/y. The lowest dose rate was 0.30 mS/y and the highest 3.31 mS/y. Kebwaro *et al*., (2011) reported an outdoor effective dose of 1.1 mS/y in the same region, which when multiplied by the conversion factor of 1.4 results in an equally high corresponding indoor gamma rate of 1.54 msv/y.

The gamma dose rate was comparatively lower in Kanana dwellings, with an average of 0.2 mS/y and a high of 0.3 mS/y. In terms of nGy/h, these values correspond to 41 nGy/h and 58 nGy/h respectively. The values are within the global averages of 18 – 93 nGy/h (UNSCEAR 2000) and also the values reported by Mustapha *et al*. (1999) for different parts of Kenya (10-176 nGy/h; average 68 nGy/h).

5.3.3 Groundwater

The results for spectral analysis of groundwater samples are summarized in Table 5.6. All samples from Kanana did not have detectable concentration (>5 Bq kg^{-1}) of ^{226}Ra.

In Mrima hill region on the other hand, 37 % of the samples had detectable concentration of ^{226}Ra, all of which were above acceptable limit of 1 Bq l^{-1}. The maximum value measured was 13.2±1.2 Bq l^{-1} while the average concentration was 4.3±0.3 Bq l^{-1}. ^{226}Ra is moderately soluble in water and therefore its presence in groundwater to some extent is a reflection of its abundance in the local geology. The value of ^{226}Ra concentration in soil reported in this study was 142 Bq kg^{-1}, which is higher than the global average by over a factor of four.

Table 5.6: Summary statistics of specific concentrations of ^{226}Ra, ^{232}Th and ^{40}K in groundwater samples

	Concentration (Bq l^{-1}**)**		
	^{226}Ra	**^{232}Th**	**^{40}K**
	Mean (Range)	**Mean (Range)**	**Mean (Range)**
Mrima hill	4.3±0.3 (BD-13.2±1.2)	2±0.1 (BD-15.8±0.8)	91.4±6.0 (45.0±2.3-131.0±8.0)
Kanana	BD	BD	54.5±4.8 (28.1±2.0-82.4±9.1)

BD-below detection limit (=5 Bq kg^{-1})

Only one sample among all the samples from the two regions had detectable concentration of ^{232}Th. This sample, collected from a well located on the slopes of Mrima hill, had ^{232}Th concentration of 15.8 Bq l^{-1} which is not unusual since ^{232}Th content in soil from the region was among the highest measured. The absence of ^{232}Th in groundwater nonetheless is not necessarily indicative of its absence in the geology. ^{232}Th preferentially adheres tightly to solid particles which essentially reduces its mobility. In sandy soil for instance, ^{232}Th concentration in soil particles is more than

3000 times higher than in interstitial water while in clay soil, its concentration in the particles is 5000 times higher.

^{40}K was detected in all the samples, with concentrations varying from 45.0±2.3 Bq l^{-1} to 131.0±8.0 Bq l^{-1} and 28.1±2.0 Bq l^{-1} to 82.4±9. Bq l^{-1} in Mrima hill and Kanana regions respectively. Regardless of the intake, ^{40}K is always maintained at a constant level within the body and therefore does not accumulate, unlike radionuclides such as ^{226}Ra. However, it will contribute to the exposure so long as it is within the human body.

5.3.3.1 Internal exposure due to groundwater consumption

To assess the risk imposed by the radionuclides on an individual's health, the concentration of ^{226}Ra, ^{232}Th and ^{232}K were related to an effective dose $E(mSv/y)$ using the WHO (2006) formula;

$$E = q\sum(C_i F_i) \qquad (55)$$

where C_i is the content of radionuclide i in water and F_i its corresponding dose coefficient given as $2.8\times10^{-4} mSv/Bq$ for ^{226}Ra, $2.3\times10^{-4} mSv/Bq$ for ^{232}Th and $0.062\times10^{-4} mSv/Bq$ for ^{40}K for adult members of the public; q is the annual ingested volume of drinking water (=730 l/y). This was based on the assumption that 2 liters of water are consumed by an individual daily.

The average annual effective dose in Mrima hill region was 1.7 mSv/y with a maximum of 3.3 mSv/y. The WHO guideline limit for annual effective dose due to

ingested radionuclides is 0.1mSv/y, representing 10 % of the ICRP recommended total exposure limit of 1 mSv/y for members of the public. In Mrima hill, the effective dose due to groundwater consumption is not only nearly 20 times higher than the prescribed limit, but also exceeds the ICRP acceptable limit by 20 %. Similar doses are reported in literature (Nwankwo *et al.*, 2013, Orloff *et al.*, 2004). In Kanana on the other hand, the exposure due to drinking water was due to ^{40}K only, resulting in an effective dose of 0.03 mSv/y.

Ingested radionuclides are of particular concern due to their accumulative nature. The lifetime risk they impose on a population can be approximated based on the nominal probability coefficient for radiation induced stochastic health effects (which include fatal cancer, non-fatal cancer and hereditary effects) for the whole population, given as 7.3×10^{-2}/Sv for adults (ICRP 1991). Assuming an average life expectancy of 60 years (in Kenya), the average lifetime risk in Mrima hill region due to ^{226}Ra and ^{232}Th approximates to 5×10^{-3}. This is significantly higher than the WHO estimated lifetime risk of 10^{-4} calculated on the basis of the exposure reference level of 0.1 mSv/y.

5.3.4 Cassava crop

Table 5.7 shows the mean and range of ^{226}Ra, ^{232}Th and ^{40}K concentrations in cassava tubers and leaves from Mrima hill region while Figure 5.9 compares the concentrations of the radionuclides in the tubers and leaves. ^{226}Ra was detected in over 70 % of cassava tubers and 85% of cassava leaves, with higher concentrations being measured in leaves.

Table 5.7: Summary statistics of specific concentration of ^{226}Ra, ^{232}Th and ^{40}K in cassava tubers and leaves

	Average concentration (range) (Bq kg^{-1})		
	^{226}Ra	^{232}Th	^{40}K
Cassava tubers	60.1±48.2 (BD - 130)	35.3±61.5 (BD - 145)	842±539 (145 - 1860)
Cassava leaves	141.7±74.6 (BD - 235)	BD	1708±552 (983 - 2603)

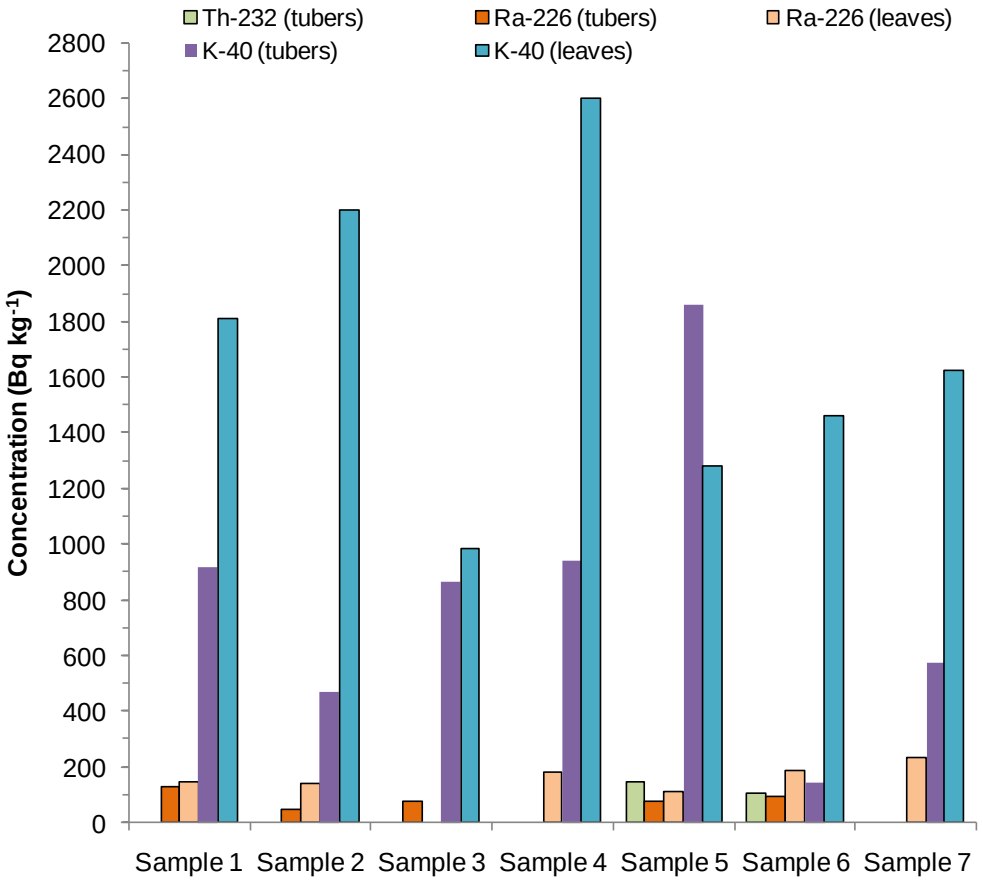

Figure 5.9: Distribution of ^{226}Ra, ^{232}Th and ^{40}K in cassava tubers and leaves from Mrima hill

The concentration in the tubers ranged from BD to 130 Bq kg^{-1} resulting in an average concentration of 60.1±48.2 Bq kg^{-1}. In the leaves, the concentration ranged from BD – 235 Bq kg^{-1} with a mean of 141.7±74.6 Bq kg^{-1}. The ^{226}Ra values in tubers were much higher than those reported by Addo *et al*. (2013) in cassava tubers (of between 19 – 28 Bq kg^{-1}) but lower than the ^{226}Ra concentration reported by Banzi *et al*., (2000) in edible vegetables of up to 399 Bq kg^{-1}. The radionuclides may be expected to be more concentrated in the outer layers of the tubers. The outer skin of the cassava tubers used for analysis was peeled off, as is done during preparation of a cassava meal. This may have contributed to the lower concentration of the radionuclides in the tubers. The effect of evapotranspiration on the other hand may have led to the high concentration of the radionuclides in leaves. Similar observations have been made with regard to cassava (Dobrin *et al*., 2004) whereby radionuclide uptake (transfer) factor was found to be higher in carrot leaves compared to the carrot tubers.

^{232}Th was not detected in the leaves although it was detected in 28 % of the tubers resulting in an average concentration of 35.3±6 Bq kg^{-1}. The highest concentration measured was 145±11 Bq kg^{-1}. The solubility of ^{232}Th is relatively low which may explain the apparent absence in the leaves. Being in contact with the soil, the tubers however may absorb the radionuclide directly from the soil.

^{40}K accounted for the greatest concentration in both the cassava tubers and leaves. Conforming to the trend, higher ^{40}K values were measured in the leaves resulting in a mean concentration of 1708±124 Bq kg^{-1}. This is in comparison to the tubers which registered a mean concentration of 842±53 Bq kg^{-1} was calculated. ^{40}K is one of the

essential elements needed by plants for proper growth and therefore high uptake of the radionuclide by the cassava crop is not unusual.

5.3.4.1 Internal exposure due to cassava crop consumption

Equation (55) was adopted for the calculation of the effective dose resulting from consumption of cassava tubers and leaves. q was taken as the crop consumption rate (kg/y) (90 kg/individual per year for the cassava tubers (Kiome, 2009), and 25 kg/individual per year for cassava leaves as generally less vegetables are eaten in most households in Kenya), and C_i the concentration of radionuclide i in the crop (Bq/kg). The dose conversion factors F_i remained unchanged.

Despite lower consumption rate, the effective dose was higher due to consumption of cassava leaves with a mean of 3.8 mSv/y compared to tubers which reported an effective dose of 2.4 mSv/y, a factor that may be attributed to the presence of high levels of ^{40}K in the leaves. The highest effective dose reported was 6.2 mSv/y due to leaf consumption. The highest dose due to tuber consumption was 5.2 mSv/y.

5.4 Physical-chemical properties of groundwater samples

Table 5.8 presents the mean and range values of pH, electrical conductivity (EC) and selected heavy metal concentration of groundwater samples from Mrima hill and Kanana regions. The pH of water samples from Mrima hill was mainly standard bordering on acidity while samples from Kanana were highly alkaline. The USEPA classifies pH as a secondary water contaminant and recommends an admissible limit of between 6.5 and 8.5. All the samples from Mrima hill had pH values below 8.5

with about 17 % having values lower than 6.5. The lowest pH measured in the region was 5.5. Samples from Kanana on the other hand registered pH values in excess of 8.5, the highest being 10.4. The geological setting coupled with sea water intrusion may have contributed to the differences in water pH between the two regions.

Electrical conductivity is a measure of water's ability to conduct electric current and although it does not give an indication of the specific elements present, it is a good indicator of the presence contaminants such as sodium, potassium or sulphates (Adegbola *et al*., 2012). The electrical conductivity was generally higher in samples from Mrima hill, with an average of 862±949 µSv/cm compared to that of 460±218 µSv/ in samples from Kanana.

Standard deviation indicates the degree of the spread of data values around the mean. In Mrima hill, the standard deviation was higher than the mean, a factor attributed to the wide range of conductivity values in the region. Here, the lowest conductivity measured was 203 µSv/cm and the highest 3730 µSv/cm. The high water conductivity in parts of Mrima hill may be due to the presence of deposits of phosphate ores reported by Gaciri (1991) and relatively high levels of ^{40}K reported in this study.

Figure 5.10 shows the percentage of samples enriched by given heavy metals. In the Mrima hill region, Mn and Cd were the most prevalent with nearly 60% of the samples exceeding the USEPA maximum contamination levels (MCL) of 0.05 mg l^{-1} for Mn and 0.005 mg l^{-1} for Cd.

Table 5.8: Mean values of pH, EC and heavy metal concentration in water samples

	Average (Range)						
	pH	**EC(µs/cm)**	**Mn (mg/l)**	**Cd (mg/l)**	**Pb (mg/l)**	**Cu (mg/l)**	**Zn (mg/l)**
Mrima	7.2±0.8 (5.5 - 8.4)	862±949 (203-3730)	0.41±0.82 (BD-1.48)	0.04±0.04 (BD-0.14)	0.002±0.01 (BD-0.03)	1.05±1.65 (BD-5.12)	0.08±0.27 (BD-1.12)
Kanana	9.9±1.2 (9.4-10.4)	460±218 (101-1000)	0.06±0.11 (BD-0.37)	0.09±0.05 (0.042-0.18)	0.09±0.14 (BD-0.46)	0.84±0.79 (BD-2.06)	0.04±0.04 (BD-0.11)

Over 70 % of the samples had detectable amounts of the metals resulting in average concentrations of 0.41±0.82 mg l^{-1} and 0.04±0.04 mg l^{-1} for Mn and Cd respectively. In the region, Cu concentration in the water samples averaged 1.05±1.65 mg l^{-1} with 29 % of the samples exceeding the USEPA limit of 1.3 mg l^{-1}. About 5 % of the samples had Pb concentrations exceeding USEPA MCL of 0.015 mg l^{-1}. Zn concentration levels were below the MCL. 90 % of groundwater samples from Mrima hill were enriched beyond MCL by at least one of the metals analysed.

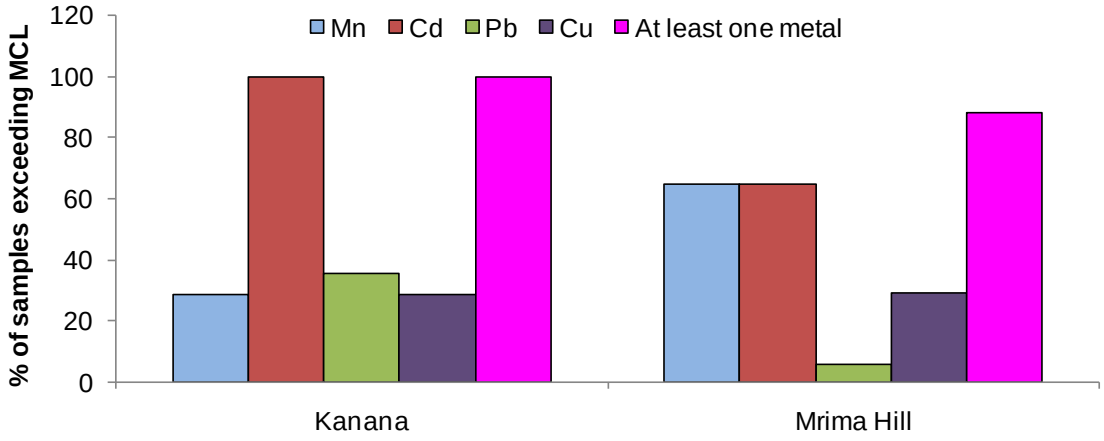

Figure 5.10: Percentage of water samples enriched by selected heavy metals

In Kanana, all the samples had detectable amounts of Cd, and all of them exceeded the USEPA MCL. The Cd concentration ranged from 0.042-0.18 mg l^{-1} with a mean of 0.09±0.05 mg l^{-1}. Pb, with an average concentration of 0.09±0.14 mg l^{-1} was present in levels above USEPA limit in 35 % of the samples; 28 % of the samples and an equal percentage had Mn and Cu levels above the respective MCL. Zn concentration in the samples did not exceed the USEPA MCL.

The existence of rich mineral background of Kwale County in general is documented in literature. Thus, there exists a possibility that the groundwater in both regions was naturally enriched through dissolution of heavy metals present in the geology. In addition, while the region has no major mining or industrial activities, small scale farming is usually undertaken by the local residents. Use of fertilizers such as those derived from phosphates may also introduce heavy metals such as Cd in the groundwater system.

5.5 Exposure associated with radioactivity in building materials, indoor air, crops and well water in the sampling region

Table 5.8 summarizes the annual effective dose associated with exposure to radioactivity in building materials, indoor air, crops and well water in Mrima hill region and Kanana village while Figure 5.11 compares the contribution of dose acquired through the different exposure path ways studied. The annual effective dose was highest in the Mrima hill region with a total of 24.1 mSv/y. 56 % of the dose was due to inhalation of indoor air. Exposure through ingestion contributed 36 % of the dose while external gamma exposure contributed 8 %.

Table 5.9: Summary of annual effective dose rates due to the various factors in the sampling regions

Sampling region	**Affective dose (mSv/y)**						
	Indoor air		Building Materials	Crops		Water	**Total**
	Radon	Thoron	Indoor γ-dose	Cassava tubers	Cassava leaves		
Mrima Hill	0.7	13.7	1.8	2.4	3.8	1.7	**24.1**
Kanana	0.17	0.7	0.2	NA	NA	0.03	**1.1**

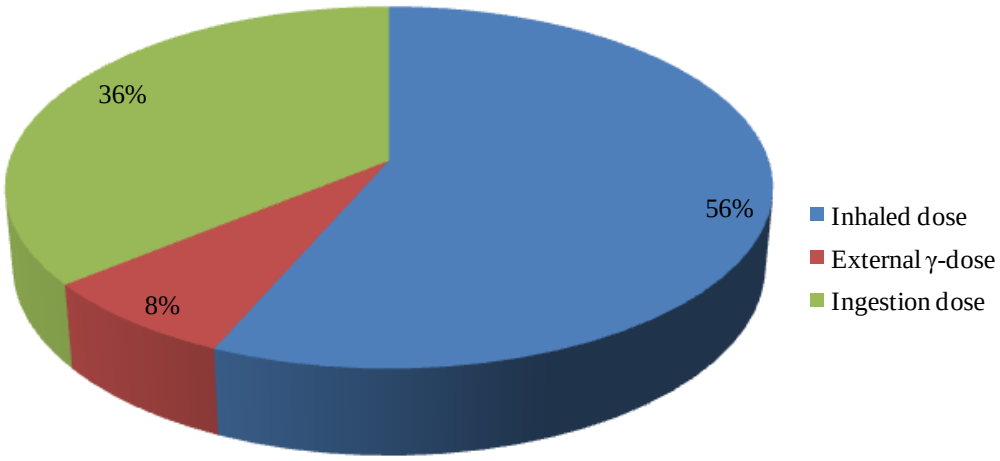

Figure 5.11: Percentage of contribution of exposure pathways to the total annual effective dose

For a combine consumption of cassava leaves and tubers in Mrima hill region, the total effective dose sums up to 6.2 mSv/y. While this is significantly higher than the acceptable limit of 0.1 mSv/y, it is lower than that reported by Banzi *et al*. (2000) of over 20 mSv/y due to consumption of crops grown around the Mijingu phosphate mines in Tanzania. The effective dose due to the studied pathways was within the prescribe limits in Kanana.

CHAPTER 6: CONLUSION AND RECOMMENDATION

6.1 Conclusion

There exists significant radiation exposure in Mrima hill region due to inhalation of indoor air, ingestion of food and water, and external gamma radiation emanating from building materials. Indoor air was responsible for most of the exposure contributing 56 % of the effective dose. 36 % of the dose was through ingestion while 8 % was due to external gamma radiation emanating from building materials. In Kanana on the other hand, the total annual effective was within the acceptable limit and therefore not a risk as concern radiation protection.

More than 90 % of the inhaled dose in Mrima hill was due to thoron which was present in indoor air in average concentration more than double the EU proposed reference level of $300\,\mathrm{Bq\,m^{-3}}$. 65 % of the dwellings had thoron concentration exceeding the EU proposed limit with 25 % of them exhibiting extremely high concentrations of over 1000 Bq m^{-3}. The positive correlation observed between measured radon/thoron exhalation rates and the content of $^{226}Ra/^{232}Th$ in the building materials and the fact that modelled exhalation rate fitted well with the measured exhalation rate implies that the content of mother radionuclide in the building materials was responsible for the concentration of the corresponding isotope in indoor air. ^{232}Th content in the earthen building materials was significantly high with an average concentration nearly 10 times the world average concentration of ^{232}Th in soil which explains the high content of thoron in Mrima hill dwellings.

Elevated external exposure was observed inside dwellings in Mrima hill region, with effective dose nearly twice the recommended dose limit of 1 mSv/y for members of the public. The high external exposure was attributed to the fact that both the walls and the floor of the dwellings sampled were earthen and contained significantly high content of ^{226}Ra and ^{232}Th.

Despite the fact that the highest exposure came from inhalation of indoor air, the risk due to ingestion was more significant in terms of radiation protection in that the dose rate was higher than the prescribed limit by the largest margin. For a combined consumption of cassava tubers, cassava leaves and groundwater in Mrima hill region, the total effective dose sums up to 7.9 mSv/y which significantly higher than the admissible ingested dose. Cassava leaves contributed the largest amount of the ingested dose followed by cassava tubers and lastly groundwater.

^{226}Ra and ^{40}K were mainly responsible for the high dose rates attributed to ingestion. ^{226}Ra was present in over 70 % of the cassava samples and in 37 % of the water samples in levels exceeding acceptable limits, a factor that may be attributed to the relative solubility of ^{226}Ra as well as its high concentration in the geology of Mrima hill region. ^{40}K was present in all samples which was not unusual since it is an essential element needed by plants for proper growth. ^{232}Th contributed to the ingested dose albeit in lesser amounts through the cassava tubers and groundwater as it was not detected in the leaves. ^{232}Th atoms preferentially adhere more to solid particles which to some extent hinders its mobility hence its apparent absence in the leaves. On the other hand, direct contact between the cassava tubers and soil may have heightened ^{232}Th transfer to the tubers while extremely high concentration of the

radionuclide in some parts of the hill may have resulted in its presence in some groundwater samples.

Groundwater from Kanana was found to be of standard pH of while that of Kanana was highly alkaline, a factor that may be attributed to sea water intrusion given its proximity to the Indian Ocean. The electrical conductivity was generally higher in samples from Mrima hill, although the high standard deviation obtained relative to the mean implied a wide variability of conductivity values around the mean; pockets of Mrima hill have rich deposits of mineral elements which may explain the wide variability of conductivity values.

In terms of heavy metals, groundwater from Kanana was of lower quality compared to that from Mrima hill as Cd was present in all the samples. In Mrima hill, 90 % of the groundwater samples were enriched by at least one metal, with Cd and Mn as the main contaminants. The state of groundwater may be attributed to the geology and to farming practices such as use of fertilizers given that small scale farming is the mainstay of the economy in the sampling regions.

6.2 Recommendations

To cut on inhaled dose, residents from Mrima hill region can adopt building techniques that reduce the exhalation of thoron such as plastering the walls of their dwellings with soil obtained from a region such as Kanana where the concentration of ^{232}Th is lower in soil. They can also using building materials of reduced porosity such as fired mud bricks.

Research should be carried out to determine the effect of fertilizer and natural compost on the radioactivity levels in crops grown in Mrima hill. This will help the residents of Mrima hill make informed choices on what to use to increase their crop yield without necessarily raising the crop's radioactivity levels.

The groundwater in both sampling regions is of poor quality either in terms of radionuclides or heavy metals or both. It is recommended that the residents be provided with alternative source of water, or with water treatment devices for home use. The groundwater analysed was collected during the dry season and as water quality evolves with time and climatic conditions, there is need to monitor the groundwater quality over a period of time for instance in the course of a year in order to establish the trend of quality with time and season.

The residents of Mrima hill and Kanana regions should also be educated on the possible consequences of radiation exposure and heavy metal toxicity.

REFERENCES

Adam A. A. and Eltayeb M. A. H., 2009. Uranium Abundance in Some Sudanese Phosphate Ores. *Journal of the Argentine Chemical Society*, **27**(2): 166-177.

Addo M. A., Darco E. O., Gordon C. and Nyarko B. J. B., 2013. A Preliminary Study of Natural Radioactivity Ingestion from Cassava Grown in and Consumed Around a Cement Production Facility in the Volta Region, Ghana. *International Journal of Environmental Sciences*, **3**(6): 2312-2323.

Adegbola, A. A. and Adewoye A. O., 2012. Impact Assessment of Selected Pollution Sources on Groundwater Quality in Wells in Gambari Community, Ogbomoso, Nigeria. *International Journal of Modern Engineering Research,* **2**(5): 3118-3122

Ahmed N. K., 2004. Natural Radioactivity of Ground and Drinking Water in Some Areas of Upper Egypt. *Turkish Journal of Engineering Environmental Sci*ence, **28**: 345-354.

Al-sharif A., 2001. Factors Affecting Radon Concentration in Houses. *Turkish Journal of Physics*, **25**(2001): 153 – 158.

Babu M. N. S., Somashekar R. K., Kumar S. A., Shivanna K., Krishnamurthy V. and Eappen K. P., 2008. Concentration of Uranium Levels in Groundwater. *International Journal of Environment Science and Technology,* **5**: 263-266.

Bailey M. R., 1994. The new ICRP Model for the Respiratory Tract. *Radiation Protection Dosimetry,* **53**: 107-114.

Banzi F. P., Kifanga L. D. and Bundala F. M., 2000. Natural Radioactivity and Radiation Exposure at the Minjingu Phosphate Mine in Tanzania. *Journal of Radiological Protection,* **20**: 41-51.

Barbier O., Jacquillet G., Tauc M, Cougnon M and Poujel P., 2005. Effects of Heavy Metals on, and Handling by, the Kidney. *Nepgron Physiology*, **99**(4): 105-110.

Battaglia A., Capra D., Queirazza G. and Sampaolo, A., 1990. Radon Exhalation Rate in Building Materials and Fly Ashes in Italy. Proceedings of the 5th International Conference on Indoor Air Quality and Climate, Toronto, 29 July - 3 August, 3: 47-52.

BEIR VII, 2006. Health Risks from Exposure to Low Levels of Ionizing Radiation. Health risks from low levels of ionizing radiation: BEIR VII, Phase 2 (2006).

Benke, R. R., and Kearfott, K. J., 1999. Soil Sample Moisture Content as a Function of Time During Oven Drying For Gamma-Ray Spectroscopic Measurements. Nuclear Instruments and Methods in Physics Research Section A, Accelerators, Spectrometers, Detectors and Associated Equipment, **422**(1-3), 817-819.

Bhandare N., Antonelli P. J., Morris C. G., Malayapa R. S. and Mendennal W. M., 2007. Ototocity after Radiotherapy for Head and Neck Tumors. *International Journal of radition Oncology, Biology, physics*, **67**(2): 469-479.

Bochicchio F., Campos V. G., Nuccetelli C., Piermattei S., Risica S., Tommasino L. and Torri G., 1996. Results of the Representative Italian National Survey on Radon Indoors. *Health Physics*, **71**: 741–748.

Briggs, D., 2003. Environmental Pollution and the Global Burden of Disease. *British Medical Bulletin*, 2003: 68: 1-24.

Callegari, I., Bezzon, G. P., Broggini, C., Buso, G. P., Caciolli, A. et al., 2013. Science: Total natural Radioactivity in Tuscany, Italy. *Journal of Maps*, **2013**: 1-7.

Chege M. W., Rathore I. V. S., Chhabra S. C. and Mustapha, A. O., 2009. The Influence of Meteorological Parameters on Indoor Radon in Selected Traditional Kenyan Dwellings. *Journal of Radiological Protection*, **29**: 95-103.

Chin J., Schroth E., MacKinlay E., Fife I., Sorimat A. and Tokanami S., 2009. Simultaneous ^{222}Rn and ^{220}Rn Measurements in Winnipeg, Canada. *Radiation Protection Dosimetry*, **34**(2): 75-78.

Colgan P. A., Organo C., Hone C. and Fenton D., 2008. Radiation Doses Received by the Irish Population: Radiological Protection Institute of Ireland: PPII08/01.

Csige I., Szabó Z. S. and Szabó C. S., 2013. Experimental Technique to Measure Thoron Generation Rate f Building Material Samples Using Rad7 Detector. *Radiation Measurements*, **59**(2013): 201–204.

D'Cunha P. and Narayan Y., 2012. Elevated Natural Radioactivity in Soil Samples of the Coastal Kerara. India. *Journal of Environmental Research and Development*, **7**(2): 700-704.

Dobrin R. I., Dulama C. N. and Toma A. L., 2004. Soil-plant Experimental Radionuclide Transfer Factors. 5th international Balkan workshop on Applied Physics. 5-7 July 2004. Constanta, Romania.

Duenas C., Fernandez M. C., Carretero J., Liger M. and Perez M., 1997. Release of ^{222}Rn from Some Soils. *Annales Geophysicae*, **15**: 124—133.

Duruibe J. O., Ogwuegbu M. O. C. and Egwurugwu J. N., 2007. Heavy Metal Pollution and Human Biotoxic Effects. *International Journal of Physical Sciences,* **2**(5): 112-118.

El-Taher A., El-Hagary M., Emam-Ismail M., El-Saied F. A., and Elgendy F. A. 2013. Radon and its Decay Products in the Main Campus of Qassim University, Saudi Arabia, and its Radiation Hazards. *Journal of American Science*, **9**(6): 257-266.

European Commission, 1998. Scientific Seminar on Radiation Protection in Relation to Radon: Directorate General, Environment, Nuclear Safety and Civil Protection.

European Commission, 2000. Risk Assessment in Relation to Indoor Air Quality. European Collaboration Action. Urban Air, Indoor Environment and Human Exposure. Environment And Quality Of Life, Report No. 22.

Gaciri S. J., 1991. Agromineral Resources of Kenya. *Nutrient Cycling in Agroecosystem,* **30**: 165-166.

Garzia, F., Brebbia C. A. and Guarascio M., 2013. Safety and Security Engineering V. WIT Press: 676.

Ghiassi-nejad M., Mortazavi S. M. J., Cameron J. R., Niroomand-rad A. and Karam P. A., 2002. Very High Background Radiation Areas of Ramsar, Iran: Preliminary Biological Studies. *Health Physics,* **82**: 87-93.

Government of Kenya, 2008. Kenya State of the Coast Report: Towards the Integrated Management of Kenya's Coastal and Marine Resources. UNEP and NEMA, Nairobi: pp 90.

Griffiths A. D., Zahorowski W., Element A. and Werczynski S., (2010). A Map of Radon Flux at the Australian Land Surface. *Atmospheric Chemistry and Physics,* **10**: 8969–8982.

Guo Q., Sun K. and Cheng J., 2004. Methodology Study on Evaluation of Radon Flux From Soil in China. The 11th International Congress of the International Radiation Protection. 23-28 May, 2004. Madrid, Spain.

Hafezi, S., Amidi, J. and Attarilar A. 2005. Concentration of Natural Radionuclides in Soil and Assessment of External Exposure to the Public in Tehran. *Iranian Journal of Radiation Research,* **3**(2): 85-88.

Hamzah H., Alias M., Saat A. and Ishak A., 2011. Measurement of Some Water Quality Parameters Related to Natural Radionuclides in Aqueous Environmental Samples from Former Tin Mining Lake. *Journal of Nuclear and Related Technologies*, **8**(2): 49-59.

Han W. and Yu K. N., 2010. Ionizing Radiation, DNA Double Strand Break and Mutation In: Advances in Genetics Research. Volume 4, Nova Science Publishers.

Harris P. M., 1965. Pandaite from the Mrima Hill Niobium Depositis (Kenya). Warren Spring Laboratory, D.S.I.R, Stevenage, Herts.

Hashim N. O., Rathore I. V. S., Kinyua A. M. and Mustapha A. O., 2004. Natural and Artificial Radioactivity Levels along the Kenya Coast. *Radiation Physics and Chemistry*, **71**: 805-806.

Hassan, N. M., Hosoda M., Iwaoka K., Sorimachi A., Janik M., Kranrod C., Sahoo S. K., Ishikawa T., Yonehara H., Fukushi M. And Tokonami S., 2011. Simultaneous Measurement of Radon and Thoron Released from Building Materials Used in Japan. *Progress in Nuclear Science and Technology*, **1**: 404-407.

Horkel A. D., Neubauer W., Niedermayr G., Okello R. E., Wachira, J. K. and Werneck W., 1984. Notes on the Geology and Mineral Resources of the Southern Kenyan Coast. Mitteilungen der Osterreichischen Geographischen Gesellschaft, **4**: 151-159.

ICRP 65, 1993. Protection against radon-222 at Home and at Work. ICRP 1993 23 (2).

ICRP, 1991. 1990 Recommendations of the International Commission on Radiological Protection. ICRP publication 60.

ICRP, 2006. International Commission on Radiological Protection. Low-dose Extrapolation of Radiation-related Cancer Risk. Publication 99. Amsterdam, the Netherlands: Elsevier, 2006.

Jereczek-Fossa B. A., Alterio D., Jassem J., Gibelli B., Tradati N. and Onecchia R., 2004. Radiotherapy Induced Thyroid Disorders. *Cancer Treatment Reviews*, **30**(4): 369-384.

Kariuki D. K., 2002. Natural Resources-Minerals: A Report of the Civil Society Review of the Implementation of Agenda 21 in Kenya NGO Earth Summit 2002 Forum.

Karuri E. E., Mbugua S. K., Karugia J., Wanda J. and Jagwe J., 2001. Marketing Opportunities for Cassava Based Products: An Assessment of the Industrial Potential in Kenya. University of Nairobi, Department of Food Science, Technology and Nutrition Food Net/International Institute of Tropical Agriculture.

Kebwaro J. M., Rathore I. V. S., Hashim, N. O. and Mustapha A. O., 2011. Radiometric Assessment of Natural Radioactivity Levels Around Mrima Hill, Kenya. *International Journal of the Physical Sciences*, **6**: 3105–3110.

Kinyua R., Atambo V. O. and Ongeri R. M., 2011. Activity Concentration of K-40, Th-232 and Ra-226 and Radiation Exposure Levels in the Tabaka Soapstone Quarries of the Kisii Region, Kenya. *African Journal of Environmental Science and Technology*, **5**(9): 682-688.

Kiome R., 2009. Food security in Kenya. Ministry of Agriculture, Republic of Kenya.

Knoll, G., F., 1989. Radiation Detection and Measurement (Second Edition). John Wiley and Sons Inc: 250.

Krewiski D. S., Rai N. Z., Hopke P. K. 1999. Characteristics of Uncertainties and Variability in Residential Cancer Risks. *Annals of the New York Academy of Science*, **895**: 245-272.

Kurttio P., Komulainen H., Leino, A., Salonen L., Auvinen A. and Saha H., 2005. Bone as a Possible Target of Chemical Toxicity of Natural Uranium in Drinking Water. *Environmental Health Perspectives*, **113**: 68-72.

Kurttio, P., Auvinen, A. and Salonen, L., 2002. Renal Effects of Uranium in Drinking Water. *Environmental Health Perspectives*, **110**: 337-342.

Kwale District Environmental Report, 1995. National Environment Secretariat, Ministry of Environment and Natural Resources.

Lintern M. J., Hann A. N., Willing M. and Talbot V., 1984. A Survey of Heavy Metals in Sediments and Waters of the Preston River - July 1984. Library Department of Conservation and Environment.

Maged A. F. and Ashraf, F. A., 2005. Radon Exhalation Rate of Some Building Materials Used in Egypt. *Environmental Geochemistry and Health*, **27** (5): 485-489.

Maina D. M., Kinyua A. M., Nderitu S. K., Agola, J .O. and Mangala M. J., 2004. Indoor Radon Levels in Coastal and Rift Valley Regions of Kenya. IAEA-CN-91/56: 401-404.

Mandour R. A. and Azab Y. A., 2010. Toxic Levels of Some Heavy Metals in Drinking Groundwater in Dakahlyia Governorate, Egypt in the Year 2010. *The International Journal of Occupational and Environmental Medicine*, **2**(2): 112-117.

Masters R. G., 1999. Poisoning the Well: Neurotoxic Metals, Water Treatment, and Human Behavior. Plenary Address to Annual Conference of the Association for Politics and the Life Sciences, Four Seasons Hotel, Atlanta, GA. Sept. 2, 1999.

Mauring, A. and Gäfvert, T., 2013. Radon Tightness of Different Sample Sealing Methods for Gamma Spectrometric Measurements of ^{226}Ra. *Applied Radiation and Isotopes*, **81**: 92–95.

McLaughlin J., Murray M., Currivan L., Pollard D., Smith V., Tokonami S., Sorimachi A. and Janik M., 2011. Long-Term Measurements of Thoron, its Airborne Progeny and Radon in 205 Dwellings in Ireland. *Radiation Protection Dosimetry*, **145**(2-3): 189-93.

Meisenberg O. and Tschiersch J., 2011. Thoron in Indoor air: Modeling for a Better Exposure Estimate. *Indoor Air*, **21**: 240–252.

Meisenberg O., Gierl S. and Tschiersch J., 2013. Measurement of Thoron and its Progeny in Traditional and Modern Earthen Buildings in Germany: Methodology and Results. 2013 International Radon Symposium: Creating New Opportunities for the Radon Professional Measurement and Mitigation. September 22-25, 2013, Springfield, Illinois.

Mlwilo N. A., Mohammed N. K. and Spyrou N. M., 2007.Radioactivity Levels of Staple Foodstuffs and Dose Estimates for Most of the Tanzanian Population. *Journal of Radiological Protection,* 27: 741-744.

Mohanty A. K., Sengupta D., Das S. K., Vijayan V. and Saha S. K., 2004. Natural Radioactivity in the Newly Discovered High Background Rradiation Area on the Eastern Coast of Orissa India. *Radiation Measurements,* **38**(2004): 153-165.

Momodu M. A. and Anyakora C. A., 2009. Heavy Metal Contamination of Ground Water: The Surulere Case Study. *Research Journal Environmental and Earth Sciences,* **2**(1): 39-43.

Mustapha A. O., Patel J. P. and Rathore I. V. S., 2002. Preliminary Report on Radon Concentration in Drinking Water and Indoor Air in Kenya. *Environmental Geochemistry and Health*, **24**: 1573-2983.

Mustapha A. O., Patel J. P. and Rathore I. V. S., 1999. Assessment of Human Exposure to Natural Sources of Radiation in Kenya. *Radiation Protection Dosimetry*, **82**: 285 – 292.

Mustapha A. O., Patel J. P., Kalambuka H. A., Achola S. O., Maina D. M. and Otwoma D., 2012. Outdoor Exposure Doses in the High Background Radiation Areas of Lambwe East Location in Southwesten Kenya. XI Radiation Physics and Protection Conference, 25-28 November, Nasr city, Cairo, Egypt.

NACADA, 2010. Report of Survey on Drug and Substance Abuse in Coast Province Kenya. Main Report. National Campaign Against Drug Abuse Authority, March 2010.

National Museums of Kenya, 2008. The World Heritage Convention: The Sacred Mijikenda Kaya Forests (Kenya).

Nawrot T., Plusquin M., Hogervovst J., Roels H. A., et al., 2006. Environmental Exposure to Cadmium and Risk of Cancer: a Perspective Population Based Study. *Lancet Oncology*, **7**(2):119-126.

NCRP 2009: Ionising Radiation Exposure of the People of the United States. National Council for Radiation Protection, NCRP No. 160.

Nwankwo L. I., 2013. Determination of Natural Radioactivity in Groundwater in Tanke-Ilorin, Nigeria. *West African Journal of Applied Ecology*, **21**(1): 111-119.

Ocheri M. and Ogwuche J., 2012. Lead in Groundwater of Benue State, Nigeria. *Journal of Environmental Science and Water Resources*, **1**(5): 115-119.

Orloff K. G., Mistry M., Charp P., Metcalf S., Marino R., Shelly, T., Melaro E., Donohoe A. M. and Jones R. L., 2004. Human Exposure to Uranium in Groundwater. *Environmental Research*, **94**: 319-326.

Osoro M. K., Rathore I. V. S, Mangala M. J. and Mustapha A. O., 2011. Radioactivity in Surface Soils around the Proposed Titanium Mining Project in Kenya. *Journal of Environmental Protection*, **2011**(2): 460-464.

Otwoma D., Patel J. P., Bartilos S. and Mustapaha A. O., 2012. Radioactivity and Dose Assessment of Rock and Soil Samples from Homa. XI Radiation Physics and Protection Conference, 25-28 November, Nasr city, Cairo, Egypt.

Oyeku O. T. and Eludoyin A. O., 2010. Heavy Metal Contamination of Groundwater Resources in a Nigerian Urban Settlement. *African Journal of Environmental Science and Technology*, **4**(4): 201-214.

Pabello N. G. and Bolivar V. J., 2005. Young Brains on Lead: Adult Neurological Consequences? *Toxicological Sciences,* **86**(2): 211-213.

Patel J. P., 1991. Environmental Radiation Survey of the Area of High Background Radiation of Mrima Hill, Kenya. *Discovery and Innovation*, **3**(3): 31-35.

Patel J. P. and Mangala M. J., 1994. Elemental Analysis of Carbonatite Samples from Mrima Hill, Kenya, by Energy Dispersive X-Ray Fluorescence. *Nuclear Geophysics*, **8**: 389-393.

Patrick L., 2006. Lead Toxicity Part II: The Role of Free Radical Damage and the Use of Antioxidants in the Pathology and Treatment of Lead Toxicity. *Alternative Medicine Review*, **11**(2): 124-127.

Prasher D. (2009). Heavy Metals and Noise Exposure: Health Effects. *Noise Health,* **1**(44): 141-4.

Reddy M. S., Reddy P. Y., Reddy K. R., Eappen K. P., Ramachandran T. V. and Mayya Y. S., 2008.Thoron Levels in Dwellings of Hyderabad city, Andhra Pradesh India. *Journal of Environmental Radioactivity*, **73**:21-28.

Sabath E and Robles O. M. L., 2012. Renal Health and the Environment: Heavy Metal Nephotoxicity. *Nefrologia*, **32**(3): 279-286.

Saghirzadeh M., Gharaati M. R., Mohammadi S. H. and Giassi-Nejad M., 2001. Evaluation of DNA Damage in the Root Cells of Allium Seeds Growing in the High Background Radiation Area of Ramsar, Iran. *Journal of Environmental Radioactivity*, **99**(2008):1698-1702.

Sakoda A., Nishiyama N., Hanamoto K., Ishimori Y., Yamamoto Y., Kataoka K., Kawabe K. and Yamaoka K., 2010. Differences of Natural Radioactivity and Radon Emanation Fraction among Constituent Minerals of Rock or Soil. *Applied Radiation and Isotopes*, **68** (2010): 1180–1184.

Salem H. M., Eweida A., Farag A., 2000. Heavy Metals in Drinking Water and their Impact on Human Health. Proceedings of the International Conference for Environmental Hazards Mitgation (ICEHM'200) 9-12 September, 2000, Cairo University, Egypt (ICHEM, 2000): 542-556.

Schumann R. R., 1993. The Radon Emanation Coefficient: An Important Tool for Geologic Radon Potential Estimations. Proceedings of the 1993 International Radon Conference: 40-47.

Shakeri A., Moore F., Mohannadi Z. and Raeisi E., 2009. Heavy Metal Contamination in the Shiraz Industrial Complex Zone Groundwater, South Shiraz, Iran. *World Applied Sciences Journal*, **7**(4): 522-530.

Shang B., Chen B., Gao Y., Wang Y., Cui H. and Li Z., 2005. Thoron Levels in Traditional Chinese Residential Dwellings. *Radiation and Environmental Biophysics*, **44**(3): 193-199.

Smith M. A., Grant L. D. and Sors A., 1989. Lead Exposure and Child Development: an International Assessment. Kleeven Academic Publishers.

Sperling D. C., 1988. The growth of Islam among the Mijikenda of the Kenya Coast, 1826-1933. Ph.D Desertation, School of Oriental and African studies, University of London.

Sreenath R. M., Yadagiri R. P., Rama K., Eappen, K. P., Ramachandran, T. V. and Mayya Y. S., 2004. Thoron levels in the Dwellings of Hyderabad City, Andhra Pradesh, India. *Journal of Environmental Radioactivity*, **73**: 21-28.

Strom D. J., 2003. Health Impacts from Acute Radiation Exposure. Prepared for the U.S. Department of Energy under Contract DE-AC06-76RL1830.

Tinga, K. K., 1998. Cultural Practice of the Midzichenda at Cross Roads: Divination, Healing, Witchcraft and Statutory Law. *Afrikanistische Arbeitspapiere (AAP),* **55**: 173-184.

Tokonami S., Sun Q., Akiba S., Zhuo W., Furukawa M., Ishikawa T., Hou C., Zhang S., Narazaki Y., Ohji B., Yonehara H., Yamada Y., 2004. Radon and Thoron Exposures for Cave Residents in Shanxi and Shaanxi Provinces. *Radiation Research*, **162**(4): 390-396.

Tschiersch J., Li W. B. and Meisenberg O., 2007. Increased Indoor Thoron Concentrations and Implication to Inhalation Dosimetry. *Radiation Protection Dosimetry*, **127**: 73-78.

Tschiersh J. and Müsch B., 2005. Radon Exposure in Homes: Is The Contribution of ^{220}Rn (Thoron) to Dose Always Negligible? GSF-Report 06/05 Neuherberg: 214.

Tubiana M, Feinendegen L. E, and Kaminski J. M., 2009. The Linear No-Threshold Relationship is Inconsistent with Radiation Biologic and Experimental Data. *Radiology*, **251**(1): 13-22.

Tzortzis T. and Haralabos T. H., 2002. Gamma-Ray Measurements of Naturally Occurring Radioactivesamples from Cyprus Characteristic Geological Rocks. Medical Physics Department, Nicosia General Hospital, Nicosia, Cyprus; UCY−PHY− 02/02 (Revised version: 2/12/2002): 1-27.

UNESCO, 2005. Policy Review Report: Early Childhood Care and Education in Kenya. UNESCO/OECD Early Childhood Policy Review Project. The Section for Early Childhood and Inclusive Education, Division of Basic Education, UNESCO Education Sector.

UNSCEAR (1982). Sources of Ionizing Radiation. United Nations Scientific Committee on Effects of Atomic Radiation, 1982 Report to the General Assembly, United Nations, New York.

UNSCEAR, 1992. Exposure to Radon and Thoron and their Decay Products. Annex D. United Nations Scientific Committee on Effects of Atomic Radiation.

UNSCEAR, 1993. Sources of Ionizing Radiation. United Nations Scientific committee on Effects of Atomic Radiation, 1993 Report, United Nations, New York, 1993.

UNSCEAR, 2000. United Nations Scientific Committee on the Effects of Atomic Radiation. Sources and Effects of Ionizing Radiation. UNSCEAR 2000 Report to the General Assembly, with Scientific Annexes, (I): New York: United Nations, 2000.

UNSCEAR, 2008. United Nations Scientific Committee on the Effects of Atomic Radiation. Sources and Effects of Ionizing Radiation. UNSCEAR 2008 Report to the General Assembly, with Scientific Annexes, (I): New York: United Nations, 2008.

UNSCEAR, 2010. Report of the United Nations Scientific Committee on the Effects of Atomic Radiation on the Effects of Atomic Radiation, 2010.

USEPA, 2003. National Primary Drinking Water Standards. U.S. Environmental Protection Agency, 2003.

USEPA, 2004. Drinking Water Advisory for Manganese. U.S. Environmental Protection Agency, 2004.

USEPA, 2005. Quick Guide to Drinking Water Sample Collection. United States Environmental Agency, USA.

Vaupoti J. and Kobal I., 2007. The Importance of Nanosize Aerosols of Radon Decay Products in Radon Dosimetry. *Croatica Chemica Acta*, **80**: 565-573.

Vengosh A., Hirschfeld D., Vinson D., Dwyer G., Raanan H., Rimawi O., Al-Zoubi A., Akkawi E., Marie A., Gustavo H., Zaarur S. and Gano J., 2009. High Natural Occuring Radioactivity in Fossil groundwater from the Middle East. *Environmental Science and Technology*, **43**(6): 1769–1775.

WHO, 2001. Water health and sanitation: Water-related Diseases. World Water Day, 2001.

WHO, 2003. World Health Organization Guidelines for Drinking Water Quality, Third edition, 2003.

WHO, 2006. Protecting Groundwater for Health: Managing the Quality of Drinking-Water Sources. Edited by O. Schmoll, G. Howard, J. Chilton.

WHO, 2006. Working Together for Health. The World Health Report, 2006.

WHO, 2007. A Safer Future: Global Public Health Security in the 21st Century. The World Health Organization Report, 2007.

WHO, 2009. World Health Organization Handbook on Indoor Radon: A Public Health Perspective. World Health Organization, 2009.

WHO, 2011. Guidelines for Drinking-water Quality. World Health Organization, 2011, 4th edition.

World Bank Report, 2008. World Bank Report on Kenya Poverty and Inequality Assessment: Volume I: Synthesis Report. Report No. 44190-KE, June 2008.

Xhixha, G., Bezzon, G. P., Broggini, C., Buso, G. P., Caciolli, A., Callegari, I. *et al*., (2013). The Worldwide NORM Production and a Fully Automated Gamma-Ray Spectrometer for their Characterization. *Journal of Radioanalitical and Nuclear Chemistry*, **295**: 445 –457.

Yamada T., 2013. Mushrooms: Radioactive Contamination of Widespread Mushrooms in Japan. Agricultural Implications of the Fukushima Nuclear Accident: 163-166.

Yamada Y., Sun Q., Tokonami S., Akiba S., Zhuo W., Hou C., Zhang S., Ishikawa T., Furukawa M., Fukutsu K. and Yonehara H.. 2006. Radon-Thoron Discriminative Measurements in Gansu Province, China, and their Implication for Dose Estimates. *Journal of Toxicology and Environmental Health, Part A*, **69**(7):723-34.

Zamora M. L., Tracy B. L., Zielinski J. M., Meyerhof, D. P. and Moss M. A. (1998): Chronic Ingestion of Uranium in Drinking Water: A Study of Kidney Bioeffects in Humans. *Toxicological Sciences*, **43**: 68-77.

Zapalac G. H., 2013. A Time-Dependent Method for Characterizing the Diffusion of Radon-222 in Concrete. *Health Physics*: 1-29.

APPENDICES

Appendix 1: ^{238}U decay chain

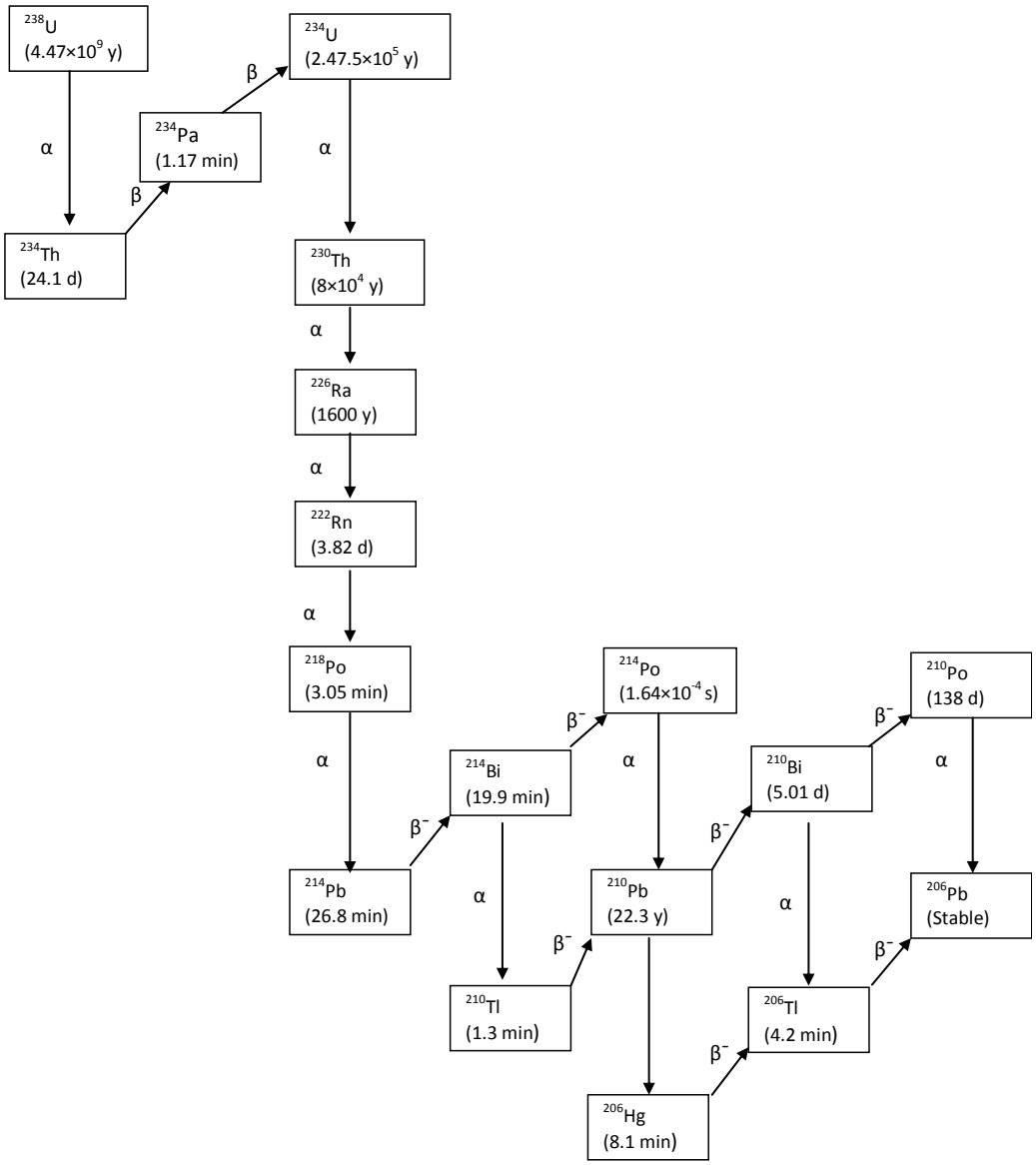

Appendix 2: Thoron decay chain

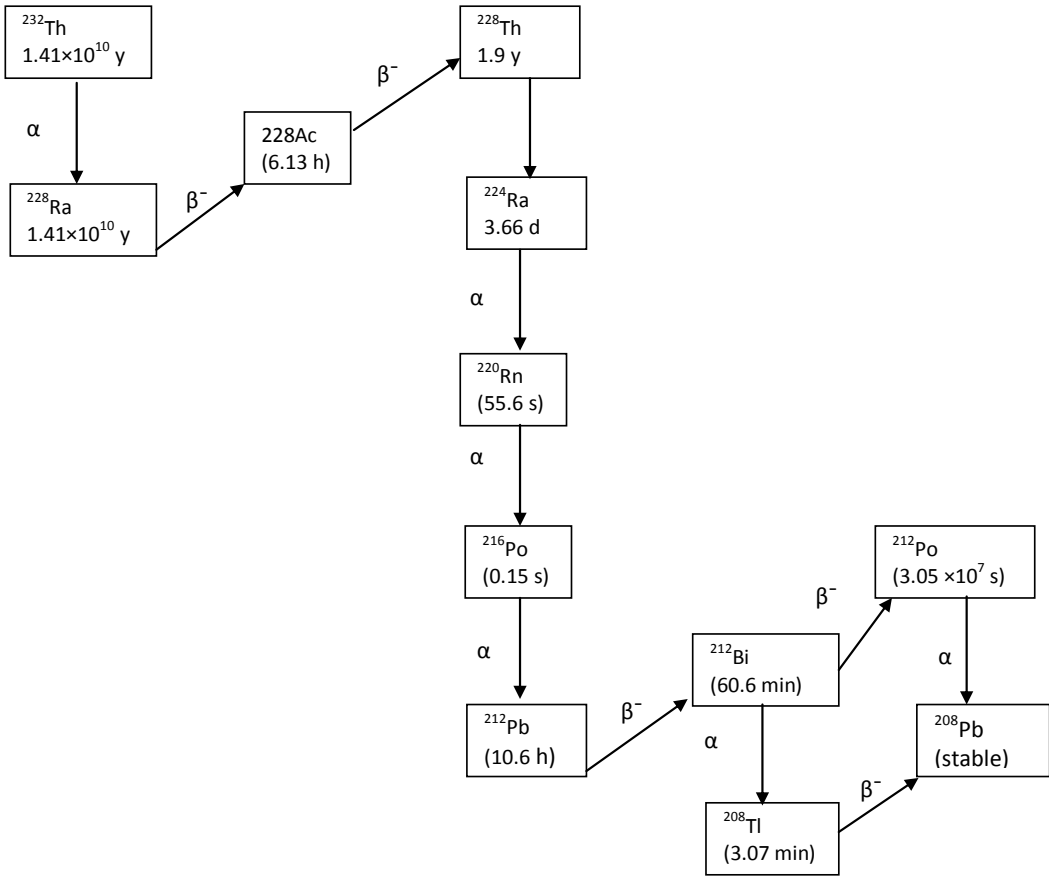

Appendix 3: Wall sample being collected from a typical mud wall of a hut in the Mrima hill region

Appendix 4: Picture of Mrima hill

Appendix 5: A local woman assisting in sample collection from an open well in Mrima hill region

Appendix 6: Calibration curves for heavy metal analysis

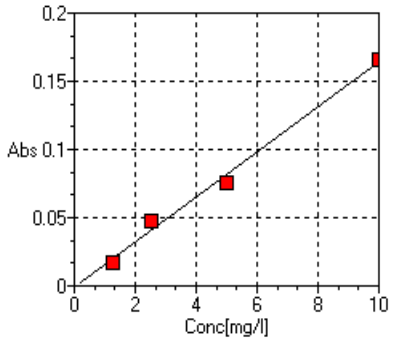

Calibration curve for Pb analysis

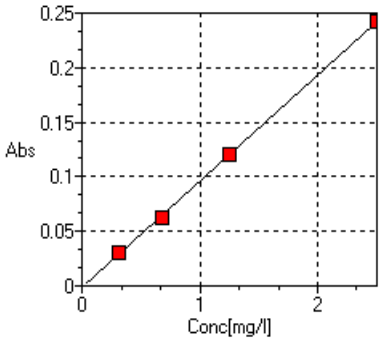

Calibration curve for Mn analysis

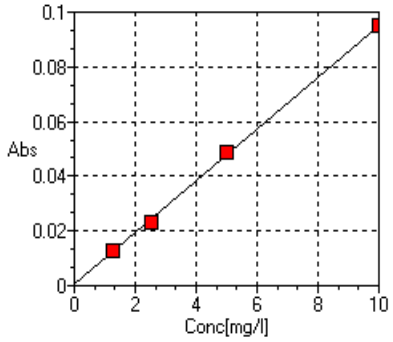

Calibration curve for Cu analysis

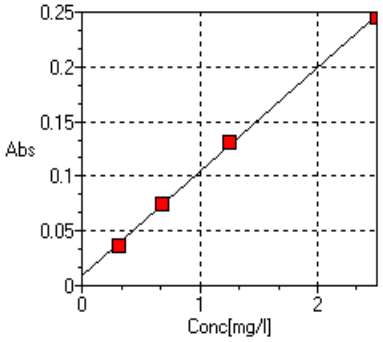

Calibration curve for Cd analysis

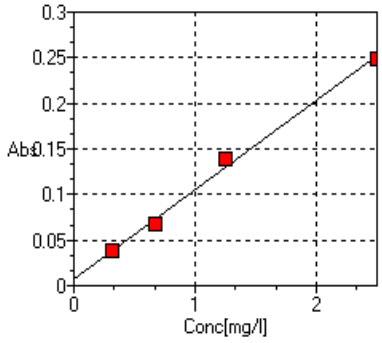

Calibration curve for Zn analysis

Appendix 7: Research papers and presentations

1 Chege, M. W., Hashim, N. O., Merenga, A. S. and Tschiersch, J., 2013 Lead contamination of traditional hand-dug wells in parts of Kwale County, Kenya. *International Journal of Physical Sciences,* **8**(18): 835-839.

2 Chege, M. W., Hashim, N. O. and Merenga, A. S., 2013. Physico-chemical analysis of groundwater in the Gazi-Mrima hill region of Kwale County, Kenya. *Asian Journal of Science and Technology*, **4**(5): 55-58.

3 Chege, M. W., Hashim, N. O., Merenga, A. S. and Tschiersch, J., 2013. Thoron concentration in mud dwellings of Mrima hill, Kenya. Presented at the WE-Heraeus Physics Summer School "Ionising Radiation and Protection of Man“ Bad Honnef, 11 - 23 August 2013. Bad Honnef, Germany.

4 Chege, M. W., Hashim, N. O., Merenga, A. S. and Tschiersch, J. (2013). Total metal concentration measurement of well water in Mrima hill region, Kwale County, Kenya. Environmental Health 2013: Science and policy to protect future generations, 3-6 March 2013 Boston, USA.

5 Chege, M. W., Hashim, N. O., Merenga, A. S. and Tschiersch, J. (2013). Heavy metal enrichment of groundwater in parts of Kwale County, Kenya. Environmental Health 2013: Science and policy to protect future generations, 3-6 March 2013 Boston, USA.

6 Chege, M. W., Hashim, N. O., Merenga, A. S., 2012. Heavy Metal Analysis of Well Water in the Gazi - Mrima hill Region of Kwale County, Kenya. Presented at the UNESCO /DAAD-ALUMNI conference “Water in Africa”: sustainable

water management In African countries. 1-3 October 2012. Maseno University (Kisumu Campus), Kenya

7 Chege, M. W., Hashim, N. O., Merenga, A. S. Tschiersch, J. and Meisenberg O., 2014. Measurement of thoron exhalation rate from earthen building materials used in rural Kenya. Presented at the International Conference on Radioecology and Environmental Radioactivity (ICRER) held from 7-12 September 2014 in Barcelona, Spain.

8 Chege, M. W., Hashim, N. O., Merenga, A. S. and Tschiersch, J., 2014. Analysis Of Internal Exposure Associated With Consumption of Crops and Groundwater from the High Background Radiation Area of Mrima Hill, Kenya. Presented at the 9th International Symposium on Natural Radiation Environment (NRE-IX) held from 23 - 26 September, 2014, Hirosaki, JAPAN.

9 Chege, M. W., Hashim, N. O., Merenga, A. S. Tschiersch, J. and Meisenberg O., 2014. Estimation of annual effective dose due to radon and thoron concentrations in mud dwellings of Mrima Hill, Kenya. Presented at the 9th International Symposium on Natural Radiation Environment (NRE-IX) held from 23 - 26 September, 2014, Hirosaki, JAPAN.

10 Modelling radon and thoron exhalation rate from earthen building materials in Kenya (preparation in progress).

11 Determination of thoron emanation coefficient in earthen building materials used in parts of Kwale County, Kenya (Under preparation).

12 Naturally occurring radionuclides content in earthen building materials and the associated indoor gamma dose rate (preparation in progress).

13 Radioactivity assessment in indoor air, well water and crops in Kanana Village of Kwale County, Kenya (preparation in progress).